AD-A210 088

(2)

UMENTATION PAGE

Form Approved OMB No 0704-0188

1a REPORT SECURITY CLASSIFICATION: (u)	1b RESTRICTIVE MARKINGS: NA
2a SECURITY CLASSIFICATION AUTHORITY: NA	3 DISTRIBUTION AVAILABILITY OF REPORT: Distribution Unlimited
2b DECLASSIFICATION / DOWNGRADING SCHEDULE: NA	
4 PERFORMING ORGANIZATION REPORT NUMBER(S): UH	5 MONITORING ORGANIZATION REPORT NUMBER: NA
6a NAME OF PERFORMING ORGANIZATION: University of New Hampshire	6b OFFICE SYMBOL (If applicable): NA
6c ADDRESS (City, State, and ZIP Code): Durham, New Hampshire 03824	7a NAME OF MONITORING ORGANIZATION: Office of Naval Research
	7b ADDRESS (City, State and ZIP Code): 800 N. Quincy St. Arlington, VA 22217-5000
8a NAME OF FUNDING / SPONSORING ORGANIZATION: Office of Naval Research	8b OFFICE SYMBOL (If applicable): ONR
	9 PROCUREMENT INSTRUMENT IDENTIFICATION NUMBER: N00014-85-K-0502
8c ADDRESS (City, State, and ZIP Code): 800 N. Quincy St. Arlington, VA 22217-5000	10 SOURCE OF FUNDING NUMBERS

PROGRAM ELEMENT NO	PROJECT NO	TASK NO	WORK UNIT ACCESSION NO
61153N	RR 4106	4413-009	

11 TITLE (Include Security Classification)

(u) Iron Associated Outer Membrane Proteins of Magnetic Bacteria

12 PERSONAL AUTHOR(S)

Blakemore, Richard Peter

13a TYPE OF REPORT	13b TIME COVERED	14 DATE OF REPORT (Year, Month, Day)	15 PAGE COUNT
Final	FROM 7/85 TO 1/89	1989/6/16	8 + reprints

16 SUPPLEMENTARY NOTATION

17 COSATI CODES			18 SUBJECT TERMS (Continue on reverse if necessary and identify by block number)
FIELD	GROUP	SUB-GROUP	Magnetism; Periplasm; Magnetosome; Bacteria; Iron Reductase; Outer Membrane; Cytochrome;
06	03		

19 ABSTRACT (Continue on reverse if necessary and identify by block number)

This project contributed to improved understanding of the growth, physiology and control of magnetite production by the magnetic bacterium Aquaspirillum magnetotacticum. As a result of the research performed under this contract it has become possible to i) culture A. magnetotacticum to high biomass yields in microaerobic continuous culture, and to ii) precisely regulate through reproducible control of culture parameters, the formation of membrane proteins and bacterial magnetosomes in vivo. This is a vital prerequisite to studies of gene expression and magnetosome biogenesis in this organism.

20 DISTRIBUTION / AVAILABILITY OF ABSTRACT	21 ABSTRACT SECURITY CLASSIFICATION
☒ UNCLASSIFIED/UNLIMITED ☐ SAME AS RPT ☐ DTIC USERS	(u)
22a NAME OF RESPONSIBLE INDIVIDUAL: M. Marron	22b TELEPHONE (Include Area Code): 202/696-4760 — 22c OFFICE SYMBOL: ONR

DD Form 1473, JUN 86 — Previous editions are obsolete — SECURITY CLASSIFICATION OF THIS PAGE: (u)

S/N 0102-LF-014-6603

DISTRIBUTION STATEMENT A
Approved for public release;
Distribution Unlimited

89 013

19.

Three outer membrane proteins (72,000 - 85,000 daltons) were coordinately produced at the high culture iron concentrations appropriate for hydroxamate siderophore production. A 55,000 dalton iron-repressible outer membrane protein present in magnetic cells was absent from non-magnetic mutant cells and may function in bacterial magnetosomes synthesis. A cd$_1$ nitrite reductase was present only in the cell outer membrane. Iron reductase initially believed to be in the outer membrane was found to be present principally in the periplasm.

A novel method of obtaining cell periplasm was developed. Periplasm obtained by this and by conventional methods was found to be the major repository of components previously unknown to be associated with bacterial cell periplasm (a soluble CO-binding c-type hemoprotein, a FeSOD, and an iron reductase).

Bacterial magnetosomes were purified by a novel magnetic separation technique. The bacterial magnetosome envelope was found to consist of a lipid bilayer with admixed protein,. Two proteins present in the magnetosome membrane were absent from the non-magnetic cell fraction and from non-magnetic mutant cells. Knowledge of their primary sequence should lead to construction of valuable probes for nucleic acid sequences specifically associated with magnetite formation in these and other bacteria.

In contrast to iron uptake by enteric bacteria, cell iron uptake was found to involve a non-specific active transport mechanism at low iron concentration. A hydroxamate siderophore was produced only with the culture iron at 10 μM, or greater.

Distribution List for Annual and Final Reports

1. Put a cover page (Form DD 1473) on your report and attach a copy of the distribution list. Mail one copy of the report to each person on the contractor subset list attached on which your name appears. The other subset list is for your information only. Please don't forget to attach this distribution list to your report - otherwise the folks below think they have mistakenly received the copy meant for the Molecular Biology Program and forward it to us.

2. Mail two copies to (include a DTIC Form 50 with these two copies too)
   Administrator
   Defense Technical Information Center
   Building 5, Cameron Station
   Alexandria, VA 22314

3. Mail one copy to each of the following:

(a) Dr. Michael Marron
ONR Code 1141
Molecular Biology Program
800 N. Quincy Street
Arlington, VA 22217-5000

(b) Administrative Contracting Officer
ONR Resident Representative
(address varies - see copy of your grant)

(c) Director,
Applied Research Directorate
ONR Code 12
800 N. Quincy Street
Arlington, VA 22217-5000

(d) Director
Office of Naval Technology
Code 22
800 N. Quincy Street
Arlington, VA 22217-5000

(e) Director
Chemical and Biological Sci Div
Army Research Office
P. 0. Box 12211
Research Triangle Park, NC 27709

(f) Life Sciences Directorate
Air Force Office of Scientific Research
Bolling Air Force Base
Washington, DC 20332

(g) Director
Naval Research Laboratory
Technical Information Div, Code 2627
Washington, DC 20375

FINAL REPORT: CONTRACT N00014-85-K-0502

DATE: JUNE 6, 1989

CONTRACT TITLE: IRON-ASSOCIATED OUTER MEMBRANE PROTEINS OF MAGNETIC BACTERIA

PRINCIPAL INVESTIGATOR: Dr. Richard P. Blakemore
Department of Microbiology

CONTRACTOR: University of New Hampshire
Durham, N.H. 03824

PROJECT PERIOD: July 1, 1985 - Jan 1, 1989

BACKGROUND AND PROJECT GOALS

The overall effort supported by this contract has been targeted at the form and formation of ultrafine intracellular magnetic particles by bacteria. Specifically, investigation was made of the iron-associated cell and magnetosome envelope proteins and hemoproteins as they relate to cell iron uptake, to magnetite formation and to oxygen toxicity. Because at the outset of this project cells grew variably and produced magnetite in a somewhat unpredictable manner, a preliminary need was to achieve improved cell growth and reproducible physiological conditions for magnetite formation. This stimulated development of microaerobic, continuous cultures of *Aquaspirillum magnetotacticum* by means of which the effects of variation in culture parameters (O_2, iron concentration, N supply) on magnetosome biogenesis could be evaluated in a reproducible way.

APPROACH

Culture conditions including iron and oxygen supply have marked effects on the magnetic state of cells in laboratory cultures of the obligately microaerophilic, magnetic spirillum *A. magnetotacticum*. An effort was initiated to establish continuous cultures to (i) improve cell growth, (ii) reproducibly obtain cells of constant and predictable composition and physiological state, (iii) investigate effects of iron and oxygen on cell physiology, and (iv) elucidate the protein composition of periplasm, magnetosome membrane and outer membranes of cells in the magnetic and non-magnetic states.

A study was also made to determine whether *Aquaspirillum magnetotacticum* cells use for iron acquisition a high affinity (siderophore) system similar to those used by other gram-negative organisms.

A novel method of obtaining cell periplasm was developed. Periplasm was examined for protein and hemoprotein components expected to be important with respect to iron and oxygen in cell physiology and magnetosome biogenesis.

RESULTS

Improved culture methods: Cells of *A. magnetotacticum* in laboratory batch culture typically achieved low cell yields and were variably magnetic or non-magnetic. Using a completely iron-free chemostat vessel with dissolved oxygen and pH control, we developed continuous culture methods for this obligate microaerophile and systematically determined limiting nutrient concentrations and controlling culture parameters such as dissolved O_2 concentration and pH (Gorby, Y.A., Ph.D dissertation, University of New Hampshire, 1989). With $D = 0.075/h$ ($T_d = 9.2$ h), control of pH (6.8) and dissolved oxygen tension at 1% of saturation, culture biomass was increased 10-fold with more predictable and reproducible cell growth and Fe_3O_4 formation than were previously possible. Denitrifying magnetic cells (NO_3^- as the limiting nutrient) and non-denitrifying cells (NH_4^+ as the limiting nutrient) became non-magnetic as the O_2 was increased from 1 to 5%. Cultures shifted back to 1% O_2 again became magnetic. This reversible transition between magnetic and non-magnetic state, regulated by culture O_2, provided a reproducible

system for examining magnetosome biogenesis and other aspects of cell physiology involving cell membrane and periplasmic components.

Iron uptake: At low concentrations iron was transported into *A. magnetotacticum* very effectively by non-specific means (Paoletti, L.C., Ph.D. dissertation, Univ. New Hampshire, 1988; Paoletti and Blakemore, Conference on Iron Biominerals, Durham, N.H., July, 1989). The Km (35 μM) and Vmax (1.25 nmol/min/mg biomass) were high compared to those of enteric bacteria; as expected for this premier iron-accumulating bacterium. In contrast to that of at least some other bacteria, the cell iron concentration (the bulk of which resided in magnetosomes) varied directly with culture medium iron concentration. The rate and extent of ferric iron transport was more than 2-fold greater than that of ferrous iron. The temperature optimum for iron uptake was that for optimum cell growth (25-30° C) and iron uptake was inhibited by metabolic poisons either totally (mercuric chloride, 2,4-dinitrophenol) or partially (sodium arsenate). These latter findings are consistent with iron uptake by an active transport mechanism.

Hydroxamate siderophores at high but not low iron: Magnetic cells of *A. magnetotacticum* produced hydroxamate material when cultured with 20 or 40 μM but not with 5μM, or less, ferric quinate (2). Cells responded similarly with iron chelated with citric acid. Moreover, they produced hydroxamates with 20 μM iron as ferric citrate when the molar ratio of citrate to iron was 1:1 but not 20:1. Since the latter situation represents low available iron (due to formation of a highly polymerized ferric citrate complex), these results are consistent with those obtained with ferric quinate: magnetic cells of this species produce secondary hydroxamates only when cultured at iron-sufficient conditions. The hydroxamate material in spent culture supernatant fluids promoted growth of a siderophore-deficient *Salmonella* mutant in demonstration of its role as a siderophore (2). Cells of *A. magnetotacticum* appear capable of dissimilatory iron reduction (14). This siderophore could promote iron availability at membrane respiratory sites in the increased amounts required for "iron respiration". Perhaps only with the metal available in sufficient amount for use as an electron acceptor is the solubilizing chelator induced.

Iron and cell outer membrane proteins: Cells of *A. magnetotacticum* possessed several major OMPs (2). Three OMPs ranging from 72,000 to 85,000 daltons were coordinately produced at the high iron concentrations conducive to hydroxamate secretion but were absent from cells cultured with less than 10 μM iron. The 72,000-, 76,00-, and 85,000-dalton OMPs detected in cells cultured at 20 or 40 μM ferric quinate may serve a role(s) in iron metabolism comparable to those of OMPs of similar sizes and produced under similar conditions by the enteric bacteria. Their coordinate production under conditions in which cells also produce hydroxamate siderophores suggests that one or more of these may be involved in hydroxamate synthesis, its secretion, or function as a cognate membrane receptor. A 55,000 dalton iron-repressible OMP (IROMP) was present in magnetic cells cultured at low but not at high ferric concentrations. The 55,000 dalton IROMP may not function in iron transport via hydroxamates as it was repressed at iron concentrations necessary for hydroxamate production. Cells of non-magnetic mutant cells (NM-1A) produced hydroxamates independant of the available iron concentration but did not produce the 55,000 dalton IROMP. Inability to form Fe_3O_4 by this mutant strain may be associated with inability to form this IROMP. The novel 58,000 dalton IROMP produced by *A. magnetotacticum* cells cultured with citrate as the chelator is most likely a component of a citrate-mediated iron uptake system in need of further study (2).

Cell magnetosome membrane composition: Intact magnetosomes were purified form *A. magnetotacticum* by a magnetic separation technique. Electron microscopical and chemical analyses revealed the Fe_3O_4 to be enclosed by a lipid bilayer admixed with proteins (9). Free fatty acids were detected in this membrane, along with glycolipids and phospholipids (phosphatidylserine and phosphatidylethanolamine). Of the many proteins detected in the magnetosome membrane, two were not found in other cell membranes or soluble fractions (9). Continuing collaborative study of magnetosome cores (crystal lattice imaging by means of high resolution transmission electron microscopy) yielded information concerning novel bullet-shaped magnetosomes known only to be produced by bacteria (7 , 8).

Recovery and analysis of cell periplasm: We developed a rapid, simple, reproducible freeze-thawing (F/T) method of selectively releasing periplasmic substances from cells of *A. magnetotacticum* (in addition to

those of *A. itersonii*, and *Azospirillum lipoferum*) without recourse to chemical treatments (6). A comparative study of this new method was carried out. Electrophoretic banding patterns and difference spectra of proteins and hemoproteins released from cells by F/T were distinct from those of membrane-associated substances and similar to those of periplasmic substances obtained by conventional fractionation methods (osmotic shock, chloroform treatment, etc.). Periplasm so obtained was examined for components expected to be of importance in cell iron and oxygen physiology. Several substances were identified as novel periplasmic components (see below). These need to be assessed in other bacterial species to better understand their possible uniqeness to magnetic bacteria and possibly to magnetite formation.

Periplasmic substances associated with iron (and oxygen): While investigating the cytochromes within cells respiring with diverse oxidants (5), we determined that more than 85% of the total cytochromes detected in *A. magnetotacticum* were of the *c*-type. Whereas virtually all of the *a*- and *b*-types were detected in cell membranes, 70% of the *c*-type hemes were soluble. Large quantities (60% of total cell cytochromes) of soluble *c*-type hemes were released with periplasm by the F/T method. Soluble c_{551} occurred in two forms: as a single compound of apparent molecular weight 17,000 daltons, which bound CO, and together with d_1 heme, as a component of nitrite reductase (Gorby, Y.A., Ph.D. dissertation, Univ. New Hampshire, 1989). Antibodies raised against the soluble, periplasmic, CO-binding c_{551}-type hemoprotein were used in Western blotting of the separated cell inner membrane, outer membrane, magnetosome membrane and periplasmic proteins. These antibodies reacted with one periplasmic and one 17,000 dalton outer membrane protein (Paoletti, L.C., Ph.D. dissertation, University of New Hampshire, 1988). Because this abundant periplasmic *c*-type hemoprotein was found to bind CO (5), it was of interest to determine whether it might also bind oxygen and function in a manner similar to *Rhizobium* leghemoglobin or *Vitrioscilla* hemoglobin; that is, to bind O_2 and keep its concentration as free O_2 low. Subsequent collaborative research with Prof. Robert Poole (King's College, London) has indicated that this hemoprotein, despite binding CO, is not a cytochrome oxidase. That is, photodissociation of bound CO at -105° C was not observed. Investigations of its properties and cell role(s) are continuing.

Recently, *c*- and *d*-type hemes were detected in the outer (but not inner) membrane by means of low temperature red-ox spectra. Moreover, NO_2^- was reduced to N_2O by outer membranes but not by periplasm or inner membrane preparations of denitrifying cells. These results indicate that a nitrite reductase of the cd_1 multiheme type is located on the *A. magnetotacticum* cell outer membrane. This is unusual in that most nitrite reductases of this type are soluble. The spectral and kinetic data indicated that the presence of this enzyme in this cell fraction was not due to contamination from another during fractionation. Nitrite reductase in the outer membrane may serve to protect the cell from excessive (toxic) nitrite accumulation at vital internal cell locations.

Cells of *A. magnetotacticum* may reduce iron during growth, thereby producing extracellular vivianite and intracellular magnetite (14). They reductively dissolve insoluble ferric oxyhydroxide present in the culture medium. We explored the possibility that iron reductase might be located in the cell outer membrane and determined the iron reductase activity in cell fractions of wild-type and non-magnetic mutant cells of this organism (11). Reductase activity was predominantly located in the cell periplasm (65-77% of total activity detected). Cytoplasm contained 20-30% and membrane fractions 3% of total iron reductase activity detected. The iron reductase activity measured in cell soluble fractions was constitutively produced over the range 0-40 μM iron and reduced uncomplexed iron or iron complexed to any of a variety of natural chelators (quinate, DHB, acetohydroxamate, ferrioxamine B, citrate). Iron complexed with quinate allowed for most effective iron reductase activity (K_m, 18μM ;V_{max}, 22 nmol Fe^{2+} formed/min/mg protein) of any chelator tested. Cells of this organism translocate protons outward in response to addition of ferric ions and should therefore be capable of "iron respiration" by reducing this oxidant. The soluble iron reductase activity was unaffected by a selection of respiratory inhibitors (HQNO, antimycin A, rotenone) at 4 μM each, whereas membrane-associated activity was inhibited by 10% of control rates by these inhibitors. Sulfhydral-binding poisons ($HgCl_2$ at 1 μM) totally destroyed activity of the soluble enzyme and activity was completely and reversibly inhibited by O_2 (11). Because iron reductase activity is important in diverse cell functions (insertion of iron into hemes, iron release from ferrisiderophores, cell respiration) including Fe_3O_4 formation cell inability to grow or produce magnetite at high O_2 may relate to the O_2 sensitivity of this enzyme. A periplasmic location of

respiratory iron reductase would (i) obviate the potential membrane barrier presented to ferric iron were its terminal reduction sites intracellular and (ii) promote a favorable proton gradient by keeping the protons that accumulate during iron reduction outside the cell. Abundant periplasmic iron reductase activity could promote iron transport and prevent accumulation of surficial ferric oxyhydroxides in this motile spirillum. Moreover, this microaerophile could be expected to be favored by low O_2 if an O_2^- susceptible iron reductase necessary for growth or survival were located near the cell surface.

Because cells are iron-rich and respire microaerobically, univalent O_2 reduction could result in iron-catalyzed toxic $OH^\cdot$ formation from O_2^- via Haber-Weiss and Fenton reactions. We examined cell superoxide dismutase (SOD) activity and the location of this oxygen-protective enzyme in cell fractions (15). The majority (roughly 95%) of total cell SOD activity was located in the cell periplasm with little or no activity in the cell membranes or cytoplasm. Iron-type SOD (FeSOD) contributed 88% of the total activity detected, although a manganese-type SOD was also present in periplasm. Cells cultured at greater than 1% dissolved oxygen tension expressed increased activity of the manganese type SOD relative to FeSOD. Magnetic cells expressed approximately 20% of the total SOD activity detected within aerobically grown cells of *E. coli*. The obligately microaerophilic nature of *A. magnetotacticum* cells appeared to relate to their inability to express measurable levels of catalase and to their relatively low level (as compared to that of aerobes) of SOD (15). The novelty of finding a periplasmic SOD may be due to the fact that other investigators nearly always have examined "membrane" and "soluble" cell fractions without separating "periplasmic" from remaining "soluble" components. A periplasmic location of SOD could be important in magnetic bacteria which have high intracellular iron concentrations by maintaining a low superoxide anion concentration at respiratory membrane sites.

PROSPECTS

Culture methods we have developed should open new possibilities for investigating magnetosome biogenesis. In particular, the newly acquired ability to control magnetosome formation (the degree of cell magnetism) and cell growth offers reproduciblity not previously available. Of immediate interest would be a study of magnetosome membrane biogenesis and membrane protein synthesis in cells shifted from the non-magnetic state to conditions "permissive" for Fe_3O_4 formation (with and without chloramphenicol treatment).

It has not yet been determined whether the hydroxamate chelator produced at high but not low iron in batch cultured cells requires induction or de-repression by iron in the medium. Moreover, the material has not yet been purified or characterized. A single attempt to do so was unsuccessful and was frustrated by the limited quantity of material then available. The unusual regulation of the production of this material, coupled with the improved culture yields now obtainable, suggests that additional study would be worthwhile.

Iron-associated OMPs and magnetosome membrane proteins have not been sequenced or characterized. They can be expected to be of value in constructing membrane vesicles with the intent of obtaining magnetosome biogenesis *in vitro*. The research is also now poised to begin identifying some of the amino acid sequences of these proteins with the purpose of producing genetic probes for identifying genes associated with bacterial magnetite production.

The F/T method of obtaining periplasmic substances, including secreted proteins, from cells should have wide-spread application in recovery of genetically engineered products from recombinant strains of gram-negative bacteria. After our ASM poster and subsequent paper, a patent covering this technology issued to employees of a biotechnology company who independantly recognized its value. The presence in periplasm of major quantities of soluble CO-binding *c*-type hemoprotein , of FeSOD or of iron reductase is without precedent and is deserving of additional study to better understand their roles in cell physiology and possibly in magnetosome formation.

PUBLICATIONS SUPPORTED

1. Rosenblatt, C., R.B. Frankel, and R.P. Blakemore. 1985. A birefringence relaxation determination of rotational diffusion of magnetotactic bacteria. Biophys. J. 47:323-325.

2. Paoletti, L. C., and R.P. Blakemore. 1986. Hydroxamate production by *Aquaspirillum magnetotacticum*. J. Bacteriol. 167:73-76.

3. Blakemore, R.P. 1986. Biomagnetism and geomagnetic field detection by organisms. Encyclopedia Universalis pp.321-325.

4. Bazylinski, D.A., E. Palome, and R.P. Blakemore. 1986. Denitrification by *Chromobacterium violaceum*. Appl. Environ. Microbiol. 52: 696-699.

5. O'Brien, W., L.C. Paoletti and R.P. Blakemore. 1987. Spectral analysis of cytochromes in *Aquaspirillum magnetotacticum*. Curr. Microbiol. 15:121-127.

6. Paoletti, L.C., K.A. Short, N. Blakemore and R.P. Blakemore. 1987. Freeze-thawing of *Aquaspirillum magnetotacticum* cells selectively releases periplasmic proteins. Appl. Environ. Microbiol. 53:2590-2592.

7. Mann, S., N.H.C. Sparks and R.P. Blakemore. 1987. Ultrastructure and characterization of anisotropic magnetic inclusions in magnetotactic bacteria. Proc. R. Soc. Lond. B 231: 469-476.

8. Mann, S., N.H.C. Sparks and R.P. Blakemore. 1987. Structure, morphology and crystal growth of anisotropic magnetite crystals in magnetotactic bacteria. Proc. R. Soc. Lond. B 231: 477-487.

9. Gorby, Y.A., T.J. Beveridge and R.P. Blakemore. 1987. Characterization of the bacterial magnetosome membrane. J. Bacteriol. 170: 834-841.

10. Blakemore, R.P., N.A. Blakemore, and R.B. Frankel. 1988. Bacterial biomagnetism and geomagnetic field detection by organisms. *in*: A.A. Marino (ed.) Modern Bioelectricity. Marcel Dekker, Inc., New York.

11. Paoletti, L.C., and R.P. Blakemore. 1988. Iron reduction by *Aquaspirillum magnetotacticum*. Curr. Microbiol. 17:339-342.

12. Moskowitz, B.M., R.B. Frankel, P.J. Flanders, R.P. Blakemore and B.B Schwartz. 1988. Magnetic properties of magnetotactic bacteria. J. Magn. Mag. Mtrls. 73: 273-288

13. Blakemore, R.P., N.A. Blakemore, D.A. Bazylinski and T.T. Moench. 1989. Magnetotactic bacteria. *in* J.E. Staley, M.P. Bryant, N. Pfennig, and J.G. Holt (eds) Bergy's Manual of Systematic Bacteriology, Vol. 3. Williams and Wilkins, Baltimore.

14. Blakemore, R.P. and R. B. Frankel. 1989. Biomineralization by magnetogenic bacteria. Chapter 6 pp.85-98 *in* R.K. Poole and G. M. Gadd (eds) Metal-microbe Interactions. IRL Press, Inc. Oxford.

15. Short, K.A. and R.P. Blakemore. 1989. Periplasmic superoxide dismutases in *Aquaspirillum magnetotacticum*. Arch. Microbiol. (in press).

ABSTRACTS AND PRESENTATIONS SUPPORTED

1. Paoletti, L.C., and R.P. Blakemore. 1985. Hydroxamate production by a magnetic spirillum at high but not low iron. Paper presented at 2nd Annu. NEMPET (New England regional morphology, physiology, ecology and taxonomy) Mtg., Ithaca, NY

2. Paoletti, L.C., K.A.Short and R.P. Blakemore. 1986. Freezing and thawing of *Aquaspirillum magnetotacticum* releases periplasmic proteins. Abstr. 86th Annu. Mtg. Am. Soc. Microbiol., Washington, D.C. I 6

3. Short, K.A., and R.P. Blakemore. 1986. Iron respiration-driven proton translocation in aerobic bacteria. Abstr. 86th Annu. Mtg. Am. Soc. Microbiol., Washington, D.C. **K 100.**

4. Paoletti, L.C. and R.P. Blakemore. 1986. Antigenic relatedness of a periplasmic c-type cytochrome and an outer membrane protein in *Aquaspirillum magnetotacticum*. 3rd Annu. NEMPET Mtg., Woods Hole, MA.

5. Gorby, Y.A., T. Beveridge and R.P. Blakemore. 1986. Ultrastructure and composition of the magnetosome sheath. 3rd Annu. NEMPET Mtg., Woods Hole, MA.

6. Short, K.A. and R.P. Blakemore 1987. Nitrite and microaerophily in *Aquaspirillum magnetotacticum*. 87th Annu. Meeting Am. Soc. Microbiol. Atlanta, GA. **I 123.**

7. Paoletti, L.C., Y.A. Gorby and R.P. Blakemore. 1987. Effects of iron on growth of *Aquaspirillum magnetotacticum* in continuous culture. 4th Annu. NEMPET mtg. Amherst, MA.

8. Paoletti, L.C. and R.P. Blakemore. 1987. Iron binding and reduction by *Aquaspirillum magnetotacticum*. 22nd Annu. Joint Mtg. NE-Conn. Valley and Eastern NY Branches of ASM. Sturbridge, MA, Oct 1987

9. Gorby, Y.A. and R.P. Blakemore. 1987. Proteins associated with the bacterial magnetosome membrane. 22nd Annu. Joint Mtg. ASM (regional) Sturbridge, MA

10. Blakemore, R.P. 1987. Form and formation of bacterial magnetite. 22nd Annu. Joint Mtg. ASM (Regional) Sturbridge, MA

11. Blakemore, R.P. 1988. Magnetite biomineralization by aquatic bacteria: roles of iron and oxygen. 111th Mtg of the Soc. for General Microbiology (U.K.) Warwick, April 1988.

12. Gorby, Y.A., L.C. Paoletti and R.P. Blakemore. 1988. Iron relieves nitrate limitation in continuous cultures of *Aquaspirillum magnetotacticum*. Abstr. 88th Annu. Mtg. Am. Soc. Microbiol., Miami, **I 58.**

13. Blakemore, R.P. 1988. Bacterial Magnets. Divisional Lecture, ASM. Miami

14. Gorby, Y.A., and R.P. Blakemore. 1988. Selective occurrence of a d-type hemoprotein in the *Aquaspirillum magnetotacticum* outer membrane. 5th Annu. NEMPET Mtgs. (regional) Amherst, MA. June 1988.

15. Paoletti, L.C., and R.P. Blakemore. 1989. Iron transport in *Aquaspirillum magnetotacticum*. 1st Iron biominerals conference, Durham, N.H.

AWARDS AND HONORS

1. Canadian Society for Microbiologists Traveling Lectureship - 1985

2. American Society for Microbiology Divisional Lecture - 1988

PERSONNEL SUPPORTED

This contract contributed partial support for the training of four Ph. D. graduate students:

Lawrence C. Paoletti - male , caucasion
Kevin A. Short - male, caucasion
Yuri A. Gorby - male, caucasion
John A. Coyle - male, caucasion

Partial suypport for a laboratory technician was also provided by the contract.

APPENDICES

1. Published papers supported by the contract.

2. Report distribution list.

A BIREFRINGENCE RELAXATION DETERMINATION OF ROTATIONAL DIFFUSION OF MAGNETOTACTIC BACTERIA

CHARLES ROSENBLATT,* RICHARD B. FRANKEL,* AND RICHARD P. BLAKEMORE‡
Francis Bitter National Magnet Laboratory, Massachusetts Institute of Technology, Cambridge, Massachusetts 02139; and ‡Department of Microbiology, University of New Hampshire, Durham, New Hampshire 03824

ABSTRACT The orientational relaxation of the magnetotactic bacterium *Aquaspirillum magnetotacticum* is observed by the decay of the optical birefringence upon switching off an aligning magnetic field. The data yield a rotational diffusion constant $D_r \simeq 0.13\ s^{-1}$ and information about cell sizes that is consistent with optical microscopy data.

The magnetotactic bacterium *Aquaspirillum magnetotacticum* (*A. magnetotacticum*) contains a chain of single magnetic-domain magnetite particles that imparts a magnetic dipole moment μ to the cell parallel to the axis of motility; the cell thus orients and swims along the earth's magnetic-field lines (1–3). The directionally averaged velocity $\langle \mathbf{V} \rangle$ is determined from the classical Boltzmann orientational distribution, and is given by $\langle \mathbf{V} \rangle = V_0 \cdot \langle \cos\theta \rangle$, where

$$\langle \cos\theta \rangle = [\coth(\mu H/k_B T) - k_B T/\mu H]. \quad (1)$$

Here k_B is Boltzmann's constant, T is temperature, and θ is the angle between the instantaneous trajectory and $\mathbf{H}$. If the swimming direction is somehow disturbed, a bacterium will feel a magnetic torque and right itself. Opposing the reorientation will be a viscous drag such that

$$\frac{k_B T}{D_r}\frac{d\theta}{dt} + \mu H \sin\theta = 0, \quad (2)$$

where D_r is the rotational diffusion constant. If the initial perturbed angle θ_i is small, the reorientation will take place on a characteristic time scale

$$\tau = \frac{k_B T}{\mu H D_r}. \quad (3)$$

Note that Brownian motion, which is responsible for $\langle \cos\theta \rangle \neq 1$ in Eq. 1, contributes an additional term to Eq. 2.

In this article we report on measurements of rotational diffusion using the method of birefringence relaxation. Because of its permanent magnetic dipole moment, *A. magnetotacticum* can be oriented within a very small solid angle about a given direction defined by an external magnetic field $\mathbf{H}_{ex}$. Moreover, oriented bacteria give rise to an optical birefringence Δn (4). When $\mathbf{H}_{ex}$ is set equal to zero, the orientations of the cells randomize, resulting in a decay of the optical birefringence Δn. Since $\Delta n \propto \langle P_2(\cos\theta) \rangle = \langle 3/2 \cos^2\theta - 1/2 \rangle$, where $\langle\ \rangle$ represents an ensemble average, measurements of Δn vs. time yield information about orientational diffusion.

Although the bacteria are actually helical in shape with a relatively small length to pitch ratio, certain approximations are used to fit the data. The simplest approximation is to assume that the bacteria are cylindrical with all principal axes of the optical anisotropy and rotational diffusion tensors coinciding. In this case both tensors are uniaxial (5) and the birefringence relaxation is determined by a single-exponential term (5, 6)

$$\Delta n = \Delta n_0 \exp(-6 D_r t), \quad (4)$$

where Δn_0 is a function of H_{ex} before the external field is turned off and D_r is the rotational diffusion constant about an axis perpendicular to the cylindrical axis. The diffusion constant D_r can be written as (7)

$$D_r = \frac{3 k_B T}{\pi \eta L^3}\left(\ln\frac{L}{d} - \gamma\right), \quad (5)$$

where η is the viscosity of the medium, L the length of the cylinder, and d the width. End effects are treated by the parameter γ, which depends upon the aspect ratio L/d and for which there is, unfortunately, no theoretical consensus (7). For sufficiently large L/d, the γ term becomes inconsequential; nevertheless, for *A. magnetotacticum* the ratio L/d is of order 5 to 10, and thus γ is not insignificant. For purposes of data analysis, we have chosen to use the form of Tirado and de la Torre (8)

$$\gamma = 0.662 - 0.92\,(d/L). \quad (6)$$

This form produces reasonable results for small aspect

ratios. Other forms for γ (7) produce only slightly different final results.

Cells of *A. magnetotacticum* were grown in culture and then killed and fixed with a small amount of gluteraldehyde. Cell concentration was $\sim 2 \times 10^8$ ml^{-1}. By measuring the static birefringence (4) vs. H_{ex}, $\langle \mu \rangle$ was found to be 2.6×10^{-13} emu with a distribution width of $\pm 1.7 \times 10^{-13}$ emu. Thus, even in a field as small as 1 G we find from Eq. 1 that $\langle \cos\theta \rangle > 0.8$. The sample was then placed in a glass cuvette of pathlength 1 cm, which in turn was placed between a pair of Helmholtz coils housed in a mu-metal can. The ambient field inside the can was <0.01 G. The entire assembly was then inserted into an optical birefringence apparatus, described in detail elsewhere (4). The field was brought to a steady-state value H_{ex} and then switched off; the transient birefringence was recorded with a Biomation model 1015 waveform recorder (Biomation Inc., Palo Alto, CA) and then output into an *xy* plotter.

A typical trace is shown in Fig. 1, where the initial field H_{ex} was 8 G. To within the expected scale factor, data taken at fields 0.24 G $\leq H_{ex} \leq$ 40 G produced virtually identical traces, as expected from Eq. 4. In Fig. 2 we have digitized the data and plotted the results on a semilog scale. Owing to the nonlinearity of this curve, it is clear that there is a distribution in D_r arising from a polydispersity of cell lengths L. Although there is no a priori form expected for the length distribution, a Gaussian was chosen for convenience

$$f(L) = \frac{1}{\Delta L \sqrt{\pi}} e^{-(L - L_0)^2/\Delta L^2}. \quad (7)$$

L_0 is the average length and ΔL the width of the distribution. Thus, combining Eqs. 4 and 7, we find the transient birefringence behaves as

$$\Delta n \propto \int dL \left(\frac{L}{d} - 1\right) e^{-6D_r t} f(L), \quad (8)$$

where D_r is given by Eqs. 5 and 6 and d is fixed at the experimental value of 0.56 μm (9). The term $(L/d) - 1$ is an approximate form that mimics the shape birefringence of a bacterium with an aspect ratio L/d.

The three parameters L_0, ΔL, and the coefficient in Eq. 8 were fit to several sets of data taken at various initial fields H_{ex}. All traces produced similar results with $L_0 = 3.4 \pm 0.5$ μm and $\Delta L = 2.1 \pm 0.6$ μm. Thus, for $L = L_0$, $D_r = 0.13\ s^{-1}$. Note that the correction term γ in Eq. 5 is of order one-third the value of ln L/d owing to the small aspect ratio.

The diffusion results for L_0 and ΔL were then compared

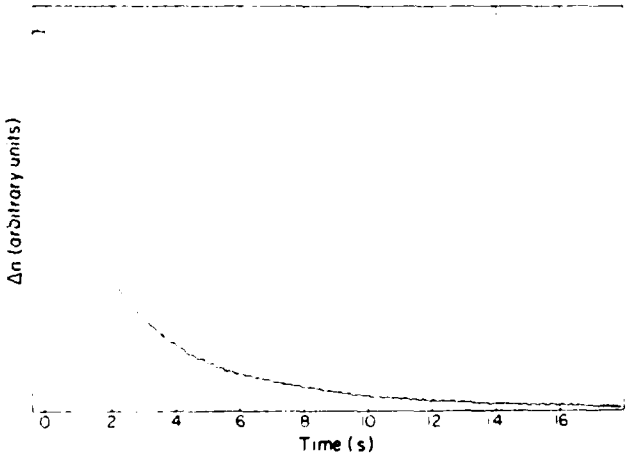

FIGURE 1 The typical decay of birefringence for initial aligning field $H_{ex} = 8$ G is shown.

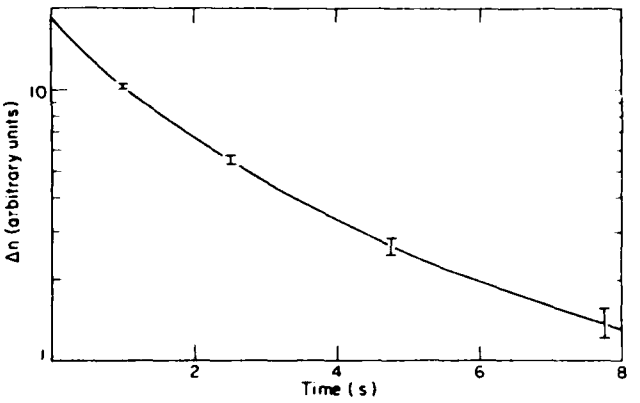

FIGURE 2 Fig. 1 is redrawn on a semilog plot. Note the nonlinearity, which indicates a distribution of effective diffusion constants. Error bars arise from uncertainty in locating base line.

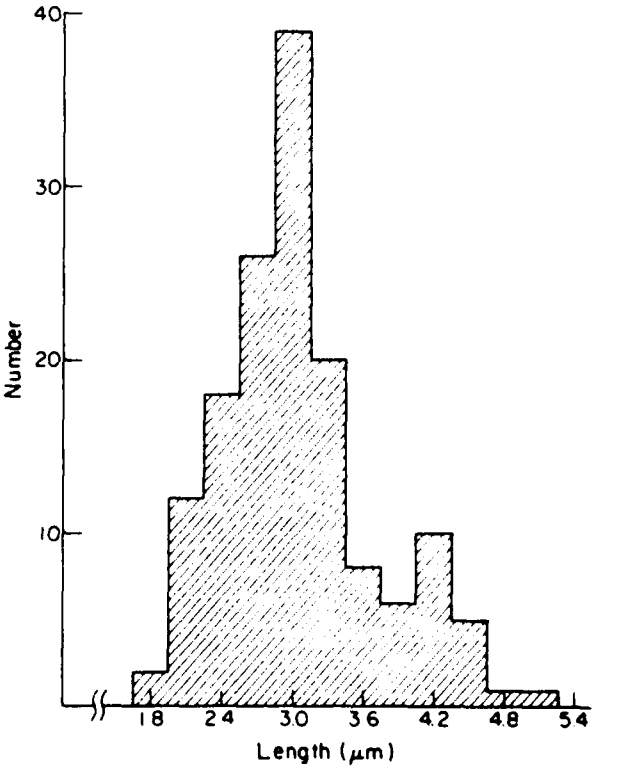

FIGURE 3 End-to-end length distribution of a sample of 148 cells is shown

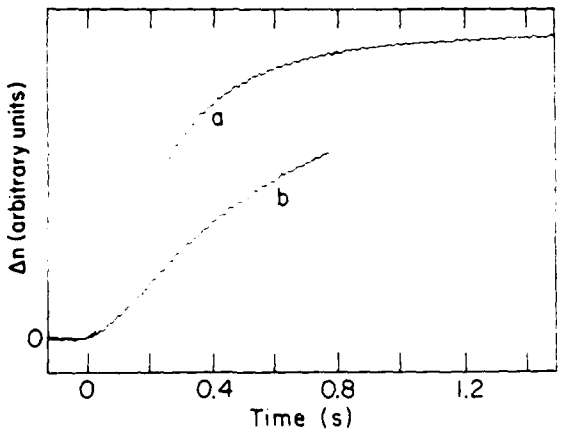

FIGURE 4 Δn vs. time upon switching on a field H_0 is shown: (*a*) 12.7 G; (*b*) 4.8 G.

with direct measurements of cell length. Photographs of 148 cells sandwiched between a pair of microscope slides spaced 1 μm apart were taken using a phase contrast microscope and measured for their end-to-end lengths. The distribution is shown in Fig. 3. From these measurements an average length $L_0 = (3.0 \pm 0.3)$ μm was determined, with a distribution width of $\sim 2\Delta L = 1.8$ μm. Although the measured length compares favorably with that obtained from the rotational diffusion measurements, the actual distribution width is somewhat narrower. To a great extent these differences have arisen from the choice of a cylindrical model for the bacteria (10). In fact, the cells are helical in shape, and thus for a sufficiently short length-to-pitch ratio the uniaxial approximation breaks down. The model also disregards coupling between rotational and translational diffusion, which at best is only a fair approximation given the shape of the bacteria. Finally, the results depend (albeit only weakly) upon the form chosen for γ. Unfortunately, there is no theoretical treatment of D_t for particles having the shape of these bacteria, and thus we chose to rely upon the cylindrical model.

The final question to be addressed is how D_r relates to the reorientation time τ. In Fig. 4 we show Δn vs. t when H_{ex} is switched from zero to some field H_0 ($H_0 = 12.7$ [*a*] and $H_0 = 4.8$ [*b*]) at $t = 0$. From Eq. 2 we find for a strong (saturating) field that

$$\theta(t) = 2\left[\tan^{-1}\left(e^{t/\tau}\tan\frac{\theta_i}{2}\right)\right]. \qquad (9)$$

Since θ_i is randomly distributed for $t < 0$, Δn vs. t can be calculated using Eq. 9

$$\Delta n(t) = 1/2\int_0^{\pi}\Delta n_0\left[\frac{3}{2}\cos^2\theta(t) - \frac{1}{2}\right]\sin\theta_i d\theta_i. \qquad (10)$$

Owing to the dependence of τ on μ, Eq. 10 implicitly assumes a knowledge of the distribution in μ as well as the distribution in L. Because of this additional uncertainty, we have not performed a full analysis of the data in Fig. 4. If, however, we make the simplifying assumptions that both the μ and L distributions are narrow and the system can be described by a single value for D_r, Fig. 4 can be fit to Eqs. 9 and 10. For trace *a*, for example, we find $\tau = 0.11 \pm 0.04$ s. Working backwards and assuming $\mu = 2.6 \times 10^{-13}$ emu, we find from Eq. 3 that $D_r \simeq 0.11$ s^{-1}, which compares favorably with the decay results.

In New England, where *A. magnetotacticum* was originally isolated, the geomagnetic field $H_G = 0.5$ G. Since the characteristic reorientation time for H_G is $\tau = 2.5$ s (see Eq. 3) and *A. magnetotacticum* swims at ~ 40 μm/s, an orientationally perturbed cell will travel a short characteristic distance $\lambda = 90$ μm before its velocity is brought into alignment with H_G. On the other hand, if a somewhat larger organism ($L_0 \sim 20$ μm) possessing the same moment μ and swimming speed V_0 were subjected to a disturbance, the characteristic reorientation length λ would be nearly 3 cm, apparently compromising the utility of magnetotaxis. It is perhaps for these dynamic reasons that larger microorganisms such as the one described by Esquivel et al. (11) have been found to possess significantly larger magnetic moments.

C. Rosenblatt and R. B. Frankel were supported in part by Office of Naval Research Contract N00014-80-C-0256 and R. P. Blakemore was supported in part by National Science Foundation Grant PCM-8215900. The Francis Bitter National Magnet Laboratory is supported by the National Science Foundation through its Division of Materials Research under Contract DMR-8211416.

Received for publication 10 July 1984

REFERENCES

1. Blakemore, R. P. 1975. Magnetotactic bacteria. *Science (Wash. DC)* 190:377–379.
2. Frankel, R. B., R. P. Blakemore, and R. S. Wolfe. 1979. Magnetite in freshwater magnetotactic bacteria. *Science (Wash. DC)* 203:1355–1356.
3. Frankel, R. B. 1984. Magnetic guidance of organisms. *Annu. Rev. Biophys. Bioeng.* 13:85–103.
4. Rosenblatt, C., F. F. Torres de Araujo, and R. B. Frankel. 1982. Birefringence determination of magnetic moments of magnetotactic bacteria. *Biophys. J.* 40:83–85.
5. Wegener, W. A., R. M. Dowben, and V. J. Koester. 1979. Time-dependent birefringence, linear dichroism, and optical rotation resulting from rigid-body rotational diffusion. *J. Chem. Phys.* 70:622–623.
6. Ridgeway, D. 1966. Transient electric birefringence of suspensions of asymmetric ellipsoids. *J. Am. Chem. Soc.* 1966:1104–1112.
7. Elias, J. G., and D. Eden. 1981. Transient electric birefringence study of length and stiffness of short DNA restriction fragments. *Biopolymers.* 20:2369–2380.
8. Tirado, M. M., and J. G. de la Torre. 1980. Rotation dynamics of rigid, symmetric top macromolecules. Application to circular cylinders. *J. Chem. Phys.* 73:1986–1993.
9. Balkwill, D. L., D. Maratea, and R. P. Blakemore. 1980. Ultrastructure of magnetotactic spirillum. *J. Bacteriol.* 141:1399–1408.
10. de la Torre, J. G., and V. A. Bloomfield. 1981. Hydrodynamic properties of complex, rigid, biological macromolecules. Theory and applications. *Q. Rev. Biophys.* 14:81–139.
11. Esquivel, D. M. S., H. C. P. Lins de Barros, M. Farina, P. H. A. Aragao, and J. Danon. 1983. Microorganisms magnetotactiques de la region de Rio de Janeiro. *Biol. Cell.* 47:227–234.

JOURNAL OF BACTERIOLOGY, July 1986, p. 73–76
0021-9193/86/070073-04$02.00/0

Vol. 167, No. 1

Hydroxamate Production by *Aquaspirillum magnetotacticum*

LAWRENCE C. PAOLETTI AND RICHARD P. BLAKEMORE*

Department of Microbiology, University of New Hampshire, Durham, New Hampshire 03824

Received 4 February 1986/Accepted 11 April 1986

Spent culture fluids from *Aquaspirillum magnetotacticum* MS-1 grown at high (20 μM) but not low (5 μM) iron concentration contained material yielding a positive hydroxamate test. Cells possessed six major outer membrane proteins. Three outer membrane proteins ranging from 72,000 to 85,000 daltons were coordinately produced at iron concentrations conducive to hydroxamate production. A 55,000-dalton iron-repressible outer membrane protein was also present in strain MS-1 cultured at low but not high ferric quinate concentration. Culture fluids from strain MS-1 which were hydroxamate positive augmented growth of a *Salmonella typhimurium* siderophore-deficient (*enb-7*) mutant in low-iron medium, suggesting a role of hydroxamate in uptake of iron by the cell.

Numerous bacterial proteins, including cytochromes, catalases, peroxidases, superoxide dismutases, ribotide reductases, and nitrogenases, contain iron (15). Because of its insolubility at neutral pH under aerobic conditions, iron is usually unavailable for direct uptake by cells (16). Under conditions of low iron concentration (less than 1 μM), many microorganisms produce iron chelators, termed siderophores (16). These are assimilated into gram-negative cells by means of specific receptor proteins located in the outer membrane (16, 18, 20).

Siderophores have been detected in spent culture fluids from aerobes and facultative anaerobes but are apparently not produced by strict anaerobes or the lactic acid bacteria (15, 16). No information exists concerning siderophore production by obligate microaerophiles.

Aquaspirillum magnetotacticum (13) is a gram-negative, obligately microaerophilic chemoheterotroph, 2.0% of which (dry weight) is iron. Although proteins and hemoproteins of this organism contain iron, most of this metal is compartmentalized within its magnetosomes, which are intracellular enveloped crystals of the iron oxide magnetite (2). Virtually nothing is known of the manner in which cells of this organism sequester iron. However, in both its natural habitat and its culture medium the total iron concentration is 20 μM. In nature, the iron may be complexed with humic substances or plant-derived organic acids. In the culture medium that we used, iron was chelated with quinic acid.

This study was initiated to determine whether *A. magnetotacticum* uses a high-affinity (siderophore) system similar to those used by other gram-negative organisms for iron acquisition.

MATERIALS AND METHODS

Bacterial strains and growth conditions. Cells of *A. magnetotacticum* MS-1 (ATCC 31632) and of a nonmagnetic mutant *A. magnetotacticum* strain, NM-1A, were cultured microaerobically in chemically defined growth medium (MSGM) as previously described (3). The iron source, ferric quinate, was provided at concentrations of 0, 5, 10, 20, or 40 μM. $FeSO_4$ was omitted from the culture medium mineral solution, and for studies involving spectrophotometric analysis of supernatant fluids, resazurin was omitted. A ferric chloride-sodium citrate mixture with a citrate-to-iron molar ratio of 1:1 or 20:1 (an iron concentration of 20 μM) was used in lieu of ferric quinate. Without added iron, MSGM contained 0.35 μM iron, as determined by the ferrozine method (19). No attempts were made to completely remove iron from the culture medium.

Salmonella typhimurium LT-2 *enb-7*, an enterobactin-deficient mutant (a gift from J. B. Neilands, Department of Biochemistry, University of California at Berkeley), and *S. typhimurium* ATCC 14028 were maintained on nutrient agar slants and subcultured twice each month. To promote siderophore production, *S. typhimurium* ATCC 14028 was cultured for 48 h at 37°C on a rotary shaker in 0.25% (wt/vol) Casamino Acids (Difco Laboratories, Detroit, Mich.) solution containing 0.2 mM $MgCl_2$ and adjusted to pH 7.5 (18).

Isolation of outer membrane proteins. *A. magnetotacticum* MS-1 and NM-1A were grown to early stationary phase in 1-liter batch cultures. Cells were harvested by centrifugation (7,000 × *g* for 15 min at 4°C) and suspended in 10 ml of 50 mM potassium phosphate buffer (pH 6.8). Outer membrane proteins (OMPs) were isolated by the procedure of Schnaitman (17). Briefly, DNase and RNase (Sigma Chemical Co., St. Louis, Mo.) were each added to cell suspensions at a final concentration of 0.1 mg/ml. Cells were ruptured by two passes through a precooled French pressure cell (16,000 lb/in^2). Unbroken cells and cellular debris were removed by centrifugation at 7,000 × *g* for 15 min at 4°C. The resulting supernatant fluid was ultracentrifuged at 200,000 × *g* for 60 min at 4°C. The brown pellet, containing both inner and outer cell membranes, was suspended in 10 ml of 10 mM *N*-2-hydroxyethylpiperazine-*N'*-2-ethane-sulfonic acid (HEPES, pH 7.4) containing 2% (vol/vol) Triton X-100 and 10 mM $MgCl_2$. The unsolubilized outer membrane fraction was collected by ultracentrifugation (200,000 × *g* for 60 min at 4°C) and washed once in 10 mM HEPES (pH 7.4) to removed residual Triton X-100. The solubilized cytoplasmic membrane proteins were precipitated with cold 95% ethanol overnight at −12°C and collected by centrifugation (7,000 × *g* for 30 min at 4°C). Protein determinations were made by the procedure of Lowry et al. (11) with bovine serum albumin as a standard. The activity of succinic dehydrogenase, a cytoplasmic membrane enzyme, was assayed in each cell fraction (5) to assess the purity of the outer membrane fraction.

Electrophoresis and analysis of OMPs. OMPs and molecular weight standards (Bio-Rad Laboratories, Richmond, Calif.) were solubilized and separated by the electrophoretic

* Corresponding author

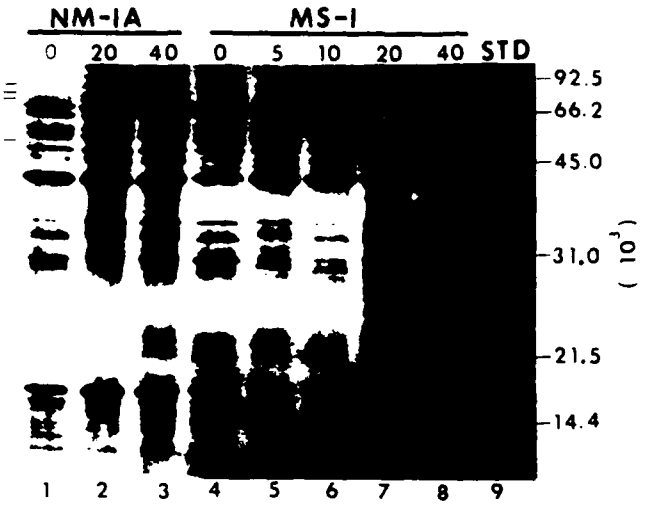

FIG. 1. Sodium dodecyl sulfate-polyacrylamide gel electrophoresis of OMP profiles from *A. magnetotacticum* NM-1A and MS-1 cultured at various iron concentrations (indicated above each lane, micromolar). Each lane contained 30 μg of purified (17) OMP. Dashes to the left of the gel indicate the positions (reading upward) of the 55,000-, 72,000-, 76,000-, and 85,000-dalton proteins. Lane 9, on the right, contained the molecular mass standards (in kilodaltons) indicated.

methods of Laemmli (9). OMPs were stacked in a 4% acrylamide gel at a constant current of 10 mA. The current was increased to 20 mA as OMPs entered a 12% acrylamide separating gel. OMPs were stained with Coomassie brillant blue and quantitated with a Helena Quick Scan R&D densitometer (Helena Laboratories, Beaumont, Tex.) at A_{500}.

Detection of iron chelators. Spirilla were grown in 500-ml batch cultures containing iron in the form of ferric quinate at 5, 20, and 40 μM or in the form of ferric citrate with a molar ratio of citrate to iron of either 20:1 or 1:1 (20 μM Fe). Spent culture fluids were freed from cells by centrifugation (7,000 × *g* for 15 min) and vacuum filtered through 0.45-μm Metricel GA-6 filters (Gelman Sciences, Inc., Ann Arbor, Mich.). The fluids were concentrated to 1/45 their original volume by flash evaporation at 35°C. Each sample was then carefully adjusted to pH 7.0 with 1 N HCl or NaOH, filter sterilized, and stored at 4°C until assayed. Uninoculated culture media at each iron concentration and spent culture fluids (concentrated 1/10 their original volume) from *S. typhimurium* ATCC 14028 cultures were prepared in an identical manner to those of controls.

The Arnow test (1) was used for the detection of phenolate-type iron chelators. The positive controls were 400 μM catechol (Sigma) and 1.5 mM 2,3-dihydroxybenzoic acid (Aldrich Chemical Co., Inc., Milwaukee, Wis.); the negative controls were 1.5 mM solutions of acetohydroxamic acid (Aldrich) and deferoxamine (a generous gift from CIBA-GEIGY Corp., Summit, N.J.). A modification of the Csaky reaction was used to detect secondary hydroxamic acids (7). The negative controls were catechol and 2,3-dihydroxybenzoic acid; the positive controls were acetohydroxamic acid and deferoxamine.

Siderophore activity. The effect of spirillum spent culture fluids on growth of the enterobactin-deficient *S. typhimurium* LT-2 *enb-7* mutant was examined. To each sidearm flask containing 100 ml of Davis minimal medium (4) with no added iron was added 1.0 ml of an overnight culture of the *S. typhimurium* LT-2 *enb-7* mutant grown in Davis minimal medium without iron or citrate. To each inoculated test flask was added 1 ml of either pre- or postgrowth fluids (prepared as described above) from strain MS-1 cultured in MSGM containing 5 or 20 μM ferric quinate. To each control flask was added 1.0 ml of either *S. typhimurium* ATCC 14028 spent culture supernatant fluid or uninoculated Davis minimal medium (prepared as described above). Growth of the *S. typhimurium* LT-2 *enb-7* mutant at 37°C (in a shaking water bath) was monitored at an optical density at 660 nm.

RESULTS

OMPs and iron. Six major OMPs, with masses ranging from 16,400 to 64,500 daltons, were produced by strains MS-1 and NM-1A (Fig. 1). The OMP preparation appeared to be relatively free of cytoplasmic membrane proteins in that it contained only 7.0% of the total succinic dehydrogenase activity of the various cell fractions.

When cultured with low (0 or 5 μM), not high (10, 20, or 40 μM), concentrations of added ferric quinate, strain MS-1 produced a 55,000-dalton OMP (Fig. 1, lanes 4 to 8). This 55,000-dalton iron-repressible OMP (IROMP) comprised 13.0 and 4.0% of the total major OMP of cells cultured with 0 and 5 μM concentrations of added ferric quinate, respectively. This IROMP also comprised 1.0% of the total OMP of strain NM-1A cells grown with no added ferric quinate (Fig. 1, lane 1). Three minor OMPs (72,000, 76,000, and 85,000 daltons) not present at low iron concentrations were produced by cells of each strain cultured with 20 or 40 μM ferric quinate (Fig. 1, lanes 2, 3, 7, and 8).

Strain MS-1 cells cultured in medium containing 400 μM sodium citrate and 20 μM ferric chloride produced, in addition to the 55,000-dalton IROMP, another IROMP, this one of 58,000 daltons (Fig. 2, lane 1). Cells cultured with 20 μM sodium citrate and 20 μM ferric chloride produced neither the 58,000- nor the 55,000-dalton IROMP (Fig. 2, lane 4). Cells grown with either 5 μM ferric quinate or 20 μM ferric citrate with a citrate-to-iron molar ratio of 20:1 (i.e., conditions of low iron availability) produced the 55,000-dalton IROMP (Fig. 2, lanes 1 and 2). This protein was absent from cells cultured with ferric quinate concentrations greater than or equal to 10 μM (Fig. 1, lanes 6 to 8) or with ferric citrate concentrations of 20 μM with a citrate-to-iron molar ratio of 1:1 (Fig. 2, lanes 3 and 4).

Siderophores. Catechol-type iron chelators were not de-

FIG. 2. Sodium dodecyl sulfate-polyacrylamide gel electrophoresis of OMP profiles from *A. magnetotacticum* MS-1 cultured with citrate-to-iron molar ratios of 20:1 or 1:1 (lanes 1 and 4, respectively) or with 5 or 20 μM ferric quinate (lanes 2 and 4, respectively). Each lane contained 30 μg of purified (17) OMP. The positions of the iron citrate-induced IROMP (58,000 daltons), the 55,000-dalton IROMP, and the major OMP (44,600 daltons) are indicated.

tected in spent culture fluids from strains MS-1 or NM-1A (by means of the Arnow reaction). Hydroxamate-type iron chelators were produced by cells of each strain (Table 1), as evidenced by positive hydroxamate tests. Hydroxamates were detected in culture media of cells grown at a 20 or 40 μM ferric quinate concentration. Surprisingly, spent medium from strain MS-1 cultured with less (5 μM) ferric quinate consistently failed to yield a positive hydroxamate reaction (Table 1). Culture fluids from cells of strain NM-1A grown at either a 5 or 20 μM ferric quinate concentration were consistently positive, however (Table 1).

Culture fluids obtained from strain MS-1 cultured with 20 μM ferric citrate at a citrate-to-iron molar ratio of 1:1 were positive in the hydroxamate test, whereas those obtained from cells grown at a 20:1 molar ratio were not (Table 1).

Siderophore activity. The enterobactin-deficient *S. typhimurium* LT-2 *enb-7* mutant did not grow in low-iron-concentration medium in the absence of exogenously supplied chelators (Fig. 3). Phenolate or hydroxamate (12, 15) siderophores have been shown to allow for the growth of this mutant in low-iron-concentration medium. Culture fluids from *S. typhimurium* ATCC 14028 (wild type) markedly stimulated the growth of the *S. typhimurium* LT-2 *enb-7* mutant, whereas uninoculated sterile Davis minimal medium (negative control) treated similarly had little effect (Fig. 3). Neither growth obtained with spent culture fluids from spirilla cultured with 5 μM ferric quinate nor growth obtained with uninoculated spirillum culture medium containing 20 μM ferric quinate exceeded that obtained with uninoculated, unsupplemented Davis minimal medium (Fig. 3). At 10 h, the *enb-7* mutant supplied with spent culture supernatant fluid from spirillum strain MS-1 cells cultured with 20 μM ferric quinate showed a 50% higher culture A_{660} than when supplied with unsupplemented Davis minimal medium (negative control) or with uninoculated medium containing 20 μM ferric quinate (Fig. 3).

DISCUSSION

Our results indicate that magnetic cells of *A. magnetotacticum* produced hydroxamate material when cultured with 20 or 40 μM added ferric quinate but not when grown with 5 μM ferric quinate. The nonmagnetic mutant, strain

TABLE 1. Hydroxamate and IROMP production by *A. magnetotacticum*

Strain and supplement (μM)	Hydroxamate production (μM)[a]	Production of 55,000-dalton IROMP[b]
MS-1		
Ferric quinate		
5	<5	−
20	49	−
40	53	−
Citrate iron		
20 (1:1)	36	−
20 (20:1)	<5	−
NM-1A		
Ferric quinate		
5	47	−[c]
20	77	−

[a] Values are deferoxamine equivalents.
[b] +, Production; −, no production.
[c] Values in parentheses indicate the ratio of citrate to iron.
[c] Inferred result based upon absence of the IROMP from electrophoretic protein profiles of strain NM-1A cells cultured with 0, 20, and 40 μM concentrations of added ferric quinate.

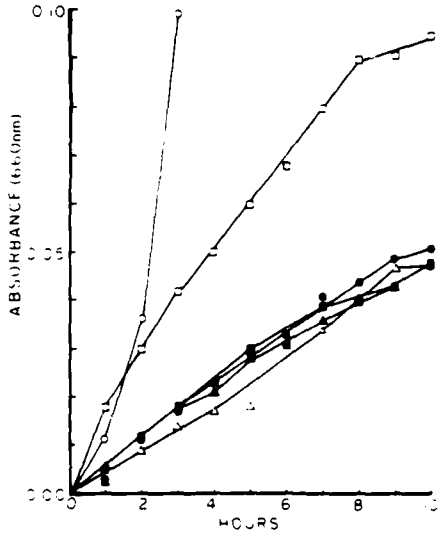

FIG. 3. Growth response of *S. typhimurium* LT-2 *enb-7* mutant cultured in Davis minimal medium supplemented with uninoculated culture medium containing 20 μM ferric quinate (■) or 5 μM ferric quinate (▲) or supplemented with spent culture fluids from strain MS-1 grown with 20 μM ferric quinate (□) or 5 μM ferric quinate (△). Controls contained Davis minimal medium (negative control) (●) or spent culture fluids from wild-type cultures of *S. typhimurium* ATCC 14028 (positive control) (○).

NM-1A, produced hydroxamates at both iron concentrations tested (5 and 20 μM ferric quinate). Because these results were unexpected in the light of iron concentration effects on siderophore production by enteric bacteria (10, 12, 15, 16), we repeated this study using an alternate source of iron, ferric citrate. At physiological pH and with a 20-fold molar excess of citrate, the ferric citrate complex can be expected to exist in a highly polymerized state (14, 16), rendering iron less available to cells. *A. magnetotacticum* MS-1 cells responded through their hydroxamate production to the available iron concentration in their culture medium. At a 20 μM concentration of iron, supplied in the form of ferric citrate, cells produced hydroxamates when the molar ratio of citrate to iron was 1:1 but not 20:1. Since the latter situation represents low available iron concentration for *A. magnetotacticum*, these results corroborated those obtained with ferric quinate: magnetic cells of this species produce secondary hydroxamates only when cultured under iron-sufficient conditions.

Although in enteric bacteria siderophore synthesis is derepressed by iron deficiency, hydroxamate synthesis by cells of *A. magnetotacticum* is apparently repressed by iron deficiency or is induced by available iron.

With low concentrations of available iron, many bacteria synthesize OMPs which function as receptors for siderophores (8, 10, 15, 16, 18). The 55,000-dalton IROMP in *A. magnetotacticum* may not function in iron transport via hydroxamates, as its synthesis was repressed at iron concentrations necessary for hydroxamate production. Thus, it may be a component of another iron uptake system not involving hydroxamates. Cells of strain NM-1A did not produce the IROMP but did produce hydroxamates, suggesting that a mutation(s) resulting in the loss of magnetite production may be associated with the gene(s) directing the synthesis of the IROMP.

In the enteric bacteria, iron storage proteins or those

involved with nonspecific iron transport are usually large (8, 16). The 72,000-, 76,000-, and 85,000-dalton OMPs detected in *A. magnetotacticum* cells cultured at a 20 or 40 μM concentration of ferric quinate may serve a role in iron metabolism comparable to those of OMPs of similar size and produced under similar conditions by the enteric bacteria (16). Alternatively, their coordinate production under conditions in which cells also produce hydroxamates suggests that these OMPs may be involved in hydroxamate secretion or binding or both.

The 58,000-dalton IROMP produced by *A. magnetotacticum* cells cultured with citrate may be a component of a citrate-mediated iron uptake system similar to that of *Mycobacterium smegmatis* (14) or *Escherichia coli* (16, 20).

The fact that only spent culture fluids which tested positively for hydroxamates stimulated growth of the *S. typhimurium* LT-2 *enb-7* mutant is consistent with a physiological role of this material in iron transport (e.g., as a siderophore) in *A. magnetotacticum*.

We do not know why hydroxamates are produced at high iron concentration and less so at low iron concentration by *A. magnetotacticum* MS-1. Two of the three catecholate siderophores of *Azotobacter vinelandii* are produced to some extent by cells cultured with 25 μM iron (6). Recently, we have detected hydroxamate production at high (20 μM) iron concentrations by *Aquaspirillum bengal*, *Aquaspirillum serpens*, and *Aquaspirillum polymorphum*, which are not magnetic (L. Paoletti and R. Blakemore, unpublished results). Thus, the magnetic spirillum appears not to be unique in this respect. This is an unusual pattern, and although not many published studies include results of hydroxamate analysis at both high and low iron concentrations, this appears to be the first report of bacterial hydroxamate production at high iron concentration. Our results also suggest that some available iron is necessary to induce synthesis of this material and of the 72,000- to 85,000-dalton OMPs detected.

Siderophore production at high iron concentration may be common among free-living organisms which accumulate this metal or require it for metabolism but live in environments in which it is normally or transiently abundant.

ACKNOWLEDGMENTS

This investigation was supported by Office of Naval Research Contract N00014-85-K-0502.

We thank N. Blakemore for providing the nonmagnetic spirillum. We also thank R. Zsigray and R. Frankel for continued advice, discussion, and encouragement.

LITERATURE CITED

1. **Arnow, L. E.** 1937. Colorimetric determination of the components of 3,4-dihydroxyphenylalanine-tyrosine mixtures. J. Biol. Chem. **118**:531–537.
2. **Blakemore, R. P.** 1982. Magnetotactic bacteria. Annu. Rev. Microbiol. **36**:217–238.
3. **Blakemore, R. P., D. Maratea, and R. S. Wolfe.** 1979. Isolation and pure culture of a freshwater magnetic spirillum in chemically defined medium. J. Bacteriol. **140**:720–729.
4. **Carlton, B. C., and B. J. Brown.** 1981. Gene mutation, p. 222–242. *In* P. Gerhardt, R. G. E. Murray, R. N. Costilow, E. W. Nester, W. A. Wood, N. R. Krieg, and G. B. Phillips (ed.), Manual of methods for general bacteriology. American Society for Microbiology, Washington, D.C.
5. **Dobrogosz, W. J.** 1981. Enzymatic activity, p. 365–392. *In* P. Gerhardt, R. G. E. Murray, R. N. Costilow, E. W. Nester, W. A. Wood, N. R. Krieg, and G. B. Phillips (ed.), Manual of methods for general bacteriology. American Society for Microbiology, Washington, D.C.
6. **Fekete, F. A., J. T. Spence, and T. Emery.** 1983. Siderophores produced by nitrogen-fixing *Azotobacter vinelandii* OP in iron-limited continuous culture. Appl. Environ. Microbiol. **46**:1297–1300.
7. **Holzberg, M., and W. M. Artis.** 1983. Hydroxamate siderophore production by opportunistic and systemic fungal pathogens. Infect. Immun. **40**:1134–1139.
8. **Klebba, P. E., M. A. McIntosh, and J. B. Neilands.** 1982. Kinetics of biosynthesis of iron-regulated membrane proteins in *Escherichia coli*. J. Bacteriol. **149**:880–888.
9. **Laemmli, U. K.** 1970. Cleavage of structural proteins during the assembly of the head of bacteriophage T4. Nature (London) **227**:680–685.
10. **Leong, J., and J. B. Neilands.** 1976. Mechanisms of siderophore iron transport in enteric bacteria. J. Bacteriol. **126**:823–830.
11. **Lowry, O. H., N. J. Rosebrough, A. L. Farr, and R. J. Randall.** 1951. Protein measurement with the Folin phenol reagent. J. Biol. Chem. **193**:265–275.
12. **Luckey, M., J. R. Pollack, R. Wayne, B. N. Ames, and J. B. Neilands.** 1972. Iron uptake in *Salmonella typhimurium*: utilization of exogenous siderochromes as iron carriers. J. Bacteriol. **111**:731–738.
13. **Maratea, D., and R. P. Blakemore.** 1981. *Aquaspirillum magnetotacticum* sp. nov., a magnetic spirillum. Int. J. Syst. Bacteriol. **31**:452–455.
14. **Messenger, A. J. M., and C. Ratledge.** 1982. Iron transport in *Mycobacterium smegmatis*: uptake of iron from ferric citrate. J. Bacteriol. **149**:131–135.
15. **Neilands, J. B.** 1981. Iron adsorption and transport in microorganisms. Annu. Rev. Nutr. **1**:27–46.
16. **Neilands, J. B.** 1982. Microbial envelope proteins related to iron. Annu. Rev. Microbiol. **36**:285–309.
17. **Schnaitman, C.** 1981. Cell fractionation, p. 52–61. *In* P. Gerhardt, R. G. E. Murray, R. N. Costilow, E. W. Nester, W. A. Wood, N. R. Krieg, and G. B. Phillips (ed.), Manual of methods for general bacteriology. American Society for Microbiology, Washington, D.C.
18. **Sokol, P.** 1984. Production of ferripyochelin outer membrane receptor by *Pseudomonas* species. FEMS Microbiol. Lett. **23**:313–317.
19. **Stooky, L. L.** 1970. Ferrozine—a new spectrophotometric reagent for iron. Anal. Chem. **42**:779–781.
20. **Wagegg, W., and V. Braun.** 1981. Ferric citrate transport in *Escherichia coli* requires outer membrane receptor protein FecA. J. Bacteriol. **145**:156–163.

Current Microbiology Vol. 15 (1987), pp. 121–127

Current Microbiology

Spectral Analysis of Cytochromes in *Aquaspirillum magnetotacticum*

Wendy O'Brien,[1] Lawrence C. Paoletti,[2] and Richard P. Blakemore[2]

[1]Bacteriology Department, University of Wisconsin, Madison, Wisconsin, and [2]Department of Microbiology, University of New Hampshire, Durham, New Hampshire, USA

Abstract. The respiratory chain of *Aquaspirillum magnetotacticum* strain MS-1 cells denitrifying microaerobically included a-, a_1-, b-, c-, cd_1-, and o-type hemes. More than 85% of the total cytochromes detected were of the c type. Virtually all of the a and b types were detected in cell membranes, whereas 70% of the c-type hemes were soluble. Large quantities of soluble c-type hemes were released with periplasm by freezing and thawing cells. Soluble c_{552} occurred in two forms: as a single compound of apparent molecular weight of 17,000 daltons, which bound CO, and, together with d_1 heme, as a component of nitrite reductase. Both a_1-type hemes (which usually comprise part of the "low aeration" cytochrome oxidase) and o types (usually part of the "high aeration" oxidase) were simultaneously expressed in microaerobically grown denitrifying cells of *A. magnetotacticum*; this indicated branching of the respiratory chain.

Cells of the magnetite (Fe_3O_4)-producing spirillum [11] *Aquaspirillum magnetotacticum* are nonfermentative, obligately microaerophilic, and oxidize organic acids [2]. They denitrify microaerobically, but will not grow anaerobically with NO_3^- [1, 2, 9]. Denitrifying cells respire, using NO_3^- and O_2 as terminal oxidants simultaneously [1, 25]. Under nondenitrifying conditions (with NH_4^+ as sole N source), only O_2 and Fe^{3+} are terminal electron acceptors in the chemically defined medium. Magnetic cells of strain MS-1 (but not those of NM-1A, a nonmagnetic mutant strain derived from it) carry out electrogenic proton translocation with Fe^{3+} [25]. It seemed possible that dissimilatory Fe^{3+} reduction might contribute to formation of intracellular Fe_3O_4 in this organism, because cells appear to produce this mineral optimally when alternate oxidants (O_2 and NO_3^-) are limiting [3]. The possibility of a link between iron respiration and Fe_3O_4 formation prompted us to identify the terminal electron transport components with the overall objective of establishing whether any might be specifically associated with iron respiration or Fe_3O_4 synthesis.

Except for a single report of a c-type cytochrome detected in cells of a magnetic coccoid bacterium (T. T. Moench, PhD thesis, Indiana University, 1978), the respiratory chains of magnetotactic bacteria have remained unexplored. Here we report results of spectrophotometric analyses of the cytochrome content of wild type and mutant *A. magnetotacticum* cells grown with NO_3^- or NH_4^+ at various values of dissolved oxygen tension (d.o.t.).

Materials and Methods

Organism and culture conditions. *Aquaspirillum magnetotacticum* strain MS-1 [20] and a nonmagnetic mutant derived from it, strain NM-1A [25], were used in this study. Cells were cultured in a chemically defined growth medium, MSGM [2], in sealed serum vials or glass carboys under microaerobic conditions (initial headspace O_2, 0.2%–2% of saturation). In lieu of 6 m*M* succinic acid, tartaric and succinic acids (3.0 m*M* each) served as carbon sources. Ferric quinate (20 μM) and 1.4 m*M* $NaNO_3$ or NH_4Cl (the latter N source to allow cell growth without denitrification) were used. Cells in batch cultures were grown to late stationary phase (11 days, 1–2 × 10^8 cells ml) at 30 C under various air–N_2 atmospheres. For the study of the effect of elevated O_2 on cytochrome content, cells in 15-liter cultures were grown at a d.o.t. of less than 5% of saturation. Upon reaching a density of approximately 10^8 cells ml, cultures were shifted to a d.o.t. between 5% and 15% of saturation. Cultures were protected at elevated d.o.t. by addition of filter-sterilized bovine liver catalase (Worthington Diagnostic Systems, Freehold, New Jersey) to the medium (120 U ml) just prior to inoculation. The culture d.o.t. was measured by means of an autoclavable galvanic O_2 electrode (New Brunswick Scientific Company, series 900; New Brunswick, New Jersey) with a New Brunswick model DO-40 dissolved O_2 analyzer. The full-scale response time was 60 s.

Cells were harvested by continuous flow centrifugation or by filtration through 0.45-μm microporous membranes in a Millipore Pellicon Cassette filtration system (Millipore Corporation, Medford, Massachusetts).

Address reprint requests to Dr. Richard P. Blakemore, Department of Microbiology, University of New Hampshire, Durham, NH 03824, USA.

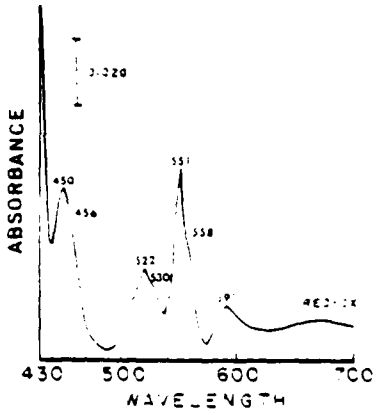

Fig. 1. Room temperature difference spectrum of dithionite-reduced minus air-oxidized small membrane particles of *Aquaspirillum magnetotacticum* MS-1. The protein concentration was 0.6 mg · ml^{-1}.

Preparation of respiratory membrane particles. Cells from 25 liters of culture (ca. 5×10^{12} cells) were washed by centrifugation at 5°C in cold 50 m*M* potassium phosphate buffer (KPB) at pH 7.0, and resuspended in 25 ml of KPB. Cells were disrupted by pulsed sonication for 3–5 min at 5°C in a Heat Systems Ultrasonics W-375 sonicator operating at 140 watts. Disrupted cells were centrifuged (10,000 *g*, 15 min, 5°C) to remove unbroken cells and debris. The supernatant fluid was centrifuged (35,000 *g*, 30 min, 5°C), yielding a pellet fraction consisting of membranous particles as evidenced by electron microscopy. These corresponded to "large respiratory membrane particles" described by Jones and Redfearn [15]. "Small respiratory membrane particles" remaining in the supernatant fluid were collected by ultracentrifugation (105,000 *g*, 90 min, 5°C) and stored on ice. The upper two-thirds of the resulting supernatant fluid comprised the small membrane particle wash fluid. Pellet fractions washed in cold KPB (pH 6.8) were resuspended in 3–6 ml of KPB. Brief sonication (15–30 s) was often necessary to effect resuspension of these particles, which, upon freezing, tended to aggregate. Freezing was avoided whenever possible.

Protein was measured by the Bio-Rad Protein Assay (Bio-Rad) or the Lowry et al. [19] method with bovine serum albumin as a standard.

Absorbance spectra. Room temperature difference spectra were measured in a Beckman Instruments DU-8 UV/VIS spectrophotometer equipped for wavelength scanning.

Reduced minus oxidized (red − ox) difference spectra were obtained by subtracting the spectrum of the air- or ferricyanide-oxidized sample from that of the same sample following either chemical (sodium dithionite) or physiological (NADH or succinate) reduction, as indicated. Difference spectra employing carbon monoxide (red_{CO} − red) were obtained by subtracting the spectrum of the cytochromes reduced with dithionite from that of the same sample after sparging with CO for 45–60 s. Identical red_{CO} − red spectra were obtained in which the CO was first deoxygenated by passage through an alkaline pyrogallol solution.

Cytochrome concentrations were estimated from published molar extinction coefficients [10]. Absorbance maxima for b-type cytochromes occurred as shoulders on major absorption peaks for c-type hemes. The relationship, $1.37\ A_{\alpha c} - 0.62\ A_{\alpha a}$ was used to estimate the amount of cytochrome c, and $1.07\ A_{\alpha c} - 0.15\ A_{\alpha a}$ was used to estimate that of cytochrome b.

Low-temperature red − ox spectra were obtained in the laboratory of Dr. B. Chance (Johnson Foundation, University of Pennsylvania, Philadelphia, Pennsylvania) with a dual wavelength recording spectrophotometer. All difference spectra were derived by computer from stored spectra.

Extraction of soluble cytochromes by freezing and thawing (F T). Washed cells (ca. 3×10^{11}) in 6 ml cold KPB (pH 6.8) were frozen at −12°C overnight. The thawed cells were centrifuged (8000 *g*, 20 min, 5°C), and the supernatant fluids were further clarified by centrifugation (32,000 *g*, 30 min, 5°C). The pink supernatant fluid was placed in a dialysis bag (Spectrapor no. 1, 6000–8000 mol wt cutoff, Spectrum Medical Industries, Los Angeles, California) and concentrated to one-sixth of its volume by use of polyethylene glycol (J. T. Baker, solid flake, 20,000 mol wt) by the method of Cliver [6]. The sample was then dialyzed overnight at 4°C against KPB (pH 6.8) and examined for cytochromes. Alkaline pyridine hemochromogens were prepared of the soluble c-type cytochromes extracted from F T supernatant fluids with cold acetone.

Soluble hemoproteins were also prepared from cells disrupted at 4°C with a French pressure cell. Cell debris was removed by centrifugation (4300 *g*, 15 min, 4°C), and the supernatant fluid was clarified by ultracentrifugation (200,000 *g*, 1 h, 4°C). The resulting light brown supernatant material was applied to a DEAE-cellulose (Sigma) column equilibrated with 20 m*M* sodium acetate (pH 6.0). Amber-colored material containing the c-type hemes eluted with the void volume.

Sodium dodecyl sulfate–polyacrylamide gel electrophoresis (SDS–PAGE). Cytochromes released by the F T method were concentrated, solubilized at 25°C, and separated on a 1.5-mm SDS–polyacrylamide gel by the buffer system described by Laemmli [18]. The concentration of acrylamide in the stack and separating gels was 4% and 17%, respectively. Each gel contained concentrated F T proteins (60 μg lane), molecular weight standards (Bio Rad), and horse cytochrome c (type II-A, Sigma). Proteins migrated through the stacking and separating gels at a constant current of 20 and 40 mA, respectively. Preparative gels contained 17–25 mg of proteins released by F T. For these gels, electrophoresis was performed at 10 mA through a 3.5-cm, 4% acrylamide stacking gel, and at 20 mA through a 7.0-cm, 12% acrylamide separating gel. Gels were observed unstained and after stain with diaminobenzidine to reveal c-type cytochromes [21], or with Coomassie blue to reveal proteins.

Results and Discussion

While the electron transport systems of several species of chemoheterotrophic spirilla have been studied [4, 5, 7, 8, 12, 13], magnetic spirilla have not been examined in this regard. Cells of *Aquaspirillum itersonii* contained an unbranched electron transport chain comprised of ubiquinone, b-, c-, and o-type cytochromes. The c-type was both membrane bound and soluble, and a considerable quantity of the soluble form was predominant when NO_3^- was present in the culture medium. Cells of the obli-

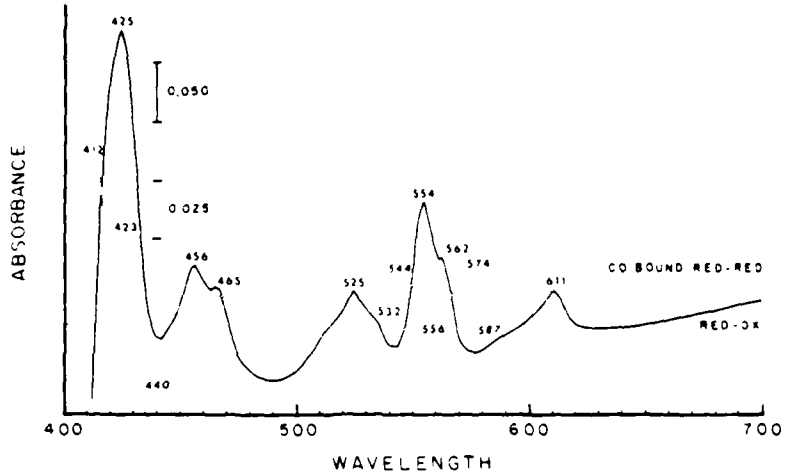

Fig. 2. Low-temperature (77 K) difference spectra of large membrane particles of *Aquaspirillum magnetotacticum* MS-1 grown with sodium nitrate as the sole nitrogen source. Samples (2.1 ml) of respiratory membrane particles, each containing 2–5 mg protein, were diluted with 100% ethylene glycol (purified on alumina) to a final concentration of 30% ethylene glycol. Each oxidized sample (1 ml) in the antifreeze was rapidly frozen in dry ice and spectrally scanned at 77 K. This spectrum (oxidized) was stored in the instrument RAM. The sample was thawed, reduced by adding 10 μl 500 m*M* sodium succinate, refrozen, scanned, and the spectrum also stored. The sample was again thawed, reduced further with several crystals of sodium dithionite, refrozen, scanned, and the spectrum stored. Finally, the thawed sample was sparged for at least 60 s with CO, refrozen, and scanned. (——) Red − ox; and (------) red_{CO} − red. The protein concentration was 4.6 mg · ml $^{-1}$.

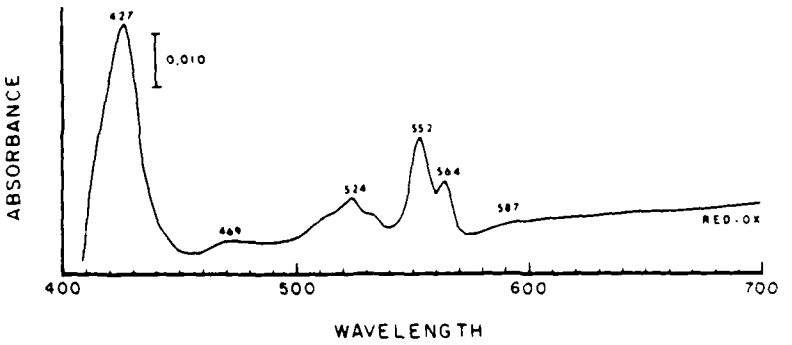

Fig. 3. Low-temperature (77 K) difference spectrum of large membrane particles of *Aquaspirillum magnetotacticum* MS-1 grown with ammonium chloride as the sole nitrogen source. The protein concentration was 1.6 mg · ml $^{-1}$.

gate microaerophile *Spirillum volutans* possessed cytochromes similar to those of *A. itersonii* and *A. serpens*, with lower quantities of cytochrome c [7].

Room-temperature red − ox spectra obtained with large or small respiratory membrane particles from magnetic cells of denitrifying *A. magnetotacticum* (Fig. 1) displayed absorption maxima of cytochromes of type c (425, 522, and 551 nm), type b (shoulders at 530 and 558 nm), and type a_1 (450 and 591 nm). Shoulders at 456 and 600 nm were consistent with the presence of either an a-type heme or the d_1 moiety of a cd_1 multiheme (nitrite reductase). The α-absorbance band attributed to c-type heme at 551 nm was frequently a split peak. The absorbance maximum in the Soret region expected for the b-type heme (425 nm) was not discernible from that resulting from c-types at room temperature.

Red − ox spectra recorded at 77 K (Fig. 2) were similar to those obtained at room temperature. Absorbance maxima at 77 K are usually shifted slightly toward the blue [26]. For unknown reasons, in our work maxima were shifted 5–10 nm toward the red end of the spectrum. Nevertheless, low temperature (Fig. 2) allowed resolution of coincident maxima and distinct peaks at 465 and 611 nm attributable to the d_1 moiety of a cd_1 nitrite reductase [28].

Table 1. Absorbance parameters of cytochromes detected in *Aquaspirillum magnetotacticum* strain MS-1 cells

Conditions	Cytochrome of type					
	a	a_1	b	c	o	d
GROWTH WITH NITRATE						
Small membrane particles						
Red – ox., room temperature						
Maxima	450			522		
	591			551		
Shoulders	456		530			
	600		558			
Freeze thaw fluids						
Red – red., room temperature						
Maxima				414		
				534		
				562		
Minima						526
						550
Red – ox., room temperature						
Maxima				419		468
				522		616
				549		
				551		
Large membrane particles						
Red – ox., 77 K						
Maxima	465	456		425		
	611			525		
				554		
Shoulders		587	532			
			562			
Red – red., 77 K						
Maxima					412	
					544	
					574	
Minima		440			526	
		590			556	
Shoulder		423				
GROWTH WITH AMMONIUM						
Red – ox., 77 K						
Maxima	469	587	532	427		
			564	524		
				552		

The room temperature absorption maximum expected for d_1-chlorin of nitrite reductase, typically at 625 nm [28], frequently appeared at 611–616 nm in our work. This is probably a pH effect in that this peak was shifted 5–10 nm toward longer wavelengths in spectra collected at higher pH. Spectral evidence for the presence of cd_1 nitrite reductase was corroborated by results of SDS–PAGE (see below).

Respiratory particles from cells grown with NO_3^- yielded low temperature carbon monoxide

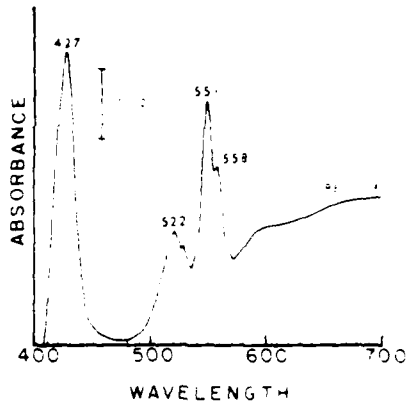

Fig. 4. Room-temperature-reduced minus oxidized difference spectrum of large membrane particles of *Aquaspirillum magnetotacticum* MS-1 cultured with sodium nitrate at elevated oxygen (5% O_2). The protein concentration was 2.7 mg · ml

(red$_{CO}$ − red) difference spectra (Fig. 2) consistent with type o (absorption maxima at 412, 544, and 574 nm, with minima at 526 and 556 nm) and a_1 (shoulder at 423 nm, a trough at 440 nm, and a slight dip at 590 nm) cytochromes. Thus, our spectral data summarized in Table 1, collectively indicate the presence of hemes of the a, a_1, b, c, cd_1, and o types in cells of *A. magnetotacticum* strain MS-1 denitrifying microaerobically. We have not yet determined the functional roles of these compounds. However, it would be interesting if this cytochrome diversity were related to the respiratory versatility of this organism.

Variations in growth conditions produced marked alterations in cytochrome content of strain MS-1. Respiratory membranes from cells cultured microaerobically with NH_4^+ as the sole N source (Fig. 3) had less a- and d_1-type cytochromes (absorption maxima at 455, 465, and 611 nm were reduced or absent) compared with those of denitrifying cells (Fig. 2). Cells cultured at a d.o.t. greater than 5% (Fig. 4) showed a 50% decrease in total cytochrome content over that of cells at 1% O_2, but were proportionally enriched in c types. They possessed 12-fold less (moles per weight membrane protein) a_1-type, threefold less b-type, and twofold less c-type hemes than cells cultured at a d.o.t. of 1% of saturation (Fig. 1).

Although photodissociation studies were not performed, our CO difference spectra suggest that the o- and a_1-type cytochromes may function as terminal oxidases. The terminal oxidase in *Escherichia coli* cells grown at high aeration consists of cytochromes b_{562} and o, which purify as a single com-

Table 2. Cytochrome concentrations in fractions of denitrifying cells of strain MS-1

Cell fraction	Quantity (nmol mg total protein) of cytochrome of type a	b	c	Total
Whole cell wash fluid	0	0	28.0 (19.9)	28.0
Large respiratory membrane particles	8.5 (91.4)	11.3 (91.9)	38.8 (27.5)	58.6
Large membrane particle wash fluid	0	0	12.0 (8.5)	12.0
Small respiratory Membrane particles	0.8 (8.6)	1.0 (8.1)	3.5 (2.5)	5.3
Small membrane particle wash fluid	0	0	58.5 (41.6)	58.5
Total	9.3 (100)	12.3 (100)	140.8 (100)	162.4

The numbers in parentheses denote percentage of each type detected.

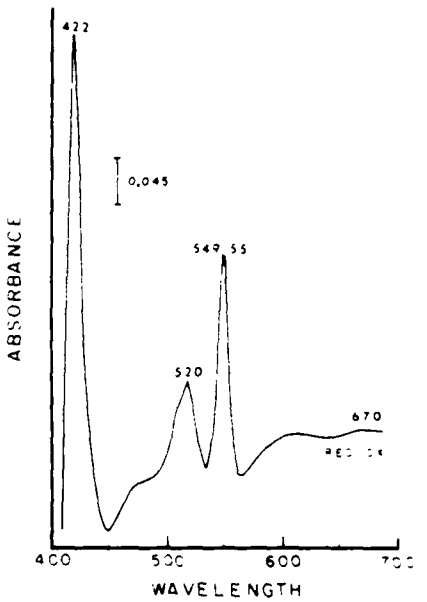

Fig. 5. Room-temperature-reduced minus oxidized difference spectrum of soluble proteins released by freezing and thawing *Aquaspirillum magnetotacticum* MS-1 cells. The protein concentration was 3.6 mg · ml

plex [14]. Low aeration results in a terminal oxidase containing b_{558}-, a_1- and d-type hemes which purify as a single complex [14]. Cytochromes of the a and a_1 types together comprise the cytochrome c oxidase of mitochondria and of some prokaryotes including *Paracoccus denitrificans* and *Rhodopseudomonas sphaeroides* [16]. However, the simultaneous occurrence of a, o, and a_1 types, as detected in this study, is uncommon. Since high aeration abolished the a-type hemes in our work, it is possible that the maxima we attribute to heme a (456 and 600 nm) are, in fact, those of a d heme associated with a "low aeration" oxidase. Nevertheless, our findings suggest branching of electron transport in this microaerophile, with dual expression of terminal oxidases of both the a_1 (low aeration) and o types (high aeration) under denitrifying conditions. Nondenitrifying cells grown microaerobically on NH_4^+ were forced to use O_2 and perhaps Fe^{3+} as terminal electron acceptors. As expected, they had greatly diminished a-type hemes ("low aeration" oxidases) cd_1 hemes (nitrite reductase), and b-type hemes (which comprise part of the enzyme nitrate reductase).

Although the two respiratory membrane particle fractions of strain MS-1 cells were qualitatively similar in cytochrome content, the large particles contained nine times more cytochrome per unit mass than the small particles. Most (91%) of the a- and b-type cytochromes were associated with the large membraneous particles; the remaining 8% was recovered in the small particle fractions (Table 2). Of considerable interest, more than 85% of the total cytochromes released from denitrifying cells of strain MS-1 or NM-1A by conventional cell fractionation procedures were of the c type (Tables 2 and 3). Furthermore, 70% of c-type hemes were soluble (Table 2), and, in fact, soluble c-type hemes comprised 60% of the total cytochromes detected (Table 2).

Red − ox difference spectra collected at 77 K, with use of the supernatant fluids obtained from washing membranous particle fractions (Table 2) exhibited absorbance maxima at 418, 522, and 551 nm with shoulders at 444, 474, and 513 nm. These indicated the presence of a soluble heme c and absence of a or b types in these wash fluids.

Suspensions of denitrifying cells in KPB (pH 7.0), when frozen overnight, thawed, and centrifuged, yielded pink supernatant fluids with spectral characteristics of c- and d_1-type hemes (Fig. 5). The absorption band in the vicinity of 551 nm was split; this suggested the presence of more than one c type. Proteins in these fluids, when concentrated and separated with SDS–PAGE, included a pink and a brown band of apparent mol wt 17,000 daltons (17.0

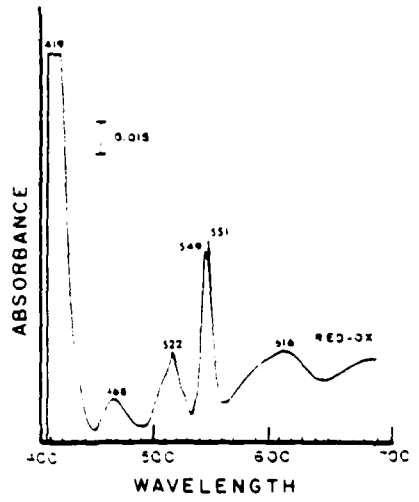

Fig. 6. Room-temperature-reduced minus oxidized difference spectrum of soluble proteins released by freezing and thawing *Aquaspirillum magnetotacticum* MS-1 cells and partially purified by treatment with DEAE–cellulose. The protein concentration was 4.0 mg · ml^{-1}.

kdal) and 85.0 kdal, respectively. Each of these exhibited peroxidase activity typical of c-type hemes [21]. When solubilized at 25°C, electrophoresed, and subsequently eluted from the unstained gel, the pink material displayed spectral characteristics (absorption maxima at 412 and 551 nm) of a c-type heme. The 85.0-kdal brown band obtained by preparative SDS–PAGE of proteins released by F/T was resolved by prolonged electrophoresis into a green (apparent mol wt of 83.0 kdal) and a pink (apparent mol wt of 81.0 kdal) band. Spectra obtained with material from the green band (dithionite-reduced minus persulfate-oxidized) had absorption maxima at 415 and 551 nm, as expected of heme c, and at 468 and 625 nm, as expected for the d_1 chlorin of cytochrome cd_1 (nitrite reductase).

A spectrum confirming the presence of soluble c-type heme (551 nm maximum) was obtained from F/T supernatant fluids extracted with acid acetone in which the residue was scanned in alkaline pyridine. This soluble c_{551} bound CO as evidenced from difference spectra (not shown) of the chemically reduced cytochromes in F/T supernatant fluids before and after treatment with CO (maxima at 414, 534, 562 nm with minima at 526 and 551 m). After treatment of F/T fluids with DEAE–cellulose, well defined red − ox maxima attributable to the d_1 (419, 468, and 616 nm) and c (419, 522, and 551 nm) hemes of nitrite reductase were observed (Fig. 6). Additional maxima characteristic of a second c-type heme (549 and 522 nm) were also present (Fig. 6).

Table 3. Total cytochromes detected in denitrifying cells of *Aquaspirillum magnetotacticum* strains MS-1 and NM-1A

	% of total cytochromes detected in strain	
Cytochrome type	MS-1	NM-1A
a	5.7	4.8
b[a]	7.5	4.0
c	86.6	91.2

[a] Includes o types.

We were surprised to find such large quantities of soluble c-type hemes in this organism. Freezing and thawing did not liberate a- or b-type cytochromes present in cell membranes, nor did it disrupt the helical cell morphology. F/T caused selective release of periplasmic proteins of this organism (not proteins in the cytoplasmic membrane) as determined from cell fractionation studies and assay of succinic dehydrogenase [23]. Thus, c-type hemes selectively released by F/T were either periplasmic or loosely associated with membranes.

Soluble c-type cytochromes are quite common [12, 13, 24] and frequently have been shown, as in our study, to bind CO [17, 22, 27]. Soluble c_{551} of strain MS-1 occurred in two forms: a 17.0-kdal free form, and together with d_1 as a component of an 85.0-kdal complex (nitrite reductase). The ability of soluble c_{551} to bind CO is suggestive of an oxidase function. CO binding by c-type cytochromes is enigmatic, since they are considered unable to bind O_2. The sixth coordination position (CO or O_2 binding site) of iron in the heme is covalently bound to the imidazole group of histidine in the protein. Therefore, their proportional abundance, soluble nature, preferential distribution in the periplasm, and apparent ability to bind CO are all properties not expected of a c-type cytochrome with a principal role in cell energy conservation (i.e., as a component of a vectorially organized electron transport chain), and alternate function(s) must be considered.

No differences were detected in the cytochrome of strains MS-1 and NM-1A (Table 3). Thus, there may not be unique cytochromes or combinations of cytochromes specifically required for iron respiration or Fe_3O_4 formation by strain MS-1. However, the mutant NM-1A, despite its inability to respire with iron [25], may be blocked in some aspect of Fe_3O_4 formation not reflected in its

cytochrome composition. Of particular interest is the fact that conditions which depress magnetite yields of cells (high d.o.t. or growth with NH_4^+) also result in diminution of a-type hemes which commonly comprise terminal oxidases. This may indicate that electron flow via particular terminal oxidases is important for optimal magnetite formation.

ACKNOWLEDGMENTS

We thank N. Blakemore, K. Short, and W. Guerin for assistance and criticism. We gratefully acknowledge Dr. L. Smith for advice and Dr. B. Chance for cooperation in carrying out low-temperature spectra. This work was supported by NSF grant DMB 85-15540 and by ONR contract N0014-85-K-0502.

Literature Cited

1. Bazylinski DA, Blakemore RP (1983) Denitrification and assimilatory nitrate reduction in *Aquaspirillum magnetotacticum*. Appl Environ Microbiol 46:1118–1124
2. Blakemore RP, Maratea D, Wolfe RS (1979) Isolation and pure culture of a freshwater magnetic spirillum in chemically defined medium. J Bacteriol 140:720–729
3. Blakemore RP, Short KA, Bazylinski DA, Rosenblatt C, Frankel RB (1985) Microaerobic conditions are required for magnetite production within *Aquaspirillum magnetotacticum*. Geomicrobiol J 4:53–71
4. Clark-Walker GD, Lascelles J (1970) Cytochrome c_{550} from *Spirillum itersonii*: purification and some properties. Arch Biochem Biophys 136:153–159
5. Clark-Walker GD, Rittenberg B, Lascelles J (1967) Cytochrome synthesis and its regulation in *Spirillum itersonii*. J Bacteriol 94:1648–1655
6. Cliver DO (1967) Detection of enteric viruses by concentration with polyethylene glycol. In: Berg G (ed) Transmission of viruses by the water route. New York: John Wiley and Sons, pp 109–120
7. Cole JA, Rittenberg SC (1971) A comparison of respiratory processes in *Spirillum volutans*, *Spirillum itersonii* and *Spirillum serpens*. J Gen Microbiol 69:375–383
8. Daily HA, Lascelles J (1977) Reduction of iron and synthesis of protoheme by *Spirillum itersonii* and other organisms. J Bacteriol 129:815–820
9. Escalante-Semerena JC, Blakemore RP, Wolfe RS (1980) Nitrate dissimilation under microaerophilic conditions by a magnetic spirillum. Appl Environ Microbiol 40:429–430
10. Estabrook R, Holowinsky A (1961) Studies on the content and organization of the respiratory enzymes of mitochondria. J Biophys Biochem Cyt 9:19–28
11. Frankel RB, Papaefthymiou GC, Blakemore RP, O'Brien W (1983) Fe_3O_4 precipitation in magnetotactic bacteria. Biochim Biophys Acta 763:147–159
12. Garrard WT (1971) Selective release of proteins from *Spirillum itersonii* by tris (hydroxymethyl) aminomethane and ethylenediaminetetraacetate. J Bacteriol 105:93–100
13. Gauthier DK, Clark-Walker GD, Garrard WT Jr, Lascelles J (1970) Nitrate reductase and soluble cytochrome c in *Spirillum itersonii*. J Bacteriol 102:797–803
14. Green GN, Gennis RB (1983) Isolation and characterization of an *Escherichia coli* mutant lacking cytochrome d terminal oxidase. J Bacteriol 154:1269–1275
15. Jones C, Redfearn ER (1966) Electron transport in *Azotobacter vinelandii*. Biochim Biophys Acta 113:467–481
16. Jones CW (1982) Bacterial respiration and photosynthesis, vol 5. Washington DC: Am Soc Microbiol
17. Knowles CJ, Calcott PH, MacLeod RA (1974) Periplasmic CO-binding c-type cytochrome in a marine bacterium. FEBS Letters 49:78–83
18. Laemmli UK (1970) Cleavage of structural proteins during the assembly of the head of bacteriophage T4. Nature (Lond) 227:680–685
19. Lowry OH, Rosebrough NJ, Farr AL, Randall RJ (1951) Protein measurement with the Folin phenol reagent. J Biol Chem 193:265–275
20. Maratea D, Blakemore RP (1981) *Aquaspirillum magnetotacticum* sp. nov., a magnetic spirillum. Int J Syst Bacteriol 31:452–455
21. McDonnel A, Staehlin LA (1981) Detection of cytochrome f, a c-class cytochrome, with diaminobenzidine in polyacrylamide gels. Anal Biochem 117:40–44
22. Nevin DF (1984) The cytochrome complement of *Haemophilus parasuis*. Can J Microbiol 30:763–773
23. Paoletti LC, Short KA, Blakemore RP (1986) Freezing and thawing of *Aquaspirillum magnetotacticum* releases periplasmic proteins. Abstr Annu Meet Am Soc Microbiol 1986:166
24. Scholes PB, McLain G, Smith L (1971) Purification and properties of a c-type cytochrome from *Micrococcus denitrificans*. Biochemistry 10:2072–2076
25. Short KA, Blakemore RP (1986) Iron respiration-driven proton translocation in aerobic bacteria. J Bacteriol 167:729–731
26. Smith L (1978) Bacterial cytochromes and their spectral characterization. Methods Enzymol 53:202–212
27. Weston JA, Knowles CJ (1974) The respiratory system of the marine bacterium *Beneckea natriegenes*. 1. Cytochrome composition. Biochim Biophys Acta 333:228–236
28. Yamanaka T, Okunuki K (1974) Cytochromes. In: Neilands J (ed) Microbial iron metabolism. New York: Academic Press, pp 349–402

APPLIED AND ENVIRONMENTAL MICROBIOLOGY, Oct. 1987, p. 2590–2592
0099-2240/87/102590-03$02.00/0

Vol. 53, No. 10

Freeze-Thawing of *Aquaspirillum magnetotacticum* Cells Selectively Releases Periplasmic Proteins

LAWRENCE C. PAOLETTI, KEVIN A. SHORT, NANCY BLAKEMORE, AND RICHARD P. BLAKEMORE*

Department of Microbiology, University of New Hampshire, Durham, New Hampshire 03824

Received 11 May 1987/Accepted 29 June 1987

Cells of the gram-negative bacterium *Aquaspirillum magnetotacticum*, when suspended in buffer and freeze-thawed, produced pinkish orange supernatant fluid. The fluid contained ≤2.0% of total extractable outer membrane component 2-keto-3-deoxyoctonate or of the cytoplasmic membrane marker succinic dehydrogenase. Electrophoretic banding patterns and difference spectra of proteins and hemoproteins released by freeze-thawing cells were distinct from those of membrane-associated substances and similar to those of periplasmic substances obtained by applying conventional fractionation methods to this organism.

Freeze-thawing (FT) is undoubtedly important in defining indigenous soil bacteria populations in temperate regions. Mc Farley et al. (11) observed a 40 to 60% decrease in bacterial viability in sandy loam soil as a direct result of FT. FT is known to have a profound effect on bacterial cells and is often used as a pretreatment for cell disruption (18, 19). Responses of gram-negative cells depend upon the cell genotype (3), the menstruum in which they are suspended, and the FT rates (4). Outer sheath material from an oral spirochete has been isolated by FT (10). Calcott and MacLeod (4) found that freeze-thawed lactose-limited *Escherichia coli* cells released considerable amounts of the periplasmic enzyme cyclic phosphodiesterase but not the cytoplasmic enzyme glucose-6-phosphate dehydrogenase. A small, constant quantity (10 to 15% of total activity) of β-galactosidase (normally cytoplasmic) released was attributed to a possible periplasmic form of this enzyme.

Periplasmic substances of *E. coli* have been separated from other cellular components by osmotic shock and spheroplast formation (12). Ames et al. (1) demonstrated selective release of periplasmic proteins from *E. coli* cells treated with chloroform.

FT of cell suspensions of *Aquaspirillum magnetotacticum* MS-1 in 10 mM *N*-2-hydroxyethylpiperazine-*N'*-2-ethanesulfonic acid (HEPES) buffer (pH 7.4) or 10 to 50 mM potassium phosphate buffer caused the release of soluble c_{553}-type hemoproteins (15; W. O'Brien, M.S. thesis, University of New Hampshire, Durham, 1982). FT did not disrupt overall helical cell form. The objective of our study was to compare FT with other cell fractionation methods applied to this organism to determine the cellular origin of the substances released, including the soluble c_{553}-type hemoprotein. This method also allowed us to partially purify this hemoprotein. Periplasmic soluble *c*-type hemoproteins of unknown function have been detected in *Alcaligenes eutrophus* (17), *Aquaspirillum itersonii* (6), *Paracoccus denitrificans* (8), and *Haemophilus parasuis* (13).

(Portions of this work have been reported previously [L. C. Paoletti, K. A. Short, and R. P. Blakemore, Abstr. Annu. Meet. Am. Soc. Microbiol. 1986, I6, p. 166].)

Denitrifying *A. magnetotacticum* MS-1 cells (ATCC 31632) were batch cultured with a chemically defined medium (2) microaerobically at a dissolved oxygen tension of less than 1% saturation. Cells were harvested by filtration (15) when they reached a density of (4×10^8) ml^{-1}. Cells were washed once by centrifugation (8,000 × *g*, 30 min, 5°C) in at least 10 pellet volumes of 50 mM potassium phosphate buffer (pH 6.8) or 10 mM HEPES buffer (pH 7.4). Cells from a single 40-liter culture were suspended in 100 ml of potassium phosphate buffer or HEPES buffer, and equal portions were fractionated by the procedures described below.

The FT technique consisted of storing washed resuspended cells at −20°C overnight. The freezing rate was 0.7°C min^{-1}. The sample was thawed at room temperature, and cells were pelleted by centrifugation (10,000 × *g*, 15 min, 5°C). The pinkish orange supernatant fluid was clarified by ultracentrifugation (100,000 × *g*, 1 h, 5°C) and concentrated by membrane dialysis (Spectrapor membrane tubing; 6,000 to 8,000 molecular weight cutoff; Spectrum Medical Industries, Inc., Los Angeles, Calif.) on a bed of solid-flake polyethylene glycol (molecular weight, 20,000; J. T. Baker Chemical Co., Phillipsburg, N.J.) at 4°C.

Periplasmic proteins were obtained by two methods, osmotic shock (12) and chloroform extraction (1). The method of Schnaitman (19) was also used to separate outer membrane proteins, cytoplasmic membrane proteins, and soluble (cytoplasm and periplasm) proteins. Cells were disrupted in a French press (10,000 lb/in^2) before treatment with 2% (vol/vol) Triton X-100 and 10 mM $MgCl_2$ in 10 mM HEPES buffer (pH 7.4). Each fraction was dialyzed overnight at 4°C against HEPES buffer before analysis.

The relative activity of succinic dehydrogenase (SDH), an integral enzyme of the cytoplasmic membrane (5, 7), and the concentration of 2-keto-3-deoxyoctonate (KDO), a constituent of outer membrane lipopolysaccharide, were used as indices of the purity of cell fractions (9). Proteins and molecular mass standards (Bio-Rad Laboratories, Richmond, Calif.) were solubilized and separated by sodium dodecyl sulfate-polyacrylamide gel electrophoresis (16) and stained with silver (14). Spectra of air-oxidized soluble protein fractions were subtracted from spectra of dithionite-reduced soluble protein fractions, both of which were at room temperature, as previously described (15). The ability of cells to survive FT was evaluated by using a standard plate assay. Logarithmic dilutions of thawed cells were prepared as pour plates in semisolid medium in triplicate. Plates were incubated for 1 week at room temperature microaerobically. Colony counts were compared with those of control (non-FT) cells plated similarly.

* Corresponding author.

TABLE 1. Membrane markers in *A. magnetotacticum* cell fractions

Fractionation method (reference), fraction	Total KDO (mg)	Total SDH (10⁻³ U)
Triton X-100-$MgCl_2$ (28)		
OMP[a]	1,330	30
Periplasm-cytoplasm	6	19
CMP[b]	149	200
Chloroform (1), periplasm	11	0.9
Osmotic shock (12), periplasm	16	2.0
FT (this study), periplasm	20	5.0

Micromoles of cytochrome *c* reduced × mg of protein⁻¹ × min⁻¹.
[a] OMP, Outer membrane protein.
[b] CMP, Cytoplasmic membrane protein.

Supernatant fluids obtained by FT contained 1.3% of the total SDH activity detected and 2.0% of the total KDO recovered (Table 1). These results suggest that FT did not markedly disrupt either the outer or the inner cell membranes with subsequent release of these markers. Soluble fractions obtained by chemical treatment (chloroform or lysozyme-EDTA) or mechanical disruption (French press) of strain MS-1 cells had comparable proportions of total detectable SDH activity and KDO (Table 1). Most (87%) of the total SDH activity and 90% of the total KDO recovered were in the cytoplasmic and outer membrane fractions, respectively, of strain MS-1 cells (Table 1).

Electrophoretograms of each soluble fraction (Fig. 1, lanes 4 to 7) exhibited similar protein-banding patterns. In each of these fractions, more than 60 proteins were evident, including several major proteins with molecular masses ranging between 28,000 and 85,000 daltons. Four proteins with apparent molecular masses of 29,000, 41,000, 44,500 and 45,000 daltons were unique to the periplasm (Fig. 1, lanes 4 to 7). The cytoplasmic membrane (Fig. 1, lane 3) contained three major proteins (16,500, 56,000, and 85,000 daltons) which were also present in the periplasmic fraction.

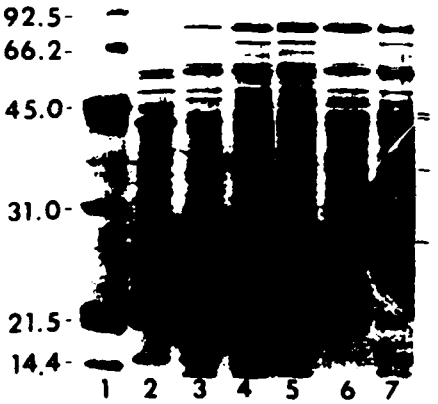

FIG. 1. Silver-stained sodium dodecyl sulfate-polyacrylamide gel electrophoretogram of *A. magnetotacticum* cell proteins. Lanes: 1, molecular mass standards (in kilodaltons); 2, outer membrane fraction; 3, inner membrane fraction; 4, periplasm-cytoplasm fraction; 5, proteins obtained by FT; 6, proteins released by osmotic shock; 7, proteins obtained with lysozyme-EDTA treatment. Each lane contained 3.5 μg of protein. Dashes to the right of the gel indicate proteins restricted to the periplasm.

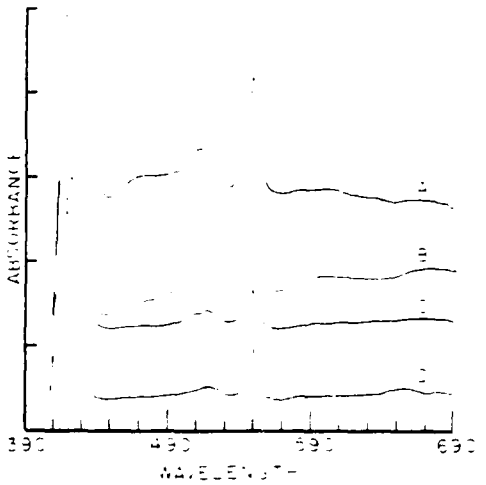

FIG. 2. Difference spectra of reduced soluble proteins minus those of oxidized proteins of *A. magnetotacticum* obtained by fractionation by (A) FT (0.7 mg of protein, absorbance divisions = 0.045), (B) the procedure of Schnaitman (0.9 mg of protein, absorbance divisions = 0.260), (C) chloroform treatment (0.04 mg of protein; absorbance divisions = 0.045), and (D) osmotic shock (0.04 mg of protein, absorbance divisions = 0.010).

The outer membrane (Fig. 1, lane 2) and periplasmic fractions (Fig. 1, lanes 4 to 7) contained few proteins in common.

Soluble fractions obtained by FT, chloroform treatment, osmotic shock, or French press disruption of strain MS-1 cells contained substances with absorption spectra (Fig. 2) typical of *c*-type hemes (maxima at 419, 522, and 551 nm). Spent growth medium and cell-wash fluids of *A. magnetotacticum* concentrated 100-fold did not contain detectable quantities of protein or *c*-type hemoproteins.

The effects of FT on strain MS-1 cells were evaluated by plate assay and electron microscopy. Only 1 to 7% of control (non-FT) cells were recovered as CFU after FT. Survivors were magnetotactic. Freeze-thawed cells which were negatively stained with uranyl acetate and observed by electron microscopy lacked flagella but appeared otherwise structurally intact as compared with control cells. They retained their helical form and did not form spheroplasts or show blebbing.

Our results indicate that FT provides a rapid, simple, reproducible method of selectively releasing periplasmic substances, including the soluble *c*-type hemoproteins, from *A. magnetotacticum* without recourse to chemical treatments.

We have applied FT to *Aquaspirillum itersonii* and *Azospirillum lipoferum* cells and obtained spectral evidence for release of *c*-type hemoproteins from these organisms as well (data not shown). Recently, FT was applied to cells of nine genera of gram-negative bacteria. The method was found to be comparable to the chloroform method (1) for the release of periplasm (B. E. Eribo, S. D. Lall, and J. M. Jay, Abstr. Annu. Meet. Am. Soc. Microbiol. 1987, I152, p. 197).

FT had several advantages over conventional techniques used to obtain periplasm from *A. magnetotacticum*. These include the following: (i) the absence of chemical treatment, such as with lysozyme, chloroform, toluene, or EDTA; (ii) the rapid and selective recovery of periplasmic substances, including enzymes; and (iii) the lack of apparent gross cell damage. This method, if generally applicable to other gram-

negative species, would prove useful in obtaining periplasm with minimal cell handling, e.g., with pathogens.

We thank Yuri Gorby for the electron microscopy.

This research was supported by National Science Foundation grant DMB-8515540 and Office of Naval Research contract N00014-85-K-0502.

LITERATURE CITED

1. **Ames, G. F.-L., C. Prody, and S. Kustu.** 1984. Simple, rapid, and quantitative release of periplasmic proteins by chloroform. J. Bacteriol. **160**:1181–1183.
2. **Blakemore, R. P., D. Maratea, and R. S. Wolfe.** 1979. Isolation and pure culture of a freshwater magnetic spirillum in chemically defined medium. J. Bacteriol. **140**:720–729.
3. **Calcott, P. H., and K. N. Calcott.** 1983. Involvement of outer membrane proteins in freeze-thaw resistance of *Escherichia coli*. Can. J. Microbiol. **30**:339–344.
4. **Calcott, P. H., and R. A. MacLeod.** 1975. The survival of *Escherichia coli* from freeze-thaw damage: permeability barrier damage and viability. Can. J. Microbiol. **21**:1724–1732.
5. **Dobrogosz, W. J.** 1981. Enzyme activity, p. 365–392. *In* P. Gerhardt, R. G. E. Murray, P. N. Costilow, E. W. Nester, W. A. Wood, N. R. Krieg, and G. B. Phillips (ed.), Manual of methods for general bacteriology. American Society for Microbiology, Washington, D.C.
6. **Garrard, W. T.** 1971. Selective release of proteins from *Spirillum itersonii* by Tris(hydroxymethyl)aminomethane and ethylenediaminetetraacetate. J. Bacteriol. **105**:93–100.
7. **Hederstedt, L., and L. Rutberg.** 1981. Succinate dehydrogenase—a comparative review. Microbiol. Rev. **45**:542–555.
8. **Husain, M., and V. L. Davidson.** 1986. Characterization of two inducible periplasmic c-type cytochromes from *Paracoccus denitrificans*. J. Biol. Chem. **261**:8577–8580.
9. **Karkhanis, Y. D., J. Y. Zeltner, J. J. Jackson, and D. J. Carlo.** 1978. A new and improved microassay to determine 2-keto-3-deoxyoctonate in lipopolysaccharide of Gram-negative bacteria. Anal. Biochem. **85**:595–601.
10. **Masuda, K., and T. Kawata.** 1982. Isolation, properties, and reassembly of outer sheath carrying a polygonal array from an oral treponeme. J. Bacteriol. **150**:1405–1413.
11. **Morley, C. R., J. A. Trofymow, D. C. Coleman, and C. Cambardella.** 1983. Effects of freeze-thaw stress on bacterial populations in soil microcosms. Microb. Ecol. **9**:329–340.
12. **Neu, H. C., and L. A. Heppel.** 1965. The release of enzymes from *Escherichia coli* by osmotic shock and during the formation of spheroplasts. J. Biol. Chem. **240**:3685–3692.
13. **Niven, D. F.** 1984. The cytochrome complement of *Haemophilus parasuis*. Can. J. Microbiol. **30**:763–773.
14. **Oakley, B. R., D. R. Kirsh, and N. R. Morris.** 1980. A simplified stain for detecting proteins in polyacrylamide gels. Anal. Biochem. **105**:361–363.
15. **O'Brien, W., L. C. Paoletti, and R. P. Blakemore.** 1987. Spectral analysis of cytochromes in *Aquaspirillum magnetotacticum*. Curr. Microbiol. **15**:121–127.
16. **Paoletti, L. C., and R. P. Blakemore.** 1986. Hydroxamate production by *Aquaspirillum magnetotacticum*. J. Bacteriol. **167**:73–76.
17. **Probst, I., and H. G. Schlegel.** 1976. Respiratory components and oxidase activities in *Alcaligenes eutrophus*. Biochim. Biophys. Acta **440**:412–428.
18. **Richardson, K., and C. D. Parker.** 1985. Identification and characterization of *Vibrio cholerae* surface proteins by radioiodination. Infect. Immun. **48**:87–93.
19. **Schnaitman, C. A.** 1981. Cell fractionation, p. 52–61. *In* P. Gerhardt, R. G. E. Murray, R. N. Costilow, E. W. Nester, W. A. Wood, N. R. Krieg, and G. B. Phillips (ed.), Manual of methods for general bacteriology. American Society for Microbiology, Washington, D.C.

Proc. R. Soc. Lond. B 231, 469–476 (1987)
Printed in Great Britain

Ultrastructure and characterization of anisotropic magnetic inclusions in magnetotactic bacteria

BY S. MANN[1], N. H. C. SPARKS[1] AND R. P. BLAKEMORE[2]

[1] *School of Chemistry, University of Bath, Bath BA2 7AY, U.K.*
[2] *Department of Microbiology, University of New Hampshire, Durham, New Hampshire* 03824, U.S.A.

(*Communicated by R. J. P. Williams, F.R.S. – Received* 18 *February* 1987)

[Plates 1 and 2]

Ovoid magnetotactic bacteria extracted from the Exeter River, New Hampshire, U.S.A., contain chains of 20–35 anisotropic magnetic inclusions running longitudinally in each of three lateral cell positions adjacent to the inner surface of the cytoplasmic membrane. The inclusions are bullet-shaped and have characteristic flattened end faces. Some particles show kinking and curvature in their morphology. In cross section the particles have a hexagonal shape. The length of the inclusions varies over a wide range (45–135 nm) with a mean value of 97.8 nm. In contrast, the width of the particles is restricted to a range of 30–45 nm with a mean value of 36.9 nm. Many particles are surrounded by an organic electron-dense envelope. The crystallographic structure of the inclusions has been determined by electron diffraction and corresponds to the mineral magnetite (Fe_3O_4). The dimensions of the crystals fall within the magnetic single-domain range for magnetite and the magnetic moment of one cell is approximately 4×10^{-12} emu (4 fJT^{-1}).

INTRODUCTION

Magnetotactic bacteria are ubiquitous in aqueous natural environments (Blakemore 1982; Sparks *et al.* 1986) from which they can be readily extracted by using small permanent magnets (Blakemore 1975). A variety of bacteria, including coccal, bacillary, vibroid and helical forms, have been reported (Blakemore 1982; Sparks *et al.* 1986). A characteristic feature of these magnetic organisms is the presence of intracellular electron-dense inclusions, often organized in chains along the long axis of the cell. The mineralogical structure of these inclusions has been determined in three different magnetotactic bacteria (Towe & Moench 1981; Frankel *et al.* 1979; Matsuda *et al.* 1983) and identified as the mixed-valence iron oxide magnetite (Fe_3O_4). The size and orientation of these intracellular magnetite particles, termed 'magnetosomes' (Balkwill *et al.* 1980) impart a permanent magnetic moment to each cell such that the bacteria are aligned in the geomagnetic field. A survey of magnetotactic bacteria found in different geographical locations indicates that cells swim almost exclusively downward in both the Northern (Blakemore & Frankel 1981) and Southern hemispheres (Blakemore *et al.* 1980; Kirschvink 1980).

The crystal morphology of bacterial magnetite has been determined in three organisms (Mann *et al.* 1984*a*, *b*; Matsuda *et al.* 1983). *Aquaspirillum magnetotacticum* synthesizes magnetite particles with a cubo-octahedral habit (Mann *et al.* 1984*a*) which is a conventional abiogenic form for this mineral. In coccoid cells (Mann *et al.* 1984*b*) and cells from an unidentified bacterium (Matsuda *et al.* 1983) the magnetite crystals adopt a parallelepiped morphology based on a hexagonal prism of {110} faces capped by {111} end faces. In contrast, the magnetic inclusions investigated in this paper show extensive anisotropy in their particle shape. The ultrastructure and characterization of these bacteria and their associated inclusions, as reported in this paper, is of fundamental biological importance in the understanding of the regulation of biomineralization processes in bacteria. In addition the unique particle shape, which is not known to be produced by abiogenic processes, indicates that they should be readily identified as being of biogenic origin in marine or freshwater sediments; this has important implications for the study of palaeobiology, palaeomagnetism and magnetostratigraphy. The nature of the inclusions is also of immediate interest to chemists and materials scientists involved in the production of crystallochemically specific materials for magnetic and catalytic application.

Materials and methods

Magnetotactic bacteria containing anisotropic magnetosomes were extracted from samples of sediment and water taken from the Exeter River, New Hampshire, U.S.A. The samples were incubated for 2 months in dim light at ambient temperature. The organisms were then separated from the sediment by using a permanent magnet, and the concentrated cells were washed once by centrifugation with filter-sterilized river water. They were then immediately fixed in 50 mM cacodylate buffer.

One drop of a cell suspension containing 1 ml river water and 0.5 ml of 50 mM cacodylate buffer was air-dried onto nitrocellulose-coated, carbon-coated, copper or nickel 3.05 mm electron microscope grids (Agar Aids). Intact cells were studied unstained or after staining with uranyl acetate. Magnetic inclusions were studied either *in situ* or after hypochlorite digestion (5% (by mass) NaOCl for 20 min at room temperature followed by washing with distilled water) of the cells air-dried onto electron-microscope grids.

Analytical transmission electron microscopy

Intact, digested and sectioned cells were investigated by using a Jeol 100CX analytical electron microscope operating at 100 keV and a Jeol 2000FX transmission electron microscope operating at 200 keV. Electron-diffraction patterns were recorded in the selected area mode. Energy-dispersive X-ray analysis (EDXA) of individual magnetic particles, either within intact cells or after hypochlorite digestion, was undertaken in the STEM mode with a Link Li-drifted, silicon detector set at 40° to the sample area. The analysis time was 100 s.

Dimensions of the magnetic particles were measured from TEM micrographs recorded at 0° tilt angle by using a vernier caliper. At least 50 particles were measured.

Sectioned cells

Cells were prepared for thin sectioning by standard procedures. A cell suspension was pelleted by centrifugation and treated with 4% (by volume) glutaraldehyde in 0.1 M cacodylate buffer for 18 h at 4 °C. The pellet was then washed twice in 0.1 M cacodylate buffer, fixed with 0.1 M osmium tetroxide for 1 h at room temperature, dehydrated in a series of acetone solutions (final solution of 100% acetone) and embedded in Taab (medium) resin. Sections (0.5–1.0 μm) were cut on a Reichert UMO3 ultramicrotome with glass knives and mounted on copper electron-microscope grids. Sections were post-stained with uranyl acetate (saturated solution in 70% (by volume) ethanol) and Reynolds lead citrate (4 g l^{-1}).

Results

Cell morphology and ultrastructure

The samples examined contained several species of magnetotactic bacterium. However, one sample became specifically enriched in ovoid cells with dimensions *ca.* 3 μm × 2 μm and with multiple sheathed flagella situated at one pole (figure 1, plate 1). Thin-sectioned material showed that the cell envelope comprised an outer membrane, with was often markedly convoluted when compared with an inner cytoplasmic membrane (figure 2, plate 1). High-magnification images indicated that the outer membrane had a trilaminate structure of the Gram-negative type. The electron-transparent periplasmic region varied considerably in dimensions (figure 2) and may represent distortion during sample preparation. These bacteria, as well as those of similar morphology collected elsewhere in New Hampshire and Vermont, U.S.A., contained magnetosomes of anisotropic morphology.

Electron-dense inclusions

The anisotropic, bullet-shaped, electron-dense magnetosomes were organized in one or more chains running longitudinally in each of three lateral cell positions (figure 1). Each chain contained 20–35 particles, of which the majority (greater than 70%) were aligned 'head-to-tail' in intact cells. In sectioned cells, however, the particles were often misoriented, presumably owing to cutting and dehydration artifacts. The chains were in close proximity to the inner surface of the cytoplasmic membrane (figure 2).

The inclusions had flattened ends oriented towards the flagellated pole of the cell and often showed curvature and kinking along their length (figures 3 and 4, plate 2). Particles viewed in cross section appeared to be rounded pseudo-hexagonal prisms with approximately equal width and thickness (figure 5, plate 2). The length of the mature particles varied over a wide range (45–135 nm) with a median value of 98.4 nm and a mean length of 97.8 nm with a standard deviation of 19.95 nm (figure 6). In contrast, the maximum width of the mature inclusions was extremely uniform (30–45 nm) with a median value of 37.9 nm and a mean of 36.9 nm with a standard deviation of 2.82 nm (figure 7).

Magnetosomes imaged in stained sectioned cells showed the presence of an electron-dense layer, *ca.* 1 nm thick, surrounding the particles (figure 8, plate 2). The layers were separated from the particle surface by a distance of *ca.* 3 nm. This

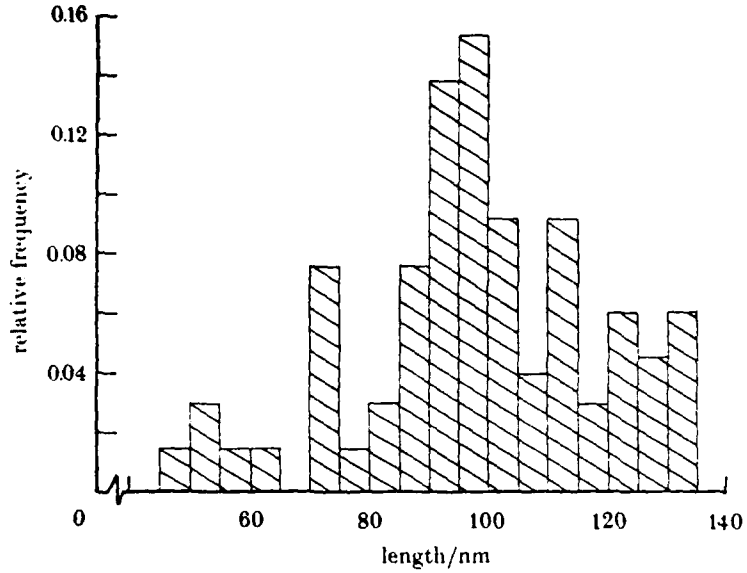

FIGURE 6. Histogram of particle lengths for mature inclusions.

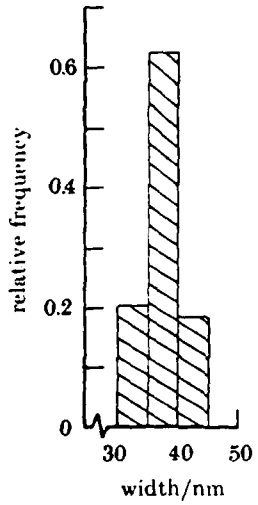

FIGURE 7. Histogram of particle widths for mature inclusions.

substructural detail was often not visible and appears to be very sensitive to sample preparation. No electron-dense structures were observed linking adjacent particles.

Mineral identification was undertaken with EDXA and selected-area electron diffraction. Compositional information from EDXA on individual particles showed that, for elements above Na in atomic number, only Fe was present (figure 9). Selected-area electron-diffraction patterns were recorded on many crystals and identified the mineral as magnetite (Fe_3O_4, *space group* $Fd3m$: $a = 8.396$ Å†)

† 1 Å = 10^{-10} m = 10^{-1} nm.

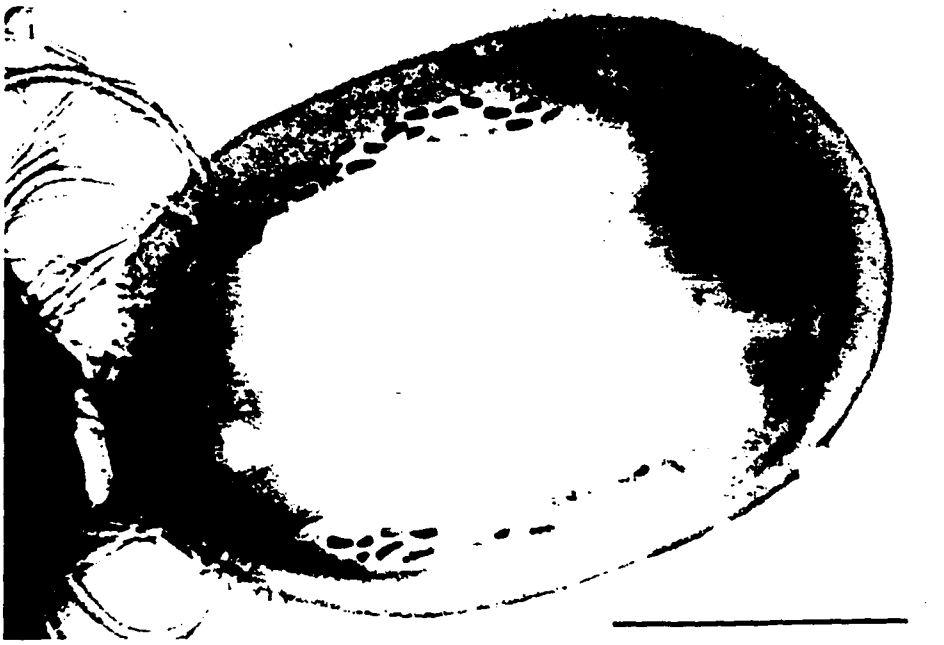

FIGURE 1. Uranyl-acetate-stained intact magnetotactic bacterium of the type described in this study. Elongated electron-dense magnetosomes are organized in longitudinal chains at three lateral positions in the cell; there are multiple sheathed flagella at one end of the cell. Scale bar 1 μm.

FIGURE 2. Transmission electron micrograph of a stained, thin-sectioned magnetotactic bacterium containing anisotropic magnetic inclusions. Abbreviations: om, outer membrane; pr, periplasmic region; cm, cytoplasmic membrane; mi, magnetic inclusions. Scale bar 1 μm.

(*Facing p.* 472)

FIGURE 3. Transmission electron micrograph of magnetic inclusions isolated from digested cells. The arrow shows a magnetosome with a flattened end-face. Electron diffraction patterns of the particles identified them as magnetite, Fe_3O_4 (table 1). Scale bar 100 nm.

FIGURE 4. Magnetic inclusion showing curvature in its growth morphology. Scale bar 10 nm.

FIGURE 5. Magnetic inclusion viewed in cross-section within a thin-sectioned cell, showing a rounded pseudohexagonal morphology. Scale bar 20 nm.

FIGURE 8. Transmission electron micrograph of a stained, thin-sectioned magnetotactic bacterium, showing the presence of electron-dense substructures (arrows) surrounding the magnetic inclusions. Scale bar 100 nm.

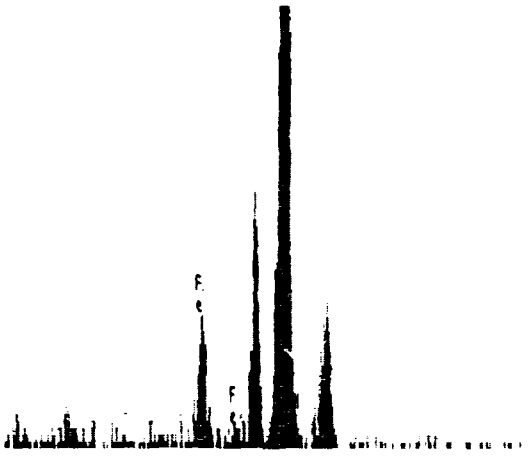

FIGURE 9. EDXA spectrum for magnetic inclusions. Cu and Ni peaks arise from the sample holder and electron microscope grid respectively. Only Fe was detected in the particles.

(table 1). Several crystals gave electron-diffraction patterns indicative of single-domain crystals. Information about the structural and morphological nature of these crystals at the nanometre level has been obtained from high-resolution transmission electron microscopy and is reported elsewhere (Mann *et al.* 1987).

TABLE 1. ELECTRON DIFFRACTION DATA FOR BACTERIAL INCLUSIONS
(*d* SPACINGS IN ÅNGSTRÖMS)

bacterial particles	magnetite (standard)[a]	Miller indices
4.88	4.85	(111)
2.99	2.967	(220)
2.54	2.532	(311)
2.12	2.099	(400)
1.75	1.715	(422)
1.59	1.616	(511)
1.49	1.485	(440)
1.10	1.093	(731)
1.06	1.050	(800)

[a] ASTM card 19–629.

DISCUSSION

This paper has described the ultrastructure and characterization of anisotropic mineral inclusions formed within the cells of a freshwater magnetotactic bacterium. The general organization of these magnetosomes within the cells is similar to that of other bacteria exhibiting a magnetotactic response to the geomagnetic field (Blakemore 1982; Balkwill *et al.* 1980). The crystals are organized in chains at three lateral positions adjacent to the inner surface of the cytoplasmic membrane. Each chain contains between 20 and 35 elongated bullet-shaped particles, with the crystal long axes lying approximately parallel to the cell length. This

arrangement establishes an optimum coupling of the motive force generated by the flagella to the torque that arises because the cells' magnetic axes are not oriented parallel to the geomagnetic field. Consequently, cells swim preferentially downwards towards a microaerobic environment. If the magnetic moment for each particle is aligned in the same direction (Frankel & Blakemore 1980), then the total magnetic moment of the cell is equal to the sum of the moments of all the particles. Magnetite has a saturation magnetization of 480 emu cm^{-3}†. Therefore the magnetic moment of an average-size anisotropic crystal (100 nm × 35 nm × 35 nm) is 5.5×10^{-14} emu. This value is close to that calculated for 50 nm isotropic magnetite crystals produced by the magnetotactic spirillum *A. magnetotacticum* (6×10^{-14} emu) (Frankel & Blakemore 1980; Frankel 1984). However, the presence of three chains of anisotropic crystals per cell in the organisms studied in this paper, in contrast to the single central chain formed in *A. magnetotacticum* cells (and many coccoid cells), generates a larger magnetic moment per bacterium (4.15×10^{-12} emu, assuming an average total of 75 particles per cell, as compared with 1.2×10^{-12} emu for 20 isotropic magnetosomes in spirillum cells). This difference is insignificant when compared with the value of 6.7×10^{-10} emu for the average magnetic moment of a magnetotactic alga recently obtained from a coastal mangrove swamp in northeastern Brazil (Torres de Araujo *et al.* 1986). Presumably the greater size of the algal cell, and the correspondingly increased viscous drag, requires a much larger magnetic moment per cell for effective geomagnetic navigation.

The dimensions of the magnetite crystals reported in this paper fall within the magnetic single-domain size range predicted by Butler & Banerjee (1975). This range represents the most magnetically efficient particle sizes. The low width: length axial ratio (0.25–0.3 for mature crystals) and corresponding shape anisotropy enables magnetic single-domain particles to be formed with lengths up to 135 nm, in contrast to isotropic bacterial magnetites, which are limited to a maximum length of 80 nm before the crystals adopt multidomain magnetic structures. Because all the bacterial magnetosomes studied to date fall within the magnetic single-domain size range, it appears that the biological organization and regulation of magnetite synthesis in bacteria are specifically related to functional properties of the magnetotactic response.

Many of the anisotropic crystals are surrounded by an electron-dense organic envelope. Similar substructures have been observed in other magnetotactic bacteria (Towe & Moench 1981; Balkwill *et al.* 1980; Y. A. Gorby & R. P. Blakemore, unpublished results) and it seems most probable that such a boundary plays an important spatial and chemical role in magnetite biomineralization (Mann 1985). However, although this feature is considered to be common to all magnetotactic bacteria, the precise crystallochemical processes which are biologically mediated within the organic boundary appear to be species-specific, resulting in a variety of crystal sizes and morphologies.

Recent reports (Peterson *et al.* 1986; Stolz *et al.* 1986) have implicated bacterial magnetite as a major source of stable remanent magnetism in marine sediments.

† 1 emu = 1 erg G^{-1} = 10^{-3} JT^{-1}.

Many of the crystals observed were cuboidal and rectangular in projection, morphologies which are characteristic of bacterial magnetite (Mann *et al.* 1984*a*, *b*) but which have similar abiogenic counterparts. However, the observation of bullet-shaped particles in these sediments indicates with certainty a biogenic contribution to the palaeomagnetic record. The identification of similar particles in extant bacteria as magnetite confirms the interpretation of magnetic coercivity spectra of marine sediments and unequivocally establishes the presence of bacterial magnetite in marine sediments. The unique morphology of such crystals should be a valuable marker in palaeontology and palaeomagnetic studies.

The magnetotactic bacteria described in this paper have the inherent ability to synthesize a mineral with an isotropic crystallographic symmetry in the form of anisotropic particles. This observation is intriguing in terms of the crystallization processes which must be mediated by the cell to provide this unusual phenomenon. The elucidation of the nucleation and crystal-growth properties of these crystals has been studied by high-resolution transmission electron microscopy and is reported elsewhere (Mann *et al.* 1987).

We thank Dr R. G. Board, University of Bath, for comments on reading the manuscript, and N. A. Blakemore for providing samples of the organism. Financial support for electron-microscopy facilities and for N.H.C.S. was from SERC. R.P.B. was supported by NSF grant DMB 85-15540 and U. S. Naval Research contract no. 0014-85-K-0502.

References

Balkwill, D. L., Maratea, D. & Blakemore, R. P. 1980 Ultrastructure of a magnetotactic spirillum. *J. Bact.* **141**, 1399–1408.

Blakemore, R. P. 1975 Magnetotactic bacteria. *Science, Wash.* **190**, 377–379.

Blakemore, R. P. 1982 Magnetotactic bacteria. *A. Rev. Microbiol.* **36**, 217–238.

Blakemore, R. P. Frankel, R. B. & Kalmijn, A. J. 1980 South-seeking magnetotactic bacteria in the southern hemisphere. *Nature, Lond.* **286**, 384–385.

Blakemore, R. P. & Frankel, R. B. 1981 Magnetic navigation in bacteria. *Scient. Am.* **245**, 42–49.

Butler, R. F. & Banerjee, S. K. 1975 Theoretical single domain grain size range in magnetite and titanomagnetite. *J. geophys. Res.* **80**, 4049–4058.

Frankel, R. B. 1984 Magnetic guidance of organisms. *A. Rev. Biophys. Bioengng* **13**, 85–103.

Frankel, R. B., Blakemore, R. P. & Wolfe, R. S. 1979 Magnetite in freshwater magnetotactic bacteria. *Science, Wash.* **203**, 1355–1356.

Frankel, R. B. & Blakemore, R. P. 1980 Navigational compass in magnetic bacteria. *J. Magn. magn. Mater.* **15–18**, 1562–1564.

Kirschvink, J. L. 1980 South-seeking magnetite bacteria. *J. exp. Biol.* **86**, 345–347.

Mann S. 1985 Structure, morphology and crystal growth of bacterial magnetite. In *Magnetite biomineralization and magnetoreception in organisms* (ed. J. L. Kirschvink, D. S. Jones & B. J. MacFadden), pp. 311–332. New York: Plenum Press.

Mann, S., Frankel, R. B. & Blakemore, R. P. 1984*a* Structure, morphology and crystal growth of bacterial magnetite. *Nature, Lond.* **310**, 405–407.

Mann, S., Moench, T. T. & Williams, R. J. P. 1984*b* A high-resolution electron microscopic investigation of bacterial magnetite. Implications for crystal growth. *Proc. R. Soc. Lond.* B **221**, 385–393.

Mann, S., Sparks, N. H. C. & Blakemore, R. P. 1987 Structure, morphology and crystal growth of anisotropic magnetite crystals in magnetotactic bacteria. *Proc. R. Soc. Lond.* B231, 477–487. (Following paper.)

Matsuda, T., Endo, J., Osakabe, N. & Tonomura, A. 1983 Morphology and structure of biogenic magnetite particles. *Nature, Lond.* **302**, 411–412.

Peterson, N., von Dobeneck, T. & Vali, H. 1986 Fossil bacterial magnetite in deep-sea sediments from the South Atlantic Ocean. *Nature, Lond.* **320**, 611–615.

Sparks, N. H. C., Courtaux, L., Mann, S. & Board, R. G. 1986 Magnetotactic bacteria are widely distributed in sediments in the U.K. *FEMS Microbiol. Lett.* **37**, 305–308.

Stolz, J. F., Chang, S. R. & Kirschvink, J. L. 1986 Magnetotactic bacteria and single-domain magnetite in hemipelagic sediments. *Nature, Lond.* **321**, 849–851.

Torres de Araujo, F. F., Pires, M. A., Frankel, R. B. & Bicudo, C. E. M. 1986 Magnetite and magnetotaxis in algae. *Biophys. J.* **50**, 375–378.

Towe, K. M. & Moench, T. T. 1981 Electron-optical characterization of bacterial magnetite. *Earth planet. Sci. Lett.* **52**, 213–220.

Proc. R. Soc. Lond. B 231, 477–487 (1987)
Printed in Great Britain

Structure, morphology and crystal growth of anisotropic magnetite crystals in magnetotactic bacteria

BY S. MANN[1], N. H. C. SPARKS[1] AND R. P. BLAKEMORE[2]

[1] *School of Chemistry, University of Bath, Bath BA2 7AY, U.K.*
[2] *Department of Microbiology, University of New Hampshire, Durham, New Hampshire* 03824, *U.S.A.*

(*Communicated by R. J. P. Williams, F.R.S. – Received* 18 *February* 1987)

[Plates 1–4]

Bacterial magnetite particles of anisotropic morphology have been studied by high-resolution transmission electron microscopy. Lattice images of individual crystals are consistent with a well-ordered magnetite cubic inverse spinel structure. The idealized morphology of the biogenic crystals is based on an elongated cubo-octahedral form comprising a hexagonal prism of {111} and {100} faces capped by $(\bar{1}\bar{1}1)$ and $(11\bar{1})$ faces with associated {111} and {100} truncations. Analysis of many particles of diverse size suggests that crystal growth takes place in two stages. The first stage is associated with the formation of well-ordered, isotropic, single-domain crystals of cubo-octahedral morphology. In this stage the crystal length and width develop concurrently up to a size of 20 nm. The second stage involves the anisotropic growth of the isotropic particles along the $[11\bar{2}]$ direction. A crystal growth mechanism is postulated which involves the specific nucleation of the $(\bar{1}\bar{1}1)$ face on a surrounding organic membrane. Unidirectional growth then occurs by selective suppression of certain crystallographic axes through spatial and chemical constraints induced by the adjacent organic boundary.

INTRODUCTION

The bioprecipitation of intracellular magnetic materials, such as the mixed-valence iron oxide magnetite (Fe_3O_4) within magnetotactic bacteria, appears to involve highly reproducible and species-dependent crystallochemical processes and illustrates the molecular specificity inherent in many biomineralization reactions. The elucidation of crystal growth mechanisms within biological environments is therefore not only relevant in the advancement of our understanding of the biological mediation of inorganic solid-state reactions but is also of potential significance in the wider field of crystal growth technology and materials science. In a recent paper (Mann *et al.* 1987) we reported the ultrastructure and characterization of elongated bullet-shaped magnetite inclusions (magnetosomes) formed within ovoid magnetotactic bacteria isolated from sediment and water taken from the Exeter River, New Hampshire, U.S.A. The particles are formed in one or more chains, each situated in three lateral positions in the cell. This organization of the magnetosomes results in a permanent magnetic moment's

being imparted to the cell such that the organism orientates in the geomagnetic field as described for other magnetotactic bacteria (Frankel 1984).

The anisotropic nature of the magnetite crystals synthesized by these bacteria is of particular interest. Magnetite has an inverse spinel structure based on a cubic close-packed arrangement of oxygen atoms with Fe^{II} atoms in octahedral sites and Fe^{III} atoms equally distributed between both tetrahedral and octahedral interstices. The cubic symmetry of this structural arrangement (space group $Fd3m$, $a = 8.396$ Å†) is exhibited in the isotropic nature of the crystal habit, with the common inorganic forms being based on octohedral, rhombododecahedral and cubic geometries. Bacterial magnetites, in contrast, have species-specific morphologies; to date, crystals with cubo-octahedral (Mann *et al.* 1984*a*), and hexagonal (Mann *et al.* 1984*b*; Matsuda *et al.* 1983) habits have been determined. The anisotropic magnetite particles described in this paper represent a highly unusual morphological form which is generated from crystals of inherent isotropic symmetry. Our interest lies primarily with the elucidation of the crystal growth mechanisms of these biogenic particles, because an understanding of the processes of biological mediation is important in the replication of similar crystal morphologies in inorganic systems involving catalytic or magnetic applications.

Here we report the crystallochemical nature of anisotropic magnetite crystals isolated from magnetotactic bacteria as determined from high-resolution transmission electron microscopy (HRTEM). Our aim has been to determine the structural perfection, morphology and processes of crystal nucleation and growth of these crystals within a biological environment. The results are discussed in light of previous HRTEM studies of other magnetotactic bacteria, and a general rationalization of magnetosome crystal development in bacteria is presented.

Materials and methods

Magnetotactic bacteria containing anisotropic magnetite inclusions were isolated from samples of sediment and water taken from the Exeter River, New Hampshire, U.S.A. as reported previously (Mann *et al.* 1987). Intact unstained magnetotactic bacteria were air-dried onto nitrocellulose covered, carbon-coated 2.3 mm and 3.05 mm copper electron microscope grids, as described previously (Mann *et al.* 1987). Unfortunately, intact cells were too thick for successful *in situ* lattice imaging of the inclusions; therefore, isolated crystals were studied after digestion of the air-dried cells with 5% (by mass) sodium hypochlorite followed by washing with distilled water. The electron microscopes used were a Jeol 200CX electron microscope, fitted with a high-brightness LaB_6 cathode, and a Jeol 2000FX electron microscope fitted with a tungsten filament. All experiments were carried out at 200 keV with objective apertures of 40 and 80 μm, capable of 2.5 and 2.8 Å point-to-point resolutions respectively.

† 1 Å = 10^{-10} m = 10^{-1} nm.

Results

(a) *Crystallographic properties of mature crystals*

Lattice images of individual crystals showed fringe spacings corresponding to {111}, {222}, {200}, {211} and {220} lattice planes of magnetite; d spacings and angles between fringes viewed along the same crystal projection were consistent with the cubic space group of magnetite (figure 1). Computational calculations of the projected charge density (Skarnulis 1979) for a stoichiometric magnetite structure under conditions of known crystal thickness and defocus matched the experimental images obtained from the electron microscope (figure 1, plate 1). Lattice fringes were well-defined, continuous and regularly spaced throughout the mature particles; these characteristics indicated that the particles were single-domain crystallites of high perfection (figure 2, plate 1). No evidence was obtained for the presence of extensive structural defects or for twin or intergrowth boundaries. Many crystals imaged along [1$\bar{1}$0] showed a high degree of order on the (111) and ($\bar{1}\bar{1}\bar{1}$) edges (see below for morphological indexing) such that surface steps in these planes could be clearly revealed (figure 4, plate 3).

The identification of different sets of lattice spacings and their corresponding angular relations within a given zone projection enabled an idealized morphology of the crystallites to be determined. In the [1$\bar{1}$0] projection the particles showed a characteristic flattened 'top' end, which ran parallel to the ($\bar{1}$1) fringes of the image, thereby identifying the corresponding face of this edge as ($\bar{1}$1) (figure 3, plate 2). Similarly, the approximately parallel long edges of the crystals viewed along [1$\bar{1}$0] were identified as well-ordered (111) and ($\bar{1}\bar{1}$1) faces (figure 3). Although other crystal faces lying parallel to [1$\bar{1}$0] were not so readily identified, the (001) face was occasionally observed running at an angle of 125° to the top end ($\bar{1}$1) face. In other projections the (200) fringes were imaged running parallel to the crystal long axis, forming well-defined edges along this direction (figure 2). These results can be rationalized in terms of an idealized three-dimensional morphology based on a cubo-octahedral habit with extensive elongation of four of the eight {111} faces and two of the six {100} faces (figure 5). The resulting crystal morphology is a hexagonal prism of elongated {111} and {100} faces capped by ($\bar{1}$1) and (11$\bar{1}$) faces with associated {111} and {100} truncations. The hexagonal cross section of the crystals has been observed by transmission electron microscopy of thin-sectioned cells (Mann *et al.* 1987).

The representation shown in figure 5 has been indexed according to a cubic crystal system and the 'top' end face has been arbitarily assigned the index ($\bar{1}$1). Figure 5 also shows the [1$\bar{1}$0] zone axis, which lies perpendicular to the line of intersection of the ($\bar{1}$1) and ($\bar{1}\bar{1}$) planes. The corresponding projection along [1$\bar{1}$0] is drawn in figure 6. The long axis of the crystal which lies perpendicular to the [111] vector is identified as [11$\bar{2}$].

We emphasize again that figure 5 is a representation of an idealized crystallographic morphology for the bacterial-cell magnetite inclusions. It does not depict the fact that most mature crystals had irregular edges and tapered in width toward their basal end. However, the top ($\bar{1}$1) and side (111) and ($\bar{1}\bar{1}$) edges (imaged in the [1$\bar{1}$0] zone), particularly towards the basal end of the crystals, often

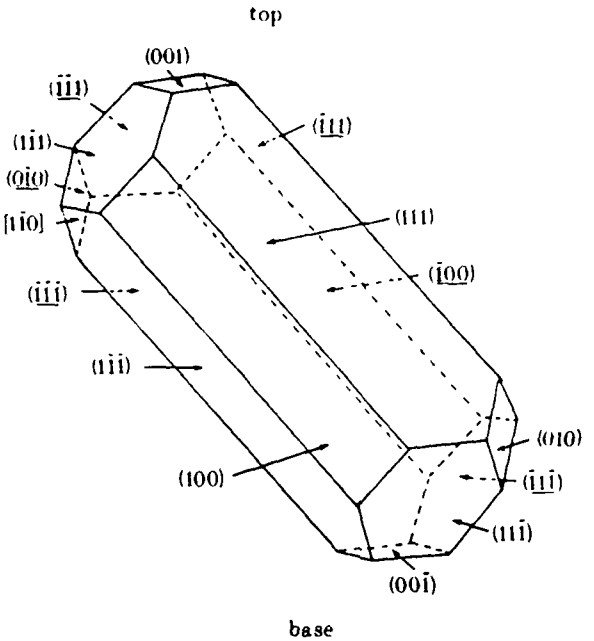

FIGURE 5. Idealized crystal morphology for anisotropic magnetite crystals. Back faces are delineated by dashed lines and identified by underlined indices. (See text for details.)

showed characteristically well-defined faces (figure 3). In some crystals the above faces were well formed but were interconnected within particles showing kinks or curvature in their growth form (figure 7, plate 3).

(*b*) *Crystal nucleation and growth*

The nucleation and anisotropic growth of the above magnetite crystals have been elucidated from lattice imaging studies of immature crystals and dimensional analysis of crystals at different stages of development. Measurements of crystal length and maximum width at different stages of growth (figure 8) showed that the crystals develop initially with concurrent increases in width and length up to a size

DESCRIPTION OF PLATES 1 AND 2

FIGURE 1. HRTEM micrograph of an individual anisotropic bacterial magnetite crystal. The enlarged image is of the [1ī0] zone of magnetite. Lattice spacings corresponding to the (1ī1) (4.85 Å), (11ī) (4.85 Å) and (002) (4.2 Å) planes, oriented at 110° and 125° to each other respectively, are shown. Inset shows a calculated image of the projected charge potential at a defocus value of −65 nm for a crystal of thickness 12 nm. Scale bar 3 nm.

FIGURE 2. Lattice image of an individual magnetite single crystal showing (200) planes running parallel to the long axis of the crystal. Note the flattened top end of the crystal and the regularity and continuity of the lattice planes. Scale bar 10 nm.

FIGURE 3. Individual anisotropic single crystal of bacterial magnetite imaged along [1ī0]. Lattice fringes imaged are the same as for figure 1. The top edge corresponds to the (1ī1) face and the well-formed side edges are the (111) and (1ī1ī) faces respectively. See figures 5 and 6 for diagrammatical representations. Scale bar 10 nm.

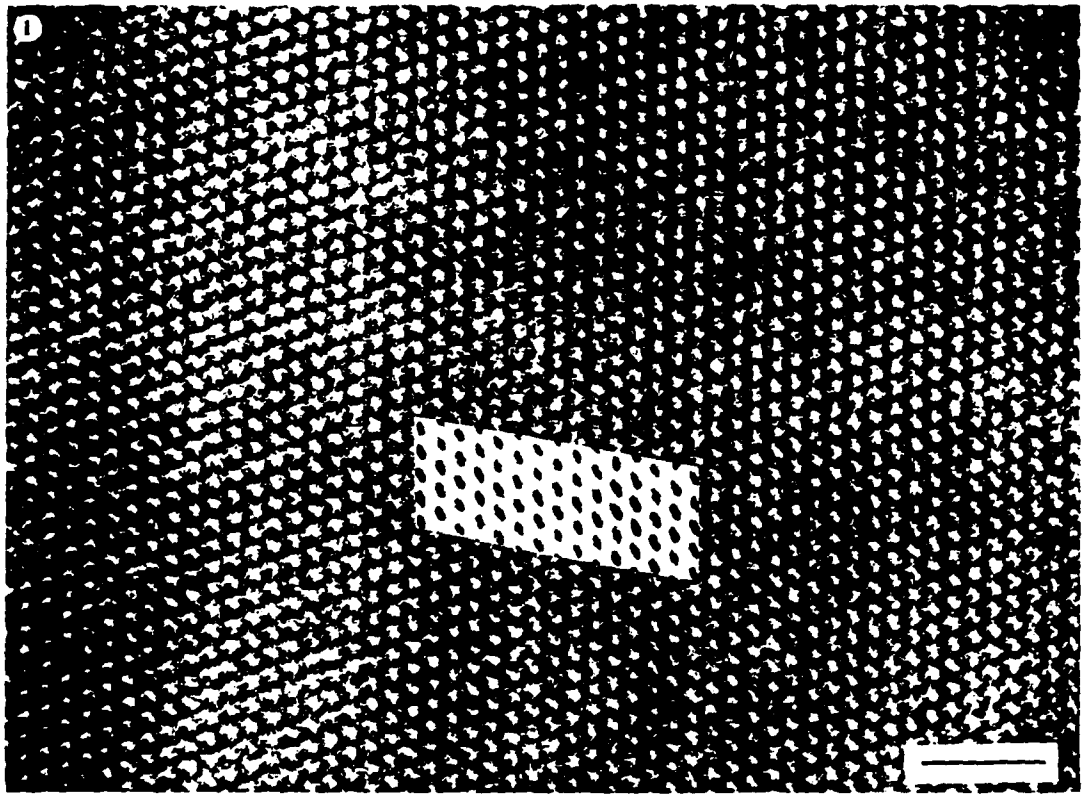

FIGURES 1 AND 2. For description see opposite. *(Facing p. 480)*

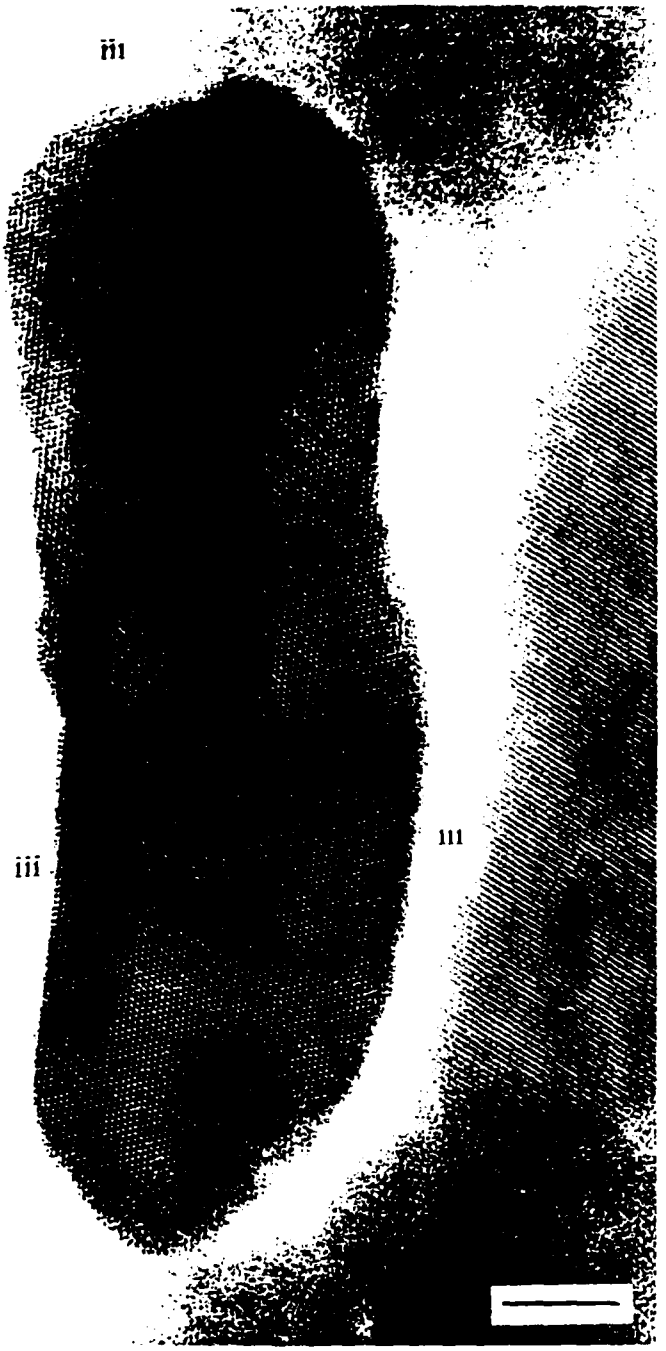

FIGURE 3. For description see p. 480.

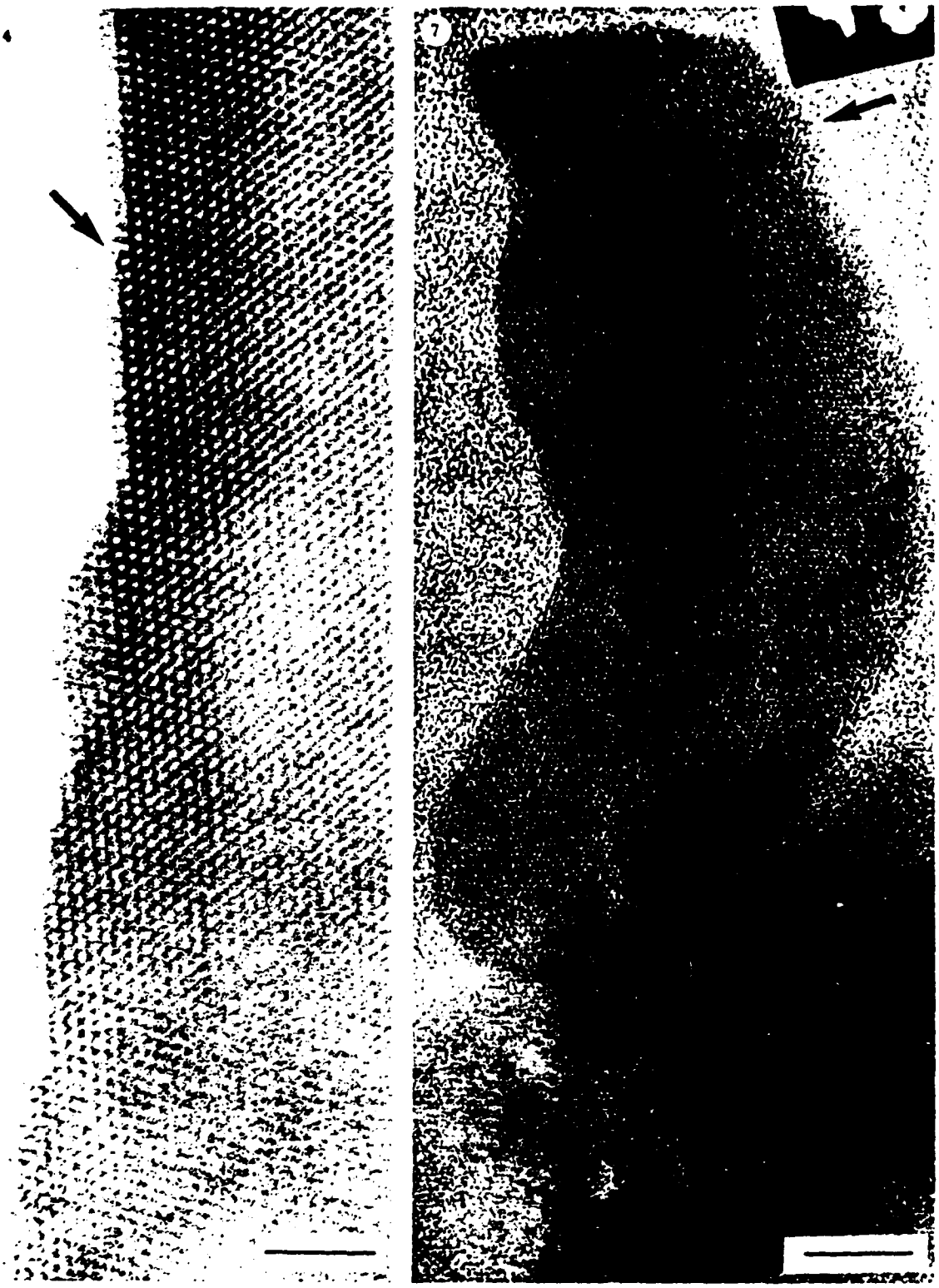

FIGURES 4 AND 7. For description see p. 481.

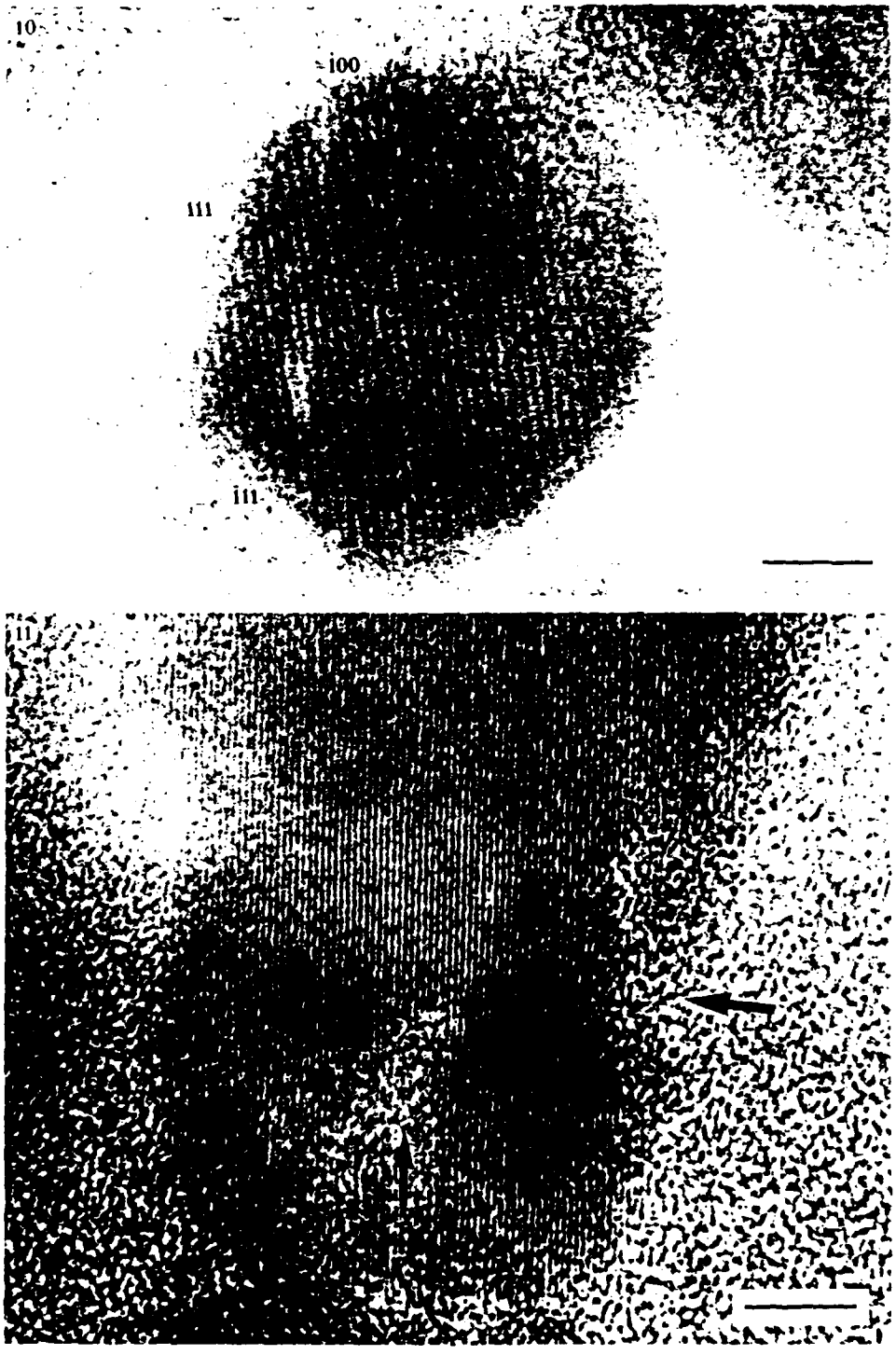

FIGURES 10 AND 11. For description see opposite.

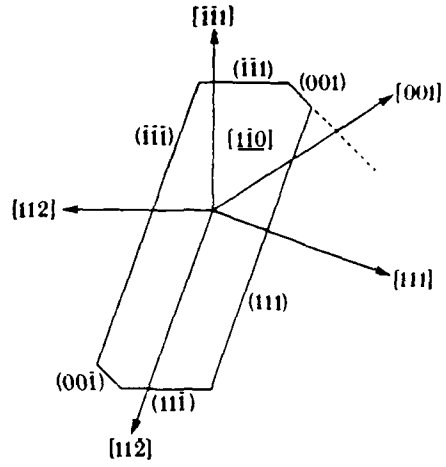

FIGURE 6. Projection of the idealized morphology for bacterial magnetite crystals along the [1$\bar{1}$0] projection. The long axis of the crystal corresponds to [11$\bar{2}$].

of 20 nm, after which the length of the crystals increases at a greater rate than the width. For particles greater than 50 nm in length there was no corresponding further increase in particle width with increase in length. Widths at this stage had a constant spread of values between 30 and 40 nm. The immature crystals are therefore formed as isotropic particles (width : length ratio = 1.0) up to a size of 20 nm, after which the width : length ratio continually decreases to values in the range 0.25–0.3 for mature particles. In accordance with these data the representation of the measured lengths and widths of mature crystals plotted as a histogram (Mann *et al.* 1987) clearly indicate that the widths of the mature particles are dimensionally constrained whereas the lengths may be within a wide range of values (65–135 nm).

Dimensional analysis was also used to determine the growth characteristics of mature particles exhibiting kinking in their crystal habit. Measurements were

DESCRIPTION OF PLATES 3 AND 4

FIGURE 4. Enlarged lattice image of the ($\bar{1}\bar{1}$1) edge of the crystal shown in figure 3. The edge is atomically flat in the basal region of the crystal except for a surface step of height 4.85 Å (arrow). In contrast, the top area of the particle has an irregular ($\bar{1}\bar{1}$1) edge. Scale bar 4 nm.

FIGURE 7. Lattice image of a bacterial crystal, imaged along [1$\bar{1}$0] and showing curvature in the growth morphology. Lattice fringes correspond to the ($\bar{1}\bar{1}$1), (111) and (002) planes (see figure 1 for details). The particle is a well-ordered single crystal with the characteristic ($\bar{1}\bar{1}$1) top face. In this crystal the development of the side (111) and ($\bar{1}\bar{1}\bar{1}$) faces appears to be inhibited; in consequence, the top (001) face is well developed (arrow). Scale bar 10 nm.

FIGURE 10. Lattice image of an immature bacterial magnetite crystal of isotropic dimension. Lattice fringes correspond to (330) (4.44 Å) planes. (These planes, although systematically absent occur due to double diffraction). Crystal edges are indexed with angles corresponding to the [01$\bar{1}$] projection. Scale bar 4 nm.

FIGURE 11. Enlarged lattice image of the basal end of a mature crystal showing structural disorder (arrows) along (220) lattice planes. Scale bar 5 nm.

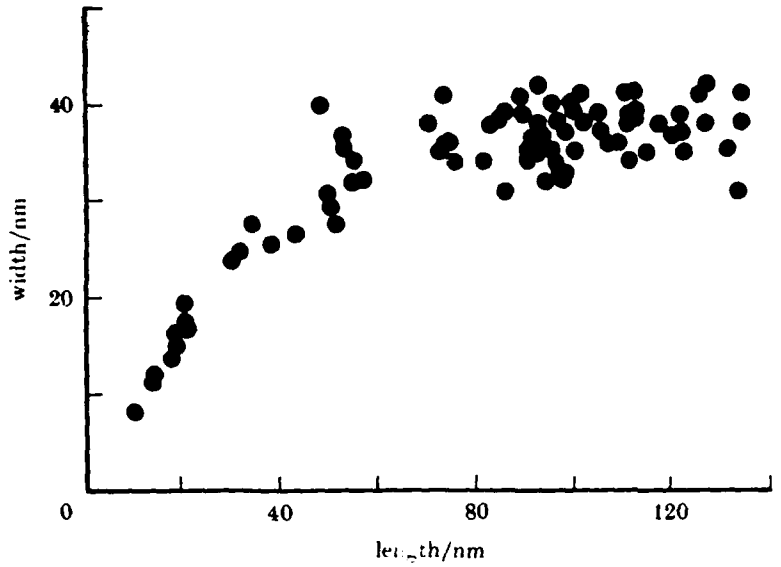

FIGURE 8. Plot of crystal length against crystal width for crystals at different stages of development.

made of the width of the top (111) face and the length from this face to the kink position and kink:width ratios were calculated (figure 9). Although there are significant errors in these measurements, owing to difficulties in determining the exact position of kinking (for example, in crystals oriented in different directions or for those showing curvature) analysis of histograms indicated that 67% of the crystals measured had width:kink length ratios in the range 0.96–1.46. Because the width of mature crystals is at a maximum and constrained to a narrow size range, the mean value of 1.21 for this ratio suggests that kinking in many crystals appears to be associated with the onset of anisotropic development.

Lattice imaging studies confirmed the isotropic nature of the immature crystals and revealed the morphological and structural characteristics of the initial mineral phase deposited. Figure 10 (plate 4) shows a lattice image of an immature isotropic particle of diameter 15 nm (approximately 18 unit-cell lengths). Regular (330) fringes can be observed traversing the particle; this observation indicates that the crystal is well defined at this early post-nucleation stage. The angles between this set of fringes and the crystal edges correspond to a particle imaged along the $\langle 110 \rangle$ projection such that the well-defined edges shown in figure 10 can be indexed. The two edges orientated at 110° to each other are {111} faces running perpendicular to the plane of the micrograph. A small (100) face can also be identified oriented at 125° to the (111) face and perpendicular to the (330) fringes. A (311) face lies at *ca.* 80° to the ($\bar{1}11$) face; however, this high-index face was not often seen in other micrographs. The results indicate that the early particles have a morphology essentially based on a cubo-octahedral geometry.

Particles as small as 10 nm were successfully imaged as well-ordered cubo-octahedral single-domain crystals. There were very few particles below this size;

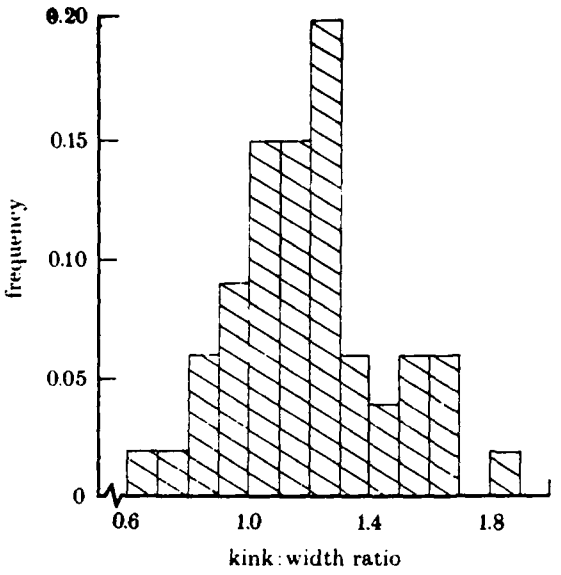

FIGURE 9. Histogram plot of the kink : width ratio for mature crystals.

this result suggests that such particles may have been dissolved or removed from the grid during the hypochlorite digestion procedure. Some crystals showed outer regions which were irregular and amorphous. It is not clear whether these results arise from particles oriented with a slight misalignment with respect to the electron beam or from real non-crystalline domains. However, no extensive regions of amorphous material were observed within these particles, in contrast with the immature magnetite crystals of spirillum cells (Mann *et al.* 1984*a*) in which non-crystalline and crystalline regions coexist within individual particles.

Figures 2–4 indicate that the development of the immature crystals proceeds such that the structural integrity of the magnetite particles is highly maintained. The very few inclusions which showed evidence for structural disorder were mature crystals in which the tapered basal end of the crystal was ill defined (figure 11, plate 4). In such cases, lattice fringes did not run to the edge of the particles and were discontinuous in localized internal regions of the mineral; these results suggest the presence of amorphous material within or overlying the bulk magnetite structure.

DISCUSSION

Although the biological organization and function of the mineral inclusions of diverse magnetotactic bacteria could have a common evolutionary origin, the crystallochemical processes which are biologically mediated are species-specific. The formation of well-defined crystals of magnetite with sizes within the magnetic single-domain range is ubiquitous in these organisms. However, the morphology, and hence the interaction, of the growing crystal and its local environment is variable. In this respect the bacterial crystals reported in this paper show unique characteristics. The inclusions are perfect single-domain crystals of magnetite

with an anisotropic cubo-octahedral morphology extensively elongated along the [11$\bar{2}$] direction. Although several crystals are longer than 100 nm the length : width ratio is such that the particles still fall within the optimum size range for single-domain remanent magnetization. The well-defined crystallographic structure of these inclusions, as shown by HRTEM lattice imaging, implies that crystal growth is relatively slow and under biological regulation.

Although only four magnetotactic bacterial species have been studied to date at the nanometre level (Mann *et al.* 1984*a*,*b*; Matsuda *et al.* 1983; and this paper) there are two common morphological relationships which are becoming apparent. Firstly, three of the four species grow crystals with elongated hexagonal habits. In addition, the cubo-octahedral habit expressed in the spirillum, *A. magnetotacticum* can, in principle, be considered as an isotropic hexagonal habit. Although the faces comprising the hexagonal prisms are different ({110} in coccoid cells (Mann *et al.* 1984*b*) and unidentified cells (Matsuda *et al.* 1983); {111} and {100} in the spirillum (Mann *et al.* 1984*a*) and in the cells described above) the adoption of this common sixfold symmetry suggests a specific relation between crystallographic development and the enclosed biological environment in which it takes place. One possibility is that the spatial organization of ion-transport centres on the surrounding membrane matches a sixfold symmetry such that the flux of ions to the crystal surface is highly directional, resulting in vectorial crystal growth along six equivalent axes. The formation of different faces making up the hexagonal prism would then be a consequence of the physicochemical properties of the biomineralization environment, such as the level of supersaturation and the presence of organic molecules of low and high relative molecular mass (Mann 1983).

Secondly, each hexagonal prism of the four species studied by HRTEM has capped faces of {111} form. The adoption of this morphological arrangement as a common feature has important implications in the magnetotactic function of the organisms and the nucleation and growth properties of these biogenic minerals. The alignment of the {111} end faces perpendicular to the primary direction of cell mobility (Mann *et al.* 1984*a*, 1987; Towe & Moench 1981) maximizes the correspondence between the easy axis of magnetization (the [111] direction) and the magnetic moment of the cell. In addition, the precise cellular organization of these faces and the consequent crystal growth direction suggests that they may be the nucleation faces expressed through some stereochemical relationship with ion-binding sites on the surrounding membrane surface. The magnetosomes of *A. magnetotacticum* are each surrounded by a membrane with characteristics of a protein-containing lipid bilayer (Balkwill *et al.* 1980; Y. A. Gorby & R. P. Blakemore, unpublished results).

It is interesting to speculate on the possible atomic relationships that could exist between the {111} faces of magnetite and a structured protein interface such as a β-pleated sheet, which is, for example, a major constituent of the monolayer gas vesicles of aquatic prokaryotes (Walsby 1978). There are two types of cation arrangement, which alternate through the magnetite structure between adjacent {111} close-packed oxygen sheets. Both arrangements have iron atoms positioned with hexagonal symmetry, although some sites are vacant. The type I arrangement has three out of four octahedral sites occupied and an Fe–Fe distance of

2.97 Å. The type II layer has one quarter of the octahedral interstices and one quarter of the tetrahedral sites filled with an Fe–Fe distance of 3.63 Å. In contrast, fibrous proteins in the β-sheet conformation have polypeptide chains separated by 4.7 Å and a repeat along the polypeptide chains of 3.4 Å per amino acid residue (Warwicker 1960). Therefore, *a priori*, there is the possibility of a close atomic correspondence in one dimension between the iron atoms in the type II arrangement on the magnetite {111} faces and a β-pleated sheet interface.

The crystal growth of anisotropic magnetite in the magnetotactic bacteria described above takes place in two stages. The first stage involves the development of isotropic magnetite crystals, of cubo-octahedral morphology, which grow to a size of 20 nm. Crystals of similar morphology have been observed in the growth of inorganic magnetite from aqueous solutions containing 5–10% orthophosphate (Couling & Mann 1985). The second stage involves anisotropic growth along the $[11\bar{2}]$ direction, resulting in three of the {111} and {100} planes becoming elongated (figures 5 and 6). Our dimensional analysis (figures 8 and 9) indicates that this stage is associated with a spatial constraint in the development of the width of the crystal and, in some crystals, kinking of the particles. Both stages are characterized by the development of structurally well-defined magnetite crystals. No extensive discontinuities, such as intergrowth boundaries, were observed. Twinning was also not apparent in contrast to many of the mature crystals formed in the magnetotactic spirillum *A. magnetotacticum* (S. Mann, unpublished data). The top $(\bar{1}\bar{1}1)$ and side (111) and $(\bar{1}\bar{1}\bar{1})$ faces are particularly well established towards the base of the crystal, being atomically flat except for the presence of a number of surface steps. In contrast, the same side faces towards the top area of the particles are irregular. This observation suggests that there are different growth processes occurring in different regions of the crystal; this in turn implies that different stages of crystal development are associated with specific growth mechanisms. The crystallographic perfection of the basal faces probably arises from the slow stepwise addition of ions at the crystal surface, whereas the roughened side edges in the top region of the particles suggest a more rapid and uncontrolled process of ion flux to the crystal surface.

The two-stage mechanism resulting in anisotropic crystal development can be rationalized in terms of a growth process which involves the spatial and chemical control of bacterial magnetite deposition. Equivalent regulatory factors have been described for magnetite synthesis in coccoid and spirillum cells (Mann 1985). Of primary importance is the presence of a thin organic sheath surrounding the anisotropic crystals (Mann *et al.* 1987). The ultrastructure and organization of this compartment can then act as a limiting boundary for crystal development such that the crystals grow to fill the space made available to them. This results in a dimensional constraint's being placed on crystal width, whereas particle length is less restricted. Kinking and curvature in crystal habits would then be the consequence of corresponding deviations in the shape of the organic compartment.

However, such a passive role for the membrane would not explain the preferential crystallographic alignment of the crystals within an elongated biological compartment. The mature crystals are characterized by a flattened top face $(\bar{1}\bar{1}1)$ and a tapered, often rounded basal end. It is difficult to envisage a crystal growth

process which involves the development of each crystal from a central origin such that the particle grows in one direction with a well-formed $(\bar{1}\bar{1}1)$ face and at the same time in the opposite direction with an ill-defined face of the same index. More probable is a process involving the unidirectional growth of the crystals from only one end. The well-defined {111} faces exhibited by the isotropic immature crystals indicate that the top flattened end of the crystals is the first end to develop and that anisotropic growth of the particle proceeds from the $(\bar{1}\bar{1}1)$ face towards the basal end. In this respect the $(\bar{1}\bar{1}1)$ face may be a nucleation face on the surrounding membrane wall such that it is inhibited from further growth. Thus the long axis of growth is generated not from this face but from the subsequent anisotropic development of the stable {111} side faces. The structural irregularities observed in the basal region of the crystals (figure 11) probably represent incomplete crystallization at the late stages of mineralization.

In conclusion, the direct imaging of bacterial magnetite crystals of anisotropic morphology provides evidence for a crystal growth process involving nucleation on a crystal face of the form {111} resulting initially in the development of isotropic cubo-octahedra particles, which subsequently grow anisotropically along the $[11\bar{2}]$ direction owing to spatial and chemical constraints generated by a surrounding membrane boundary. Further work will attempt to model these concepts in inorganic systems.

We thank N. A. Blakemore for samples; Professor R. J. D. Tilley, University College, Cardiff, for the use of a Jeol 200CX transmission electron microscope; Dr A. J. Skarnulis, University of Oxford, for the use of computer programs; and SERC for the purchase of a Joel 2000FX electron microscope and financial support for N.H.C.S. R.P.B. was supported by NSF grant DBM 85-15540 and U.S. Office of Naval Research contract no. 0014-85-K-0502.

References

Balkwill, D. L., Maratea, D. & Blakemore, R. P. 1980 Ultrastructure of a magnetotactic spirillum. *J. Bact.* **141**, 1399–1408.

Couling, S. B. & Mann, S. 1985 Influence of inorganic phosphate on the crystallization of magnetite (Fe_3O_4) from aqueous solution. *J. Chem. Soc. chem. Commun.*, pp. 1713–1715.

Frankel, R. B. 1984 Magnetic guidance of organisms. *A. Rev. Biophys. Bioengng* **13**, 85–103.

Mann, S. 1983 Mineralization in biological systems. *Struct. Bond.* **54**, 125–174.

Mann, S. 1985 Structure, morphology and crystal growth of bacterial magnetite. In *Magnetite biomineralization and magnetoreception in organisms; a new biomagnetism* (ed. J. L. Kirchvink, D. S. Jones & B. J. MacFadden), pp. 311–332. New York: Plenum Press.

Mann, S., Frankel, R. B. & Blakemore, R. P. 1984*a* Structure, morphology and crystal growth of bacterial magnetite. *Nature, Lond.* **310**, 405–407.

Mann, S., Moench, T. T. & Williams, R. J. P. 1984*b* A high resolution electron microscopic investigation of bacterial magnetite. Implications for crystal growth. *Proc. R. Soc. Lond.* B **221**, 385–393.

Mann, S., Sparks, N. H. C. & Blakemore, R. P. 1987 Ultrastructure and characterization of anisotropic magnetic inclusions in magnetotactic bacteria. *Proc. R. Soc. Lond.* B **231**, 469–476. (Preceding paper.)

Matsuda, T., Endo, J., Osakabe, N. & Tonomura, A. 1983 Morphology and structure of biogenic magnetite particles. *Nature, Lond.* **302**, 411–412.

Skarnulis, A. J. 1979 A system for interactive electron image calculations. *J. appl. Crystallogr.* **12**, 636–638.

Towe, K. M. & Moench, T. T. 1981 Electron-optical characterization of bacterial magnetite. *Earth planet. Sci. Lett.* **52**, 213–220.

Walsby, A. E. 1978 The gas vesicles of aquatic prokaryotes. *Symp. Soc. gen. Microbiol.* **28**, 327–358.

Warwicker, J. O. 1960 The crystal structures of various fibroins. *J. molec. Biol.* **2**, 350–362.

JOURNAL OF BACTERIOLOGY, Feb. 1988, p. 834–841
0021-9193/88/020834-08$02.00/0

Vol. 170, No. 2

Characterization of the Bacterial Magnetosome Membrane

YURI A. GORBY,[1] TERRY J. BEVERIDGE,[2] AND RICHARD P. BLAKEMORE[1]*

Department of Microbiology, Spaulding Life Sciences Building, University of New Hampshire, Durham, New Hampshire 03824,[1] and Department of Microbiology, College of Biological Science, University of Guelph, Guelph, Ontario, Canada N1G 2W1[2]

Received 28 August 1987/Accepted 4 November 1987

Intact magnetosomes of *Aquaspirillum magnetotacticum* were purified from broken cells by a magnetic separation technique. Electron microscopic and chemical analyses revealed the magnetite to be enclosed by a lipid bilayer admixed with proteins. Lipids were recovered in fractions expected to contain (i) neutral lipids and free fatty acids, (ii) glycolipids and sulfolipids, and (iii) phospholipids (in a weight ratio of 1:4:6). Phospholipids included phosphatidylserine and phosphatidylethanolamine. Two of the numerous proteins detected in the magnetosome membrane were not found in other cell membranes or soluble fractions.

The permanent-magnetic character of magnetotactic bacteria (3) and algae (27) results from a conspicuous intracellular structure characterizing the group, the magnetosome (1). Those magnetosomes which have been studied are enveloped single crystals of the iron oxide magnetite, commonly arranged in one or more linear arrays within the cytoplasm (7, 14, 17, 28). Magnetite crystal morphology may vary among species. In some bacterial species, the crystals are truncated hexagonal prisms as revealed by crystal lattice imaging (17); in others they are bullet shaped (3). Those within the axenically cultivable species *Aquaspirillum magnetotacticum* (16) are truncated octahedrons (14) which lie in a single helical line along the cell axis and adjacent to the cytoplasmic membrane. The structure and composition of the magnetosome envelope has not been widely studied, although trilaminate membrane structures have occasionally been observed surrounding magnetosomes of thin-sectioned magnetotactic bacteria collected directly from mud (2). Balkwill et al. (1) considered the possibility that magnetite particles of *A. magnetotacticum* were each surrounded by a lipid bilayer. However, because of the high electron density of the magnetite core, it was not possible to discern the electron-opaque inner leaflet expected of a closely apposed lipid bilayer in these stained preparations. We applied magnetic separation methods to disrupted cells as a unique and effective means of purifying magnetosomes for chemical and structural analyses, and from these magnetosomes we obtained definitive proof of an attendant bilayer envelope.

MATERIALS AND METHODS

Media and culture conditions. *A. magnetotacticum* was grown in 15-liter batch cultures as previously described (4). The chemically defined mineral medium contained 4 mM $NaNO_3$ and lacked organic forms of nitrogen. Iron, at a final concentration of 20 μM, chelated with an equimolar concentration of quinic acid, was added to autoclaved and cooled medium. To study iron limitation, cells were transferred at least three times in medium from which iron compounds were omitted. The total trace iron concentration in media to which no iron was intentionally added was less than 1 μM, as determined with ferrozine (26).

Cells concentrated by filtration were centrifuged at 5,000 × *g* for 10 min at 4°C. They were suspended and washed three times in buffer A, consisting of 10 mM *N*-2-hydroxyethylpiperizine-*N*′-2-ethanesulfonic acid buffer (pH 7.4) containing 10 μg of the protease inhibitor phenylmethylsulfonyl fluoride per ml.

Magnetosome purification. Approximately 10^{12} cells suspended in 30 ml of buffer A were disrupted by three passes through a French pressure cell at 18,000 lb/in^2. DNase (50 μg/ml), RNase (100 μg/ml), and $MgCl_2$ (10 μM) were added to the disrupted cells and incubated for 60 min at 23°C. Disrupted cells in a centrifuge tube were placed in the gap of a large (2 kG) radar magnet. The black magnetic fraction accumulated within 10 min at the sides of the tube nearest the magnet. The nonmagnetic fluid fraction was removed by aspiration, and the magnetic phase was suspended in 100 times its volume of buffer A. This procedure was repeated at least 10 times. The partially purified magnetosome fraction was suspended in 100 times its volume of buffer A containing 1 M NaCl. The salt was added to remove adventitious electrostatically associated proteins. Purified magnetosomes were washed at least 10 more times with buffer A.

Fractionation of nonmagnetic subcellular components. The nonmagnetic cell fraction was separated into outer membrane, inner membrane, and soluble fractions by methods described by Schnaitman (24). Nonmagnetic cellular debris (approximately 30 ml obtained from 10^{12} cells) was centrifuged at 500 × *g* for 15 min at 4°C to remove unbroken cells. The supernatant fluid was centrifuged (200,000 × *g*; 1 h; 4°C) to remove membranes, and the supernatant fluid from this high-speed centrifugation, considered to contain soluble proteins, was stored on ice. The brown pellet, containing outer and inner membranes, was suspended in 30 ml of buffer A containing 2% (vol/vol) Triton X-100 and 10 mM $MgCl_2$. The solubilized cytoplasmic membrane proteins were precipitated with cold 95% ethanol overnight at 0°C and collected by centrifugation (500 × *g*; 15 min; 4°C). Fractionation was evaluated by assaying specific activity of succinic dehydrogenase, an inner membrane enzyme (6), and by measuring the quantity of 2-keto-3-deoxyoctonate, a constituent of outer membrane lipopolysaccharide (20).

Freeze-etching. Cells of *A. magnetotacticum* MS-1 and the nonmagnetic mutant strain NM-1A were flash frozen in Freon 22 kept at liquid nitrogen temperature. Frozen preparations were fractured and etched for 10 s, and platinum-carbon replicas were made at −100°C in a Balzers BA 360M freeze-etching apparatus. Magnetically purified magnetosomes were similarly prepared. Replicas were examined at

* Corresponding author.

60 kV with a Philips EM300 or EM400 electron microscope equipped with a goniometer stage under standard operating conditions.

Thin sections. Cells grown with or without 20 μM iron were fixed for 1 h with glutaraldehyde (5% [vol/vol]), followed by washing and secondary fixation for 30 min with osmium tetroxide (2% [wt/vol]) in 50 mM cacodylate buffer (pH 6.8) containing 10 mM $MgCl_2$. Samples were dehydrated in ethanol, followed by propylene oxide, and embedded in Epon 812 or Epon 812-Araldite. Thin sections obtained with an LKB 8800 Ultratome III ultramicrotome were stained with 5% uranyl acetate and 0.4% lead citrate (22) and viewed with either a Hitachi H600 or a Philips EM400 STEM at 80 kV in the transmission electron microscopy mode.

Lipid analysis. Lipids were extracted from purified magnetosomes with chloroform-methanol as described by Bligh and Dyer (5) and purified by the Sephadex bead (Pharmacia Fine Chemicals, Piscataway, N.J.) method of Wurthier (29). The purified total lipids were separated into three fractions by an acid-treated Florisil (Sigma Chemical Co., St. Louis, Mo.) column (9). The fractions were expected to contain (i) neutral lipids and free fatty acids, (ii) glycolipids, sulfolipids, and possibly phosphatides, and (iii) phospholipids. Each lipid fraction was dried and weighed.

The dry phospholipid fraction was dissolved in 0.3 ml of chloroform-methanol (1:1 [vol/vol]), spotted onto a glass thin-layer chromatography plate [20 by 20 cm] of silica gel, and chromatographed in chloroform-methanol-water (65:25:4 [vol/vol]). Subsequently, the plate was air dried, rotated 90°, and chromatographed in the second dimension with chloroform–methanol–7 N ammonium hydroxide (60:35:5 [vol/vol]). The developed plate was completely air dried. Lipids were stained with iodine vapors. Each spot was scraped from the thin-layer chromatography plate and transferred to a Pasteur pipette plugged with glass wool. Phospholipids were eluted from the pipettes with 2 ml of chloroform-methanol (1:1 [vol/vol]), followed by 2 ml of absolute methanol. Each sample was collected in a 5-ml glass ampoule and evaporated to dryness under a stream of nitrogen. The residues were each dissolved in 2 ml of 1 N HCl and, after sealing of the ampoule, heated to 100°C for 4 h. Cooled ampoules were opened, and 2 ml of redistilled hexane was added. The mixture was vigorously shaken and allowed to separate, and the aqueous phase was removed and lyophilized. The residues were dissolved in 0.1 ml of distilled water and spotted onto Whatman no. 1 chromatography paper. The chromatogram was developed with redistilled phenol-absolute ethanol-glacial acetic acid (50:5:6 [vol/vol]), air dried, and sprayed with ninhydrin reagent, which stains serine and ethanolamine. A duplicate chromatogram was sprayed with Dragendorf reagent (9), which stains choline and dimethylethanolamine. The color and R_f value of each unknown sample were compared to those of lipid standards.

Gel electrophoresis. The protein concentration of each subcellular fraction was determined by the method of Lowry et al. (13). Magnetite, liberated from organic material during the Lowry assay, was removed by centrifugation before spectrophotometric analysis at A_{560}. Proteins (5 μg) from each subcellular fraction were separated by sodium dodecyl sulfate-polyacrylamide gel electrophoresis through a 4% stacking gel and a 12% separating gel as described by Laemmli (10).

Proteins from partially purified magnetosomes and nonmagnetic fractions from cells of strain MS-1 were separated by two-dimensional gel electrophoresis. Samples (30 μg of protein each) were separated in a pH gradient ranging from 3.5 to 10.0 with tube gels as described by O'Farrell (19). At 16 h, the constant voltage (400 V) was increased to 800 V for an additional hour. Each tube gel was fixed with 1% agarose to the top of a sodium dodecyl sulfate-polyacrylamide gel (10 to 20% linear gradient of acrylamide). Proteins were separated in the second dimension of constant current (15 mA) for 9 h. The gels were stained with silver as described by Oakley et al. (18).

RESULTS

Magnetosome purification. Magnetosomes within *A. magnetotacticum* cells were always arranged in a linear array in the manner described by Balkwill et al. (1). They appeared to be enveloped and were separated from one another by a distance of about 9.0 nm. The interparticle spacing decreased to about 6.8 nm in crude preparations of magnetosomes, although particles remained attached end to end and were still enveloped (Fig. 1A). After NaCl treatment and extensive washing, magnetosomes appeared free of contaminating cellular components. However, each particle remained enveloped and separated from adjacent particles by a distance of 5.0 nm (Fig. 1B). Purified magnetosomes did not exhibit succinic dehydrogenase activity or contain 2-keto-3-deoxyoctonic acid. Sodium dodecyl sulfate detergent or Triton X-100 treatment, which dissolves lipid bilayers, removed the enveloping material, destroyed the linear arrangement of the electron-dense particles, and allowed them to clump with virtually no interparticle spacing (Fig. 1C).

Freeze-etching. In frozen and etched preparations of magnetic cells of strain MS-1 (Fig. 2A), intact magnetosomes appeared as convex protrusions ($\widehat{MM}$). Cup-shaped depressions with raised rims ($\widecheck{MM}$) were interpreted to be regions through which the fracture plane had passed with removal of magnetite cores. The raised edges making up the rim were attributed to a magnetosome envelope differing in composition and structure from adjacent cytoplasm. A number of representative fracture surfaces associated with magnetosomes within strain MS-1 cells are shown in Fig. 2B. The results are those expected if a lipid bilayer were present around each magnetite crystal. Some fractures appeared to expose the external surfaces of intact magnetosomes ($\widehat{MM}$). In other cases, the magnetite crystal appeared to have been extracted (as revealed by characteristic raised rims), and the internal surface of the magnetosome-enveloping layer ($\widecheck{MM}$) was evident. Occasionally, the fracture appeared to have penetrated the magnetosome envelope without removal of the mineral core, thereby exposing a surface which was either the magnetite core or the external face of the internal leaflet of the magnetosome envelope ($M\widehat{M}F$). The latter would be possible only if the boundary were a lipid bilayer which fractured internally along its hydrophobic region.

Frozen and etched magnetosomes, isolated from cells, displayed these same structural features. When the alignment of magnetosomes to the fracture angle was correct, the particles appeared to be arranged in linear arrays (Fig. 3). Replicas of magnetosomes treated with detergent to remove enveloping layers (data not shown) did not exhibit fractures characteristic of intact magnetosomes.

Frozen and etched cells of a nonmagnetic mutant strain lacked features associated with magnetite cores or associated enveloping layers (Fig. 4), although fracture surfaces associated with the inner and outer membranes appeared similar to those of other gram-negative bacteria. Fracture surfaces associated with external wall layers, such as capsules or surface arrays, were not observed with either the magnetic or the nonmagnetic strain.

FIG. 1. Electron microscopic evaluation of magnetosome purity. (A) Magnetosomes liberated from cells after three passages through a French pressure cell. Particles, separated by a distance of 6.8 nm, remain in chains. Note the contaminating cellular debris. (B) Purified magnetosomes after treatment with 1 M NaCl and extensive washing. Interparticle spacing has decreased to 5.0 nm, yet magnetosomes remain in chains. Note the covering around each particle and the lack of contaminating cellular debris. (C) Magnetosomes after treatment with 10% sodium dodecyl sulfate. Enveloping material has been removed, and particles are randomly oriented. Bar, 250 nm.

Thin sections. Magnetosomes within cells cultured in medium containing 20 μM iron (Fig. 5) appeared in thin sections as electron-dense crystalline iron cores, each enveloped by a 1.7-nm-thick, electron-transparent layer and a 2.0-nm electron-dense layer. These results were comparable to those of Balkwill et al. (1). Stereo views of our thin sections (not shown) offered additional evidence of the bilayer nature of this envelope and suggested that it was not merely an electron phase artifact.

Magnetic cells cultured with no added iron contained some typical magnetosomes (Fig. 6A). In addition, however, numerous 40-nm-diameter membranous vesicles were present. These vesicles lacked electron-dense cores and were adjacent to one another along the long axis of the cell

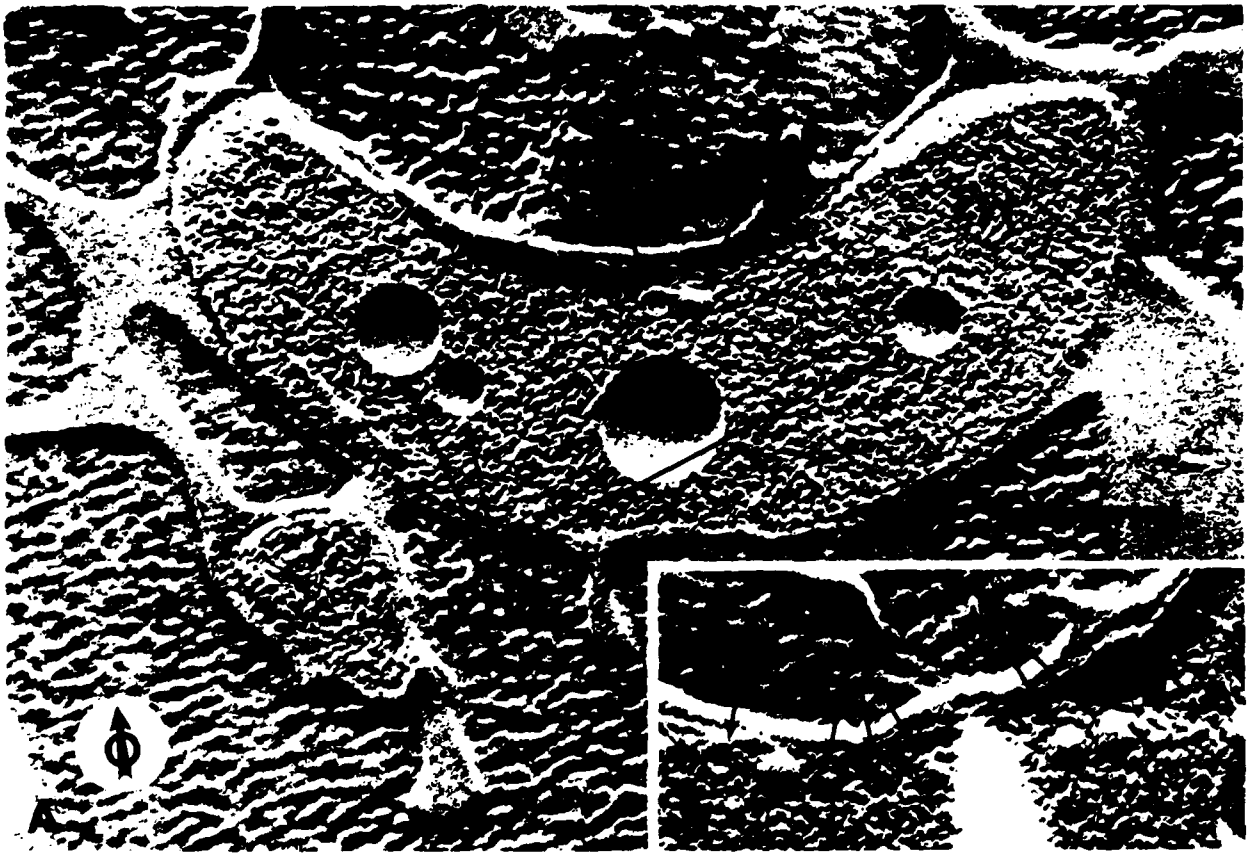

FIG. 2. Freeze-etch preparations of magnetic cells of strain MS-1. (A) An intact magnetosome appears convex, with the magnetosome membrane surface ($\widehat{MM}$) exposed, whereas a magnetosome from which the iron core has been removed by the fracture appears concave, revealing the inside of the membrane ($\widecheck{MM}$). Poly-β-hydroxybutyrate, PHB; cytoplasm, cyt. (B) The fracture has penetrated the magnetosome membrane and exposed what appears as either the face of the magnetite particles or the convex fracture of the inner leaflet of the magnetosome membrane ($\widehat{MMF}$). The circled arrow indicates the direction of the shadow. Bar, 250 nm.

in the position normally occupied by intact magnetosomes within cells cultured with iron. Each "empty" membrane vesicle consisted of two 1.7-nm-thick, electron-dense layers separated by a 2.2-nm-thick electron-transparent layer as characteristic of a lipid bilayer unit membrane (23). Sometimes these vesicles were not filled with crystalline magnetite. Instead (as determined from energy-dispersive X-ray analysis and selected-area electron diffraction), they contained amorphous iron (Fig. 6B) which was presumably a derivative of polyferric hydroxide.

Lipid analysis. Magnetically separated and washed magnetosomes from 25 g of wet-packed cells yielded 25 mg of purified lipids and 150 mg of purified magnetite. Lipids associated with this magnetosome fraction included (i) neutral lipids and free fatty acids making up 8% of total lipids by weight, (ii) a fraction expected to contain glycolipids, sulfolipids, and phosphatides making up 30% of total lipids by weight, and (iii) phospholipids making up 62% of total lipids by weight. The neutral and free fatty acids were not identified, nor were the components of the glycolipid fraction. The phospholipids included phosphatidylethanolamine and phosphatidylserine, as determined by thin-layer chromatography.

Gel electrophoresis. Proteins of the cell outer and inner membranes and of the soluble cell fraction were compared with those associated with the purified magnetosome fraction (Fig. 7). The outer membrane protein profile of this

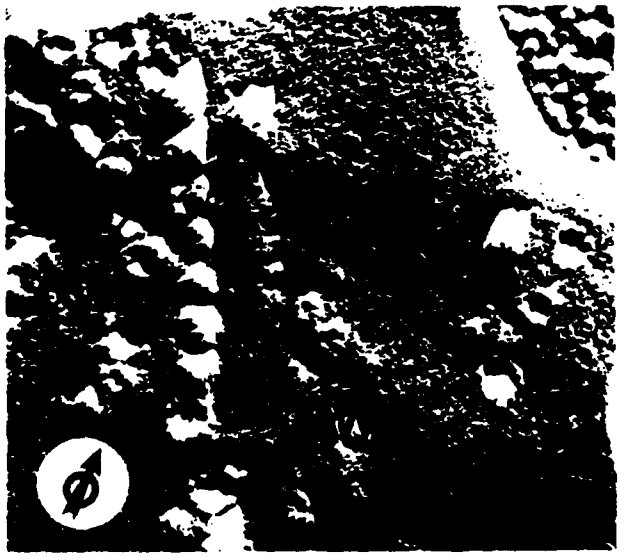

FIG. 3. Freeze-etch preparation of purified magnetosomes. Note the chain formation of characteristic fracture surfaces. Abbreviations: outer surface of the magnetosome membrane, $\widehat{MM}$; inside surface of the magnetosome membrane, $\widecheck{MM}$; either the face of the magnetite particle or the convex fracture of the inner leaflet of the magnetosome membrane, $\widehat{MMF}$. The circled arrow indicates the direction of the shadow. Bar, 100 nm.

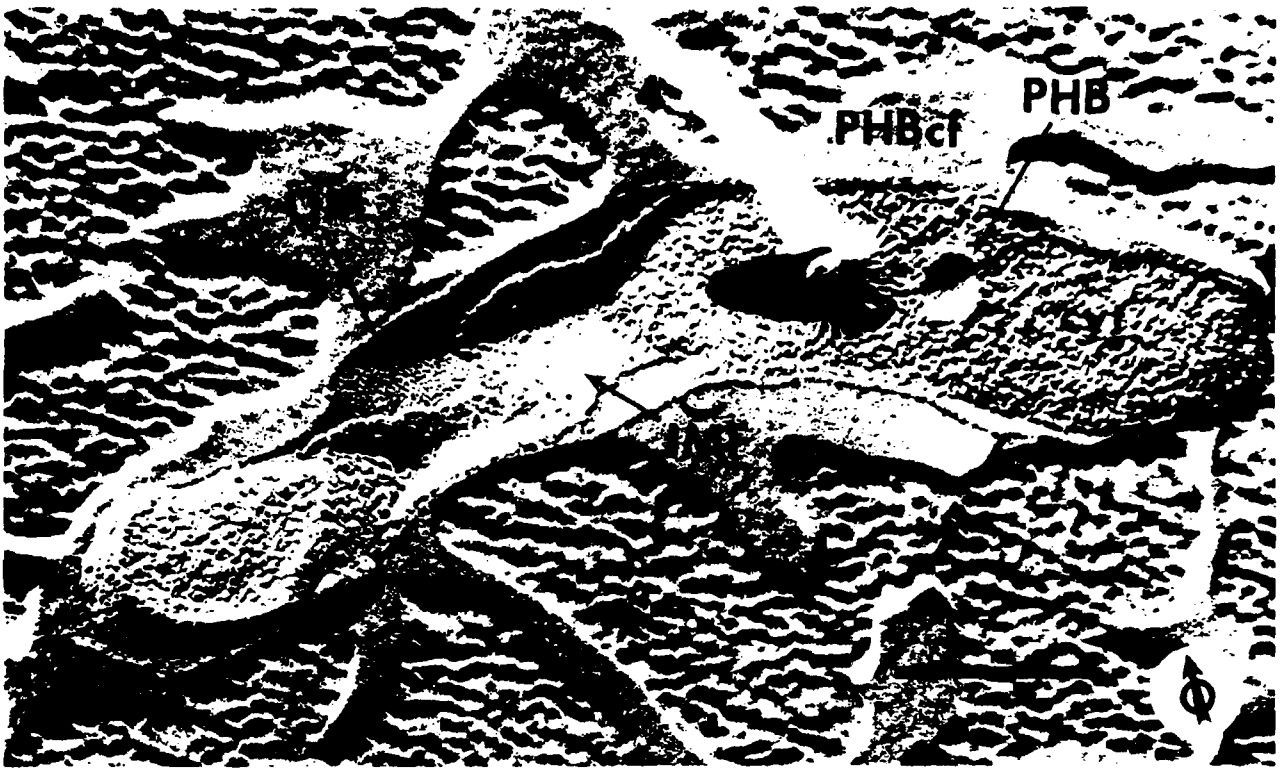

FIG. 4. Freeze-etch preparation of nonmagnetic mutant strain NM-1A. Note the lack of magnetic particles. Abbreviations: inner surface of the outer membrane, OM; convex fracture of the inner leaflet of the inner membrane, IMF; poly-β-hydroxybutyrate, PHB; cross-fracture of a PHB particle, PHBcf. The circled arrow indicates the direction of the shadow. Bar, 250 nm.

organism was similar to that described by Paoletti and Blakemore (21). Several proteins of identical molecular masses were shared between the magnetosome membrane and either the outer or inner membrane, but the intensities of the sodium dodecyl sulfate-polyacrylamide gel electrophoresis bands differed, reflecting concentration differences. Two

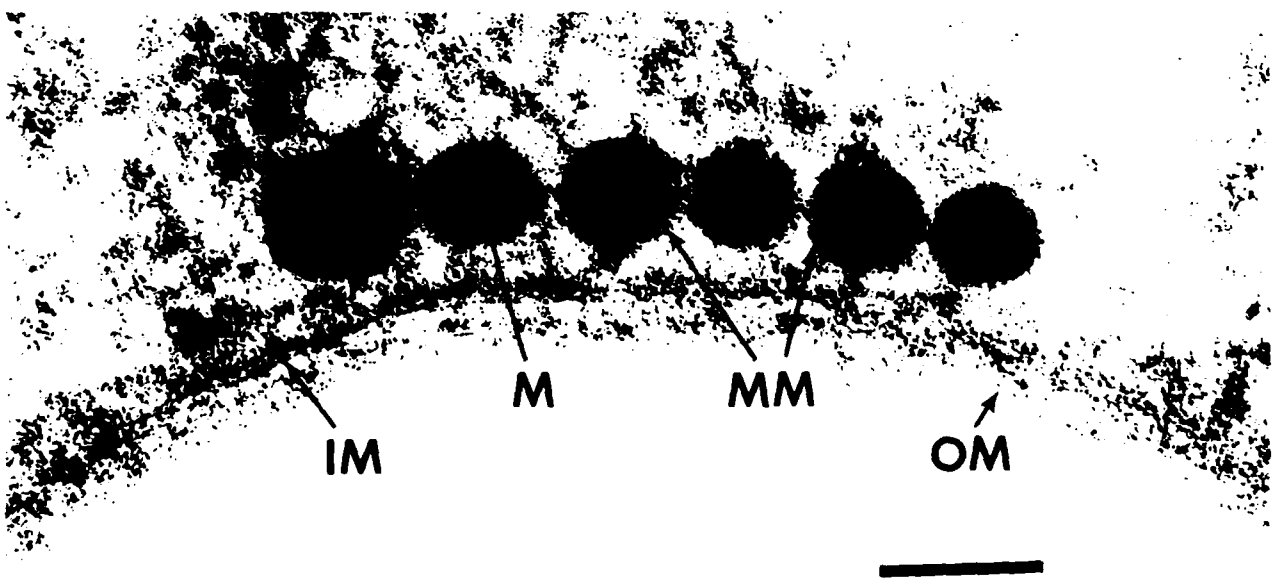

FIG. 5. Thin section of a magnetic cell. Abbreviations: outer membrane, OM; inner membrane, IM; magnetosome membrane, MM; magnetite, M. Bar, 100 nm.

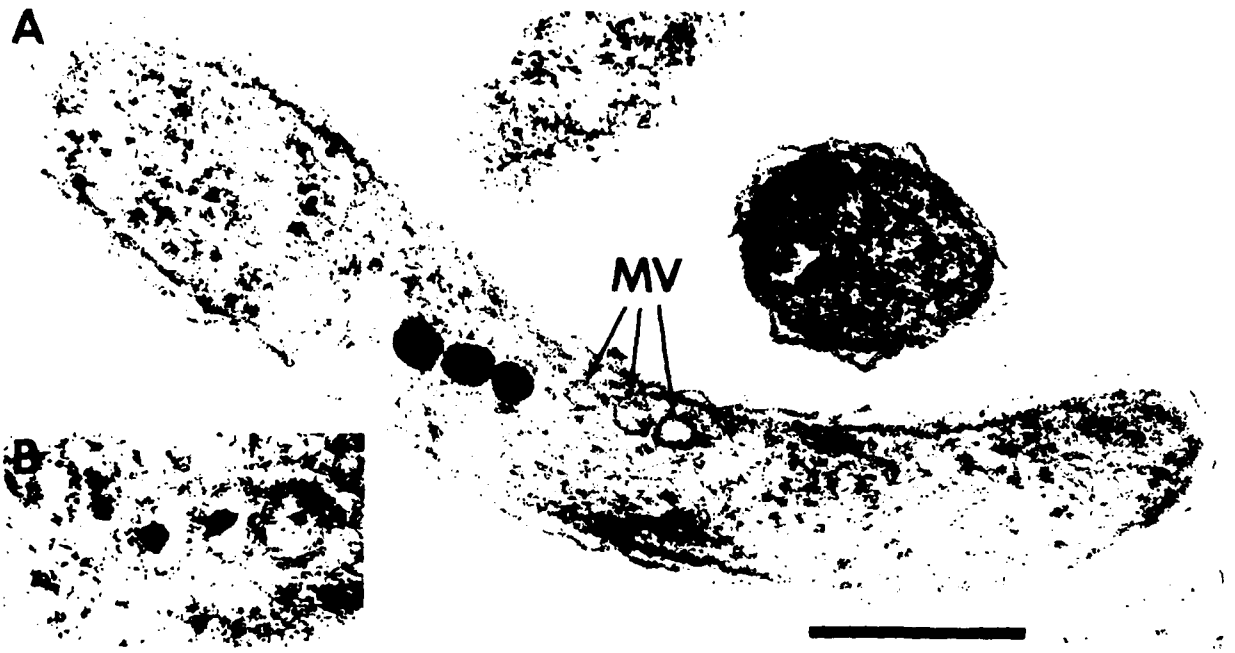

FIG. 6. Thin sections of cells cultured under iron limitation. (A) Note the trilaminate structure of the membranous vesicles (MV), which lie along the same axis as complete magnetosomes. Bar, 250 nm. (B) Note the small electron-dense deposits of amorphous iron within the membranous vesicles.

proteins, with apparent molecular masses of 15,000 and 33,000 daltons, appeared to be restricted to the magnetosome membrane fraction.

Characteristic magnetosome protein profiles obtained after two-dimensional gel electrophoresis are shown in Fig. 8. Two abundant anodically migrating proteins, with apparent molecular masses of 15,500 and 16,500 daltons, were present only in the magnetosome fraction. In concert, the one- and two-dimensional gels showed the magnetosome membrane to be distinct from the other outer and inner cell membranes.

DISCUSSION

Previous studies (1, 2) provided suggestive evidence for a lipid bilayer envelope surrounding the bacterial magnetosome. However, conclusive evidence has been lacking because of the difficulty in interpreting thin sections and the absence of data on purified magnetosomes. We extended previous cytological studies and used a magnetic separation method to recover intact magnetosomes from cellular debris. Our data, obtained by freeze-etching and thin sectioning of both cells and magnetically extracted magnetosomes, indicate the presence of a trilaminate membrane surrounding each magnetite core. This membranous envelope was absent from purified magnetosomes treated with detergent to remove lipids and proteins. Trilaminate membrane vesicles with dimensional and spatial characteristics of magnetosomes, but devoid of magnetite cores, were present in wild-type magnetic cells grown without iron. Amorphous iron was occasionally present in small quantity within these vesicles. Magnetosomes, vesicles with amorphous iron, or empty vesicles were not present within cells of the nonmagnetic mutant strain NM-1A. It was apparent, therefore, that these membranes were an integral part of magneto-

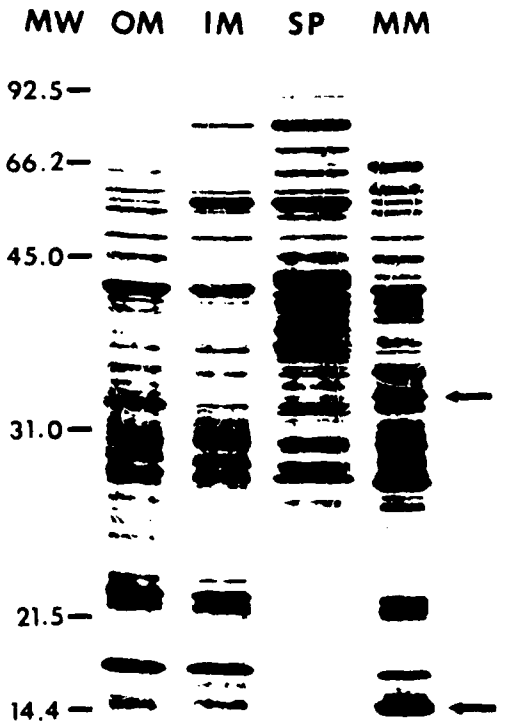

FIG. 7. Sodium dodecyl sulfate-polyacrylamide gel electrophoresis of cell fractions of strain MS-1. Lanes: Outer membrane proteins, OM; inner membrane proteins, IM; magnetosome membrane proteins, MM; soluble proteins, SP; molecular weight standards, MW. Arrows indicate the positions of the 15,000- and 33,000-dalton magnetosome membrane proteins.

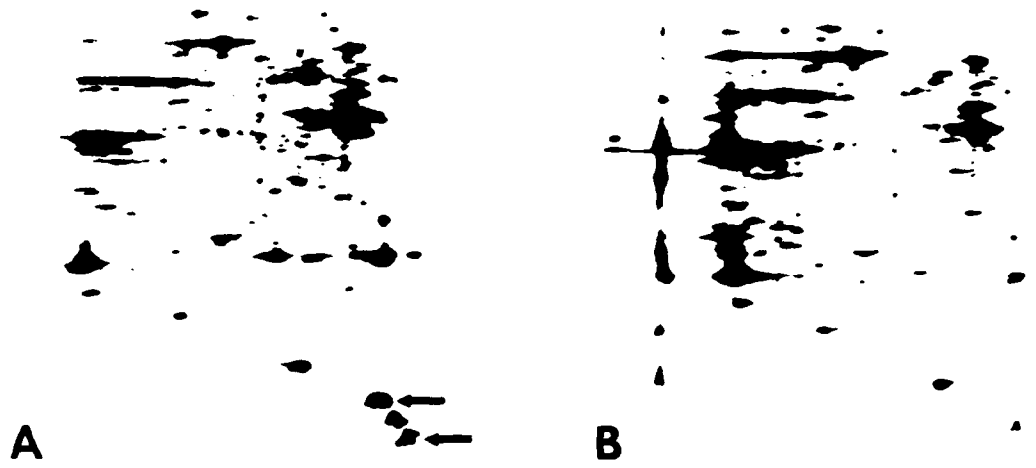

FIG. 8. Two-dimensional gel electrophoresis of proteins recovered from the magnetic (A) and nonmagnetic (B) fractions from strain MS-1. Arrows indicate the positions of the 15,500- and 16,500-dalton anionic proteins present only in the magnetic fraction.

somes, and we consider them to be magnetosome boundary membranes.

Magnetosome membranes do not appear to be contiguous with the cytoplasmic membrane. We have never observed connections between the two membranes in numerous thin sections, including stereo views, of magnetic cells. If the magnetosome membranes were invaginations of the cytoplasmic membrane, we would expect freeze-etching to reveal severed connections as pits in the inner surface of this membrane (as observed with freeze-etched preparations of cyanobacteria which possess photosynthetic membranes as vesicular intrusions of the cytoplasmic membrane [11]); it did not. Furthermore, when spheroplasts were made, they did not evert their magnetite crystals as would be expected of particles within surficial invaginations of the cytoplasmic membrane.

The magnetosome membrane does not appear significantly different in overall composition from other cell membranes. We detected protein and lipid as components. Lipids were present in fractions expected to contain (i) neutral lipids and fatty acids, (ii) glycolipids, sulfolipids, and phosphatides, and (iii) phospholipids. The ratio of the abundance of the lipid components is that expected for a biological membrane (23). Although most proteins detected in envelopes of purified magnetosomes were of a mass (but not a quantity) similar to that of the cytoplasmic membrane, two were unique to the magnetosome envelope. It is tempting to speculate that these have a specific role in magnetite production. As enzymes, they could promote the accumulation of supersaturating quantities of iron within vesicles, serve to oxidize iron, or reduce and dehydrate the ferrihydrite precursor (8) of bacterial magnetite. They could also be ferrihydrite-associated proteins such as bacterioferritin (25) apoprotein. As structural proteins, they might contribute to the compartmentalization deemed essential for "organic matrix-mediated" (12) biomineralization. The use of artificial membranous vesicles to study iron biomineralization, as recently initiated by Mann et al. (15), would undoubtedly be advanced by purification and inclusion of these magnetosome-specific proteins.

ACKNOWLEDGMENTS

We thank N. Blakemore, R. Frankel, T. Laue, and F. Rodgers for helpful advice and discussions. J. Cherry and B. McGrew provided help with electrophoresis.

A portion of this research was performed by the Natural Sciences and Engineering Council of Canada Guelph Regional STEM Facility in the Department of Microbiology, College of Biological Science, University of Guelph, and was supported by Natural Sciences and Engineering Council and Medical Research Council operating grants to T.J.B. Research conducted in the laboratory of R.P.B. was supported by Office of Naval Research contract N00014-85-K-0502 and National Science Foundation grant DMB-85-15540. Y.A.G. gratefully acknowledges partial support from University of New Hampshire Central University Research Fund award S396.

LITERATURE CITED

1. **Balkwill, D. L., D. Maratea, and R. P. Blakemore.** 1980. Ultrastructure of a magnetotactic spirillum. J. Bacteriol. **141**: 1399–1408.
2. **Blakemore, R. P.** 1975. Magnetotactic bacteria. Science **190**: 377–379.
3. **Blakemore, R. P.** 1982. Magnetotactic bacteria. Annu. Rev. Microbiol. **36**:217–238.
4. **Blakemore, R. P., D. Maratea, and R. S. Wolfe.** 1979. Isolation and pure culture of a freshwater magnetic spirillum in chemically defined medium. J. Bacteriol. **140**:720–729.
5. **Bligh, E. G., and W. S. Dyer.** 1951. A rapid method for total lipid extraction and purification. Can. J. Biochem. Physiol. **37**:911–917.
6. **Dobrogosz, W. J.** 1981. Enzymatic activity, p. 365–392. *In* P. Gerhardt, R. G. E. Murray, R. N. Costilow, E. W. Nester, W. A. Wood, N. R. Krieg, and G. B. Phillips (ed.), Manual of methods for general bacteriology. American Society for Microbiology, Washington, D.C.
7. **Frankel, R. B., R. P. Blakemore, and R. S. Wolfe.** 1979. Magnetite in freshwater bacteria. Science **203**:1355–1356.
8. **Frankel, R. B., G. C. Papaefthymiou, R. P. Blakemore, and W. O'Brien.** 1983. Fe_3O_4 precipitation in magnetotactic bacteria. Biochim. Biophys. Acta **763**:147–159.
9. **Hanson, R. S., and J. A. Phillips.** 1981. Chemical composition, p. 328–364. *In* P. Gerhardt, R. G. E. Murray, R. N. Costilow, E. W. Nester, W. A. Wood, N. R. Krieg, and G. B. Phillips (ed.), Manual of methods for general bacteriology. American

Society for Microbiology, Washington, D.C.
10. **Laemmli, U. K.** 1970. Cleavage of structural proteins during the assembly of the head of bacteriophage T4. Nature (London) **227**:680–685.
11. **Lommen, M. A. J., and J. Takemoto.** 1978. Comparison, by freeze-fracture electron microscopy, of chromatophores, spheroplast-derived membrane vesicles, and whole cells of *Rhodopseudomonas sphaeroides*. J. Bacteriol. **136**:730–741.
12. **Lowenstam, H. A.** 1981. Minerals formed by organisms. Science **211**:1126–1131.
13. **Lowry, O. H., N. J. Rosebrough, A. L. Farr, and R. J. Randall.** 1951. Protein measurement with the Folin phenol reagent. J. Biol. Chem. **193**:265–275.
14. **Mann, S., R. B. Frankel, and R. P. Blakemore.** 1984. Structure, morphology and crystal growth of bacterial magnetite. Nature (London) **310**:405–407.
15. **Mann, S., J. P. Hannington, and R. J. P. Williams.** 1986. Phospholipid vesicles as a model system for biomineralization. Nature (London) **324**:565–567.
16. **Maratea, D., and R. P. Blakemore.** 1981. *Aquaspirillum magnetotacticum* sp. nov., a magnetic spirillum. Int. J. Syst. Bacteriol. **31**:452–455.
17. **Matsuda, T., J. Endo, N. Osakabe, and A. Tonomura.** 1983. Morphology and structure of biogenic magnetite particles. Nature (London) **302**:411–412.
18. **Oakley, B. R., D. R. Kisch, and N. R. Morris.** 1980. A simplified stain for detecting proteins in polyacrylamide gels. Anal. Biochem. **105**:361–363.
19. **O'Farrell, P. H.** 1975. High resolution two dimensional electrophoresis of proteins. J. Biol. Chem. **250**:4007–4021.
20. **Osborn, M. J., and H. C. P. Wu.** 1980. Proteins of the outer membrane of gram-negative bacteria. Annu. Rev. Microbiol. **34**:369–422.
21. **Paoletti, L. C., and R. P. Blakemore.** 1986. Hydroxamate production by *Aquaspirillum magnetotacticum*. J. Bacteriol. **167**:73–76.
22. **Reynolds, E. S.** 1963. The use of lead citrate at high pH as an electron-opaque stain in electron microscopy. J. Cell Biol. **17**:208–212.
23. **Rogers, H. J.** 1983. Bacterial cell structure, p. 28–53. American Society for Microbiology, Washington, D.C.
24. **Schnaitman, C.** 1981. Cell fractionation, p. 52–61. *In* P. Gerhardt, R. G. E. Murray, R. N. Costilow, E. W. Nester, W. A. Wood, N. R. Krieg, and G. B. Phillips (ed.), Manual of methods for general bacteriology. American Society for Microbiology, Washington, D.C.
25. **Stiefel, E. I., and G. D. Watt.** 1979. *Azotobacter* cytochrome $b_{557.5}$ is a bacterioferritin. Nature (London) **279**:81–83.
26. **Stookey, L. L.** 1970. Ferrozine—a new spectrophotometric reagent for iron. Anal. Chem. **42**:779–781.
27. **Torres De Araujo, F. F., M. A. Pires, R. B. Frankel, and C. E. M. Bicudo.** 1986. Magnetite and magnetotaxis in algae. Biophys. J. **50**:375–378.
28. **Towe, K. M., and T. T. Moench.** 1981. Electron-optical characterization of bacterial magnetite. Earth Planet. Sci. Lett. **52**:213–220.
29. **Wurthier, R. E.** 1966. Purification of lipids from nonlipid contaminants on Sephadex bead columns. J. Lipid Res. **7**:558–561.

2

Bacterial Biomagnetism and Geomagnetic Field Detection by Organisms

RICHARD P. BLAKEMORE, NANCY A. BLAKEMORE, RICHARD B. FRANKEL*

Department of Microbiology, University of New Hampshire
Durham, New Hampshire, and *Francis Bitter
National Magnet Laboratory, M.I.T.
Cambridge, Massachusetts

INTRODUCTION

The Earth is a magnet. Its dipole character results from massive currents within the molten portion of its core. These currents, driven presumably by gravitational energy, induce, in the manner of a self-sustaining dynamo, a global dipolar magnetic field with a magnitude of roughly 0.7 gauss at the poles. Although the ancient Chinese were familiar with the polar alignment of magnetized needles, geomagnetism became science with the publication in 1600 of William Gilbert's classic exposition De Magnete, Magneticisque Corporibus Et De Magno Magnete Tellure: Physiologia Nova, Plurimis & Argumentis & Experimentis Demonstrata. Gilbert's predecessor, Peter Peregrinus de Maricourt in his Epistola de Magnete of 1269, had noted that a magnetized needle (compass) left free to float on water, merely rotates, coming to rest with its axis lying in the north-south plane, and is not pulled in a northward direction. He did not perceive that the source of the magnetism causing the compass deflection was the Earth itself. Other predecessors of William Gilbert had believed such magnetism was extraterrestrial or was due to some remote "magnetic mountains." Gilbert fashioned lodestone spheres which he called terrellas or little Earths; a term indicating his suspicion that the Earth itself was a magnet. By studying the interactions between his terellas and small bits of iron wire, he arrived at a novel and experimentally based philosophy of the attractive behavior or "coition" of ferromagnets, and presented in his book the first inductive rationale for the concept of terrestrial magnetism.

CURRENT MICROBIOLOGY Vol. 17 (1988), pp. 339–342

Current Microbiology

Iron Reduction by *Aquaspirillum magnetotacticum*

Lawrence C. Paoletti and Richard P. Blakemore

Department of Microbiology, University of New Hampshire, Durham, New Hampshire, USA

Abstract. Iron reductase activity in cell extracts of *Aquaspirillum magnetotacticum* strain MS-1 (wild type) or nonmagnetotactic mutant strain NM-1A was located primarily in the periplasm. Cytoplasm contained 20%–35% and membrane fractions 3% of total iron reductase activity detected. Iron reduction was reversibly inhibited by oxygen, required β-NADH, and was enhanced by flavins. Reduced disulfide bonds and uncomplexed sulfhydryl groups were necessary for reductase activity. Respiratory inhibitors did not appreciably affect iron reductase activity. Iron complexed with quinic acid, dihydroxybenzoic acid, acetohydroxamic acid, citric acid, or deferrioxamine B was reduced by soluble iron reductases of strain MS-1.

Enzymatic reduction of ferric iron to the more soluble ferrous form may be an important and common feature of bacterial iron assimilation [1–4, 7–9, 11, 16]. Some bacteria also couple iron reduction to substrate dissimilation [6, 15].

Magnetotactic bacteria assimilate extracellular ferric iron by incompletely understood means [5, 13]. They convert much of it to intracellular magnetite (a mixed-valence iron oxide) by steps involving iron reduction [5]. One species available for pure culture studies, *Aquaspirillum magnetotacticum* strain MS-1, is also apparently capable of dissimilatory iron reduction because it exhibits iron respiration-driven proton translocation [15]. However, despite this indirect evidence that they reduce iron, measurements of iron reductase (FeRed) activity by cells of this premier iron-accumulating bacterium are needed. In this paper, we report the cellular locations and biochemical characteristics of FeRed activity detected in cell fractions of *A. magnetotacticum* strains MS-1 and NM-1A grown under conditions appropriate for magnetite formation.

Materials and Methods

Bacterial strains and growth conditions. *Aquaspirillum magnetotacticum* strains MS-1 (ATCC 31632) and NM-1A [15] were batch-cultured microaerobically in magnetic spirillum growth medium [13].

Preparation of cell extracts. Cells were harvested [14] and washed once in 10 m*M* Tris (2-amino-2-hydroxymethylpropane-1,3-diol) buffer, pH 8.0. Washed cells suspended in 6–8 ml of buffer were disrupted by two passes through a French pressure cell at 16,000 lb in^{-2}. Undisrupted cells and debris were removed by centrifugation (10,000 *g*, 15 min, 4 C). The cell membrane and soluble fractions were obtained from the supernatant fluids by ultracentrifugation (100,000 *g*, 1 h, 4 C). Membranes in the pellet fraction were suspended in 1–2 ml of buffer and stored on ice. Periplasm was obtained by the freeze-thaw method [14], and cytoplasm was subsequently released from thawed cells by disruption in a French pressure cell. Outer and cytoplasmic membranes were separated with Triton X-100 (Sigma Chemical Co., St. Louis, Missouri), as previously described [13]. Samples were immediately assayed for FeRed activity. Protein concentrations were determined by the method of Lowry et al. [10].

Iron reductase assay. Iron reduction by cell extracts was measured with ferrozine (ε_{562} = 28,000 M^{-1} cm^{-1}) as described by Dailey and Lascelles [4]. Assays were performed anaerobically in Thunberg cuvettes at 25 C in a Beckman Instruments DU-8 spectrophotometer equipped for kinetic analysis. Reaction mixtures (final volume of 2.0 ml) consisted of 10 m*M* Tris-acetate buffer (pH 8.1) containing 10% (vol/vol) glycerol and 10 μg/ml phenylmethylsulfonyl fluoride; 0.8 m*M* β-NADH; 0.5 m*M* ferrozine; 0.2 m*M* ferric citrate; and 10 μ*M* flavin mononucleotide (FMN). Cell extract (0.5–2.0 mg protein) was placed in the sidearm, and the cuvette contents were sparged with O_2-free N_2 for 5 min. The reaction was initiated by mixing the extract with the assay mixture. Apparent K_m and V_{max} values were calculated from Lineweaver-Burke plots obtained with a minimum of three substrate concentrations.

Iron chelates. Ferric chloride (4 m*M*) was combined with each of the following chelators (4 m*M* each in Milli-Q water): quinic acid (Sigma Chemical Co.), 2,3-dihydroxybenzoic acid (DHB, Aldrich Chemical Co., Milwaukee, Wisconsin), acetohydroxamic acid (Aldrich Chemical Co.), and deferrioxamine B (a generous gift from Ciba-Giegy Corp., Summit, New Jersey).

Address reprint requests to: Dr. Richard P. Blakemore, Department of Microbiology, University of New Hampshire, Durham, NH 03824, USA.

Table 1. Cellular distribution of iron reductase activity in *Aquaspirillum magnetotacticum*

	Activity in strain			
	MS-1		NM-1A	
Cell fraction	% total	Sp. act	% total	Sp. act
Periplasm	77	25	64	37
Cytoplasm	20	9	35	7
Membranes	3	2	3	1

Specific activity, nmol Fe(II) formed · min⁻¹ · mg protein⁻¹. Assay conditions are described in *Materials and Methods*.
[a] Obtained by freeze-thaw method [14].
[b] Includes outer plus cytoplasmic membranes.

Chemicals. β-NADH, β-NADPH, FMN, FAD, rotenone, antimycin A, and 2-heptyl-4-hydroxyquinoline-N-oxide (HQNO) were purchased from Sigma Chemical Co.

Results and Interpretations

Distribution of FeRed activity. Of the total FeRed specific activity detected in strains MS-1 and NM-1A, 77% and 64%, respectively, were in the cell periplasmic fraction (Table 1). Approximately 20% (strain MS-1) to 35% (strain NM-1A) of the total FeRed activity was present in the cytoplasm, and 3% was detected in the combined membrane fractions (Table 1). The outer membrane fraction contained approximately 1% of the total activity, and frequently no activity was detected in the cytoplasmic membrane fraction. Specific activity values of soluble or membrane-associated FeRed of *Aquaspirillum magnetotacticum* (Table 1) were similar to those reported for other organisms [1, 2, 4, 9, 11].

The preponderant distribution of FeRed activity in periplasm could be important in iron assimilation [13], in formation of the periplasmic hemes detected previously in this organism [12], in substrate dissimilation [15], or in a combination of these. Cytoplasmic FeRed of *A. magnetotacticum* could be associated with iron transport or with reduction of intracellular ferrihydrite ($5Fe_2O_3 \cdot 9H_2O$) to magnetite ($Fe_2O_3 \cdot FeO$) [5].

Biochemical properties of FeRed. We detected FeRed activity in soluble fractions from cells cultured over the range of 0–40 μM added iron (data not shown); this indicated that this enzyme was constitutively produced. Specific activity of either soluble or membrane-associated FeRed in strain MS-1 cells was at least twofold higher with β-NADH than with β-NADPH as the reductant (Table 2). Succinate did not serve as a reductant for either soluble or membrane-associated FeRed (Table 2). Flavins have been shown to stimulate FeRed activity [8, 9, 11]. The activity of both soluble and membrane-associated FeRed of strain MS-1 cells was enhanced by adding FMN or FAD to the assay mixture (Table 3). Activity was not detected in cell combined (outer plus cytoplasmic) membrane fractions in the absence of added flavins. Reduction was not observed with either 0.8 mM β-NADH (or β-NADPH) or 10 μM FMN (or FAD) added to the assay mixture in the absence of enzyme. Activity was completely destroyed by boiling of the cell fractions.

Preferential use of β-NADH over β-NADPH and the stimulatory effect of flavins are characteristics shared by FeRed in *Neisseria gonorrhoeae* [8], *Rhodopseudomonas sphaeroides* [11], *Pseudomonas aeruginosa* [2], and *Agrobacterium tumefaciens* [9].

Table 2. Effect of reductants on iron reductase activity of *Aquaspirillum magnetotacticum* strain MS-1

	Specific activity[a] in	
Reductant (mM)	Soluble fraction	Membrane fraction[b]
NADH (0.8)	8.2	2.4
NADPH (0.8)	2.0	1.0
Succinate (4.0)	N.D.[c]	N.D.[c]

[a] nmol Fe(II) formed · min⁻¹ · mg protein⁻¹. Assay conditions are described in *Materials and Methods*.
[b] Includes outer and cytoplasmic membranes.
[c] No detectable activity.

Table 3. Effect of flavins on iron reductase activity of *Aquaspirillum magnetotacticum* strain MS-1

	Specific activity[a] in	
Flavin (10 μM)	Soluble fraction	Membrane fraction[b]
None	1.2	N.D.[c]
FMN	8.9	1.6
FAD	11.8	2.4

[a] Specific activity, nmol Fe(II) formed · min⁻¹ · mg protein⁻¹. Assay conditions are described in *Materials and Methods*.
[b] Includes outer and cytoplasmic membranes.
[c] No detectable activity.

As with other bacteria [4, 9], the FeRed activity was measured was totally and reversibly inhibited by oxygen (data not shown). Inhibition was relieved by sparging mixtures with O_2-free N_2 or by adding 2-mercaptoethanol (0.1% vol/vol) to the assay mixture. Lodge et al. [9] have reported bacterial FeRed inhibition by sulfhydryl-binding agents such as mercuric or cadmium chloride and N-ethylmaleimide. *Mercuric chloride (1 mM)* completely abolished iron reduction by the soluble cell fraction of strain MS-1. These results suggest that reduced disulfide bonds, which can be disrupted by O_2, and uncomplexed sulfhydryl groups may be necessary for soluble FeRed activity in this bacterium.

Respiratory inhibitors HQNO, antimycin A, or rotenone (4 μM each) inhibited iron reduction by combined membrane fractions of *A. magnetotacticum* MS-1. The inhibition was 11% or less of that of untreated controls. Because the cytoplasmic membrane fraction exhibited little or no FeRed activity, our results indicate that the FeRed activity we measured was not associated with cell respiration. These results are at variance with those of Short and Blakemore [15] which demonstrated that intact cells of this strain (cultured similarly) carry out iron respiration-driven proton translocation, a process that was inhibited by respiration inhibitors. Although some organisms apparently use respiratory chain components for iron reduction [4, 7], recent evidence was presented showing that iron reduction by *Escherichia coli* K12 cells was not linked to respiration [16]. Differences between our work and that of Short and Blakemore [15] may relate to our use of cell membranes rather than intact cells.

The specific activity of the membrane FeRed of strain MS-1 with ferric-DHB was fourfold higher than with other ferric chelates tested. Except for this effect, we observed no differences in the specific activity of either periplasmic, cytoplasmic, or membrane reductases of strain MS-1 with any of the six iron chelates tested (those listed in Table 4). Cox [2] correctly predicted that *Pseudomonas aeruginosa* cells possessed two different soluble iron reductases based, in part, upon measured differences in specific activity of extracts with two iron chelates. By this reasoning, because we observed similar activity with diverse chelates, *A. magnetotacticum* may contain one soluble FeRed able to process iron uncomplexed or bound to a variety of chelates.

Apparent K_m and V_{max} values. Apparent K_m values of soluble (periplasmic and cytoplasmic) FeRed from strain MS-1 ranged from 18 μM for ferric quinate to 212 μM for ferric citrate (Table 4). The V_{max} values ranged from 9 nmol · min^{-1} · mg protein^{-1} for ferric DHB to 52 nmol · min^{-1} · mg protein^{-1} for ferric citrate (Table 4). These data indicate that *A. magnetotacticum* cells are able to reduce uncomplexed iron or iron complexed to citrate, phenolates, or to primary or secondary hydroxamates. Ferric quinate appeared to be an especially suitable iron substrate. This may reflect the culture history of cells because ferric quinate is the iron source in our growth medium.

Table 4. Apparent K_m and V_{max} values of *Aquaspirillum magnetotacticum* strain MS-1 soluble iron reductase with various iron compounds

Iron compound	K_m	r	V_{max}
Ferric quinate	18	0.98	22
Ferric DHB	26	0.99	9
Ferric acetohydroxamate	56	0.98	16
Ferric chloride	105	0.99	38
Ferric ferroxamine B	154	0.99	15
Ferric citrate	212	0.99	52

μM

r = correlation coefficient; K_m and V_{max} values were calculated from Lineweaver-Burke plots of enzyme activity at three or more substrate concentrations.

nmol Fe(II) formed · min^{-1} · mg protein^{-1}

Conclusions

Our data show that FeRed activity of *A. magnetotacticum* was predominantly located in the periplasm. The enzyme reduced uncomplexed iron or iron complexed to any of several chemically different chelators and was constitutively produced over the range of culture iron from 0 to 40 μM. Enzyme activity required β-NADH, was enhanced by flavins, and was reversibly inactivated by oxygen. Soluble FeRed was unaffected by a selection of respiratory inhibitors.

Cells of mutant strain NM-1A accumulate substantial amounts of iron as ferrihydrite but not magnetite [5]. We did not observe substantial differences between the magnetic and nonmagnetic strains with regard to the location and specific activity of FeRed. Our results corroborate earlier findings (D.A. Bazylinski, Ph.D. thesis, University of New Hampshire, Durham, 1984) and suggest that iron-reducing ability is not a factor explaining the inability of NM-1A cells to produce magnetite.

In some organisms, iron is apparently released from ferrisiderophores by reduction [1–4, 7–9, 11,

16]. However, in few studies have comparisons been made of FeRed activity in separated periplasmic, cytoplasmic, and membrane cell fractions. Iron accumulates intracellularly in both wild-type strain MS-1 and nonmagnetic mutant strain NM-1A as magnetite or ferrihydrite, respectively. Because it does not accumulate at the cell surface, transport through cell boundary layers and periplasm cannot be a rate-limiting step in iron acquisition by these strains. Abundant periplasmic iron reductase activity could promote iron transport and prevent accumulation of surficial ferric oxyhydroxides in this motile spirillum.

ACKNOWLEDGMENTS

We thank R. Valleri and T. Laue for helpful advice. This work was supported by Office of Naval Research Contract N00014-85-K-0502 and National Science Foundation grant DMB 85-15540. L.C.P. was supported by a University of New Hampshire Graduate Student Summer Fellowship.

Literature Cited

1. Arceneaux JE.L, Byers BR (1980) Ferrisiderophore reductase activity in *Bacillus megaterium*. J Bacteriol 141:715–721
2. Cox CD (1980) Iron reductases from *Pseudomonas aeruginosa*. J Bacteriol 141:199–204
3. Crichton RR, Charloteaux-Wauters M (1987) Iron transport and storage. Eur J Biochem 164:485–506
4. Dailey Jr HA, Lascelles J (1977) Reduction of iron and synthesis of protoheme by *Spirillum itersonii* and other organisms. J Bacteriol 129:815–820
5. Frankel RB, Papaefthymiou GC, Blakemore RP, O'Brien W (1983) Fe_3O_4 precipitation in magnetic bacteria. Biochim Biophys Acta 763:147–159
6. Jones CW (1982) Bacterial respiration and photosynthesis. Washington DC: American Society for Microbiology. pp 58–63
7. Lascelles J, Burke KA (1978) Reduction of ferric iron by L-lactate and DL-glycerol-3-phosphate in membrane preparations from *Staphylococcus aureus* and interactions with the nitrate reductase system. J Bacteriol 134:585–589
8. Lefaou, AE, Morse SA (1987) Ferric reductase activity in *Neisseria gonorrhoeae*. Abstract: Annual Meeting, American Society of Microbiology, D-20, p 75
9. Lodge JS, Gaines CG, Arceneaux JE.L, Byers BR (1982) Ferrisiderophore reductase activity in *Azotobacter* [illegible] J Bacteriol 149:771–774
10. Lowry OH, Rosebrough NJ, Farr AL, Randall RJ (1951) Protein measurement with Folin phenol reagent. J Biol Chem 193:265–275
11. Moody MD, Dailey HA (1985) Ferric iron reductase of *Rhodopseudomonas sphaeroides*. J Bacteriol 163:1120–1125
12. O'Brien W, Paoletti LC, Blakemore RP (1987) Spectral analysis of cytochromes in *Aquaspirillum magnetotacticum*. Curr Microbiol 15:121–127
13. Paoletti LC, Blakemore RP (1986) Hydroxamate production by *Aquaspirillum magnetotacticum*. J Bacteriol 167:73–76
14. Paoletti LC, Short, KA, Blakemore [illegible] Blakemore RP (1987) Freeze-thawing *Aquaspirillum magnetotacticum* cells selectively releases periplasmic proteins. Appl Environ Microbiol 53:2590–2592
15. Short K, Blakemore RP (1986) Iron respiration-driven proton translocation in aerobic bacteria. J Bacteriol 167:729–731
16. Williams HD, Poole RK (1987) Reduction of iron (III) by *Escherichia coli* K-12: lack of involvement of the respiratory chains. Curr Microbiol 15:319–324

Journal of Magnetism and Magnetic Materials 73 (1988) 273–288
North-Holland, Amsterdam

MAGNETIC PROPERTIES OF MAGNETOTACTIC BACTERIA

B.M. MOSKOWITZ [1]

Department of Geological and Geophysical Sciences, Princeton University, Princeton, NJ 08544, USA

R.B. FRANKEL [2]

Francis Bitter National Magnet Laboratory, Massachusetts Institute of Technology, Cambridge, MA 02319, USA

P.J. FLANDERS

Physics Department and Laboratory for Research on the Structure of Matter, University of Pennsylvania, Philadelphia, PA 19104, USA

R.P. BLAKEMORE

Department of Microbiology, University of New Hampshire, Durham, NH 03824, USA

and

B.B. SCHWARTZ

Biomagnetech Corporation New York, NY 10017, USA

Received 20 January 1988; in revised from 1 April 1988

This paper reports on the magnetic properties of magnetosomes in the freshwater magnetotactic bacterium *Aquaspirillum magnetotacticum*. The magnetosomes are well crystallized particles of magnetite with dimensions of 40 to 50 nm, which are arranged within cells in a single linear chain and are within the single-magnetic-domain (SD) size range for magnetite. A variety of magnetic properties have been measured for two samples of dispersions of freeze-dried cells consisting of (1) whole cells (M-1) and (2) magnetosomes chains separated from cells (M-2). An important result is that the acquisition and demagnetization of various type of remanent magnetizations are markedly different for the two samples and suggest that remanence is substantially affected by magnetostatic interactions. Interactions are likely to be much more important in M-2 because the extracted magnetosome chains are no longer separated from one another by the cell membrane and cytoplasm. Other experimental data for whole cells agree with predictions based on the chain of spheres model for magnetization reversal. This model is consistent with the unique linear arrangement of equidimensional particles in *A. magnetotacticum*. The magnetic properties of bacterial and synthetic magnetites are compared and the paleomagnetic implications are discussed.

1. Introduction

Magnetotactic bacteria in marine or freshwater aquatic sediments orient and navigate along geomagnetic field lines [1]. These bacteria are typically microaerophillic, inhabiting the microaerobic sediment between the aerobic surface and anoxic deep layers. All species of magnetotactic bacteria contain magnetosomes, which are intracytoplasmic, membrane-bound particles of magnetite, Fe_3O_4 [2]. Magnetotactic bacteria synthesize Fe_3O_4 by accumulating ferric or ferrous iron, or both, from their environment to intracellular concentration that are 10^4 to 10^5 times higher than ex-

[1] Present address: Department of Geology, University of California, Davis, DA 95616, USA.

[2] Present address: Physics Department, California Polytechnic State University, San Luis Obispo, CA 93407, USA.

0304-8853/88/$03.50

tracellular concentrations [3]. Magnetosome morphologies are species dependent [4], but are invariable within the single-magnetic-domain (SD) size range for Fe_3O_4. Magnetosomes within cells are often arranged in one or more chains with the chain axis more or less parallel to the axis of motility of the cell. Because of interparticle interactions among the magnetosomes in a chain, all the particle moments are aligned parallel to each other along the chain direction. The chain of magnetosomes thus has a permanent magnetic dipole moment which is responsible for the magnetotactic response of the organism in the geomagnetic field [5].

Magnetotactic bacteria are found in the sediments of many aquatic environments [1]. When

Fig. 1. Electron micrograph of *A. magnetotacticum* used in this study. The scale bar is 1.0 μm.

cells die, their magnetosomes or magnetosome chains could remain in the sediments, making substantial contributions to the paleomagnetic record preserved in sedimentary rocks [6]. It has been suggested that fossil magnetosomes may be the primary source of stable natural remanent magnetization in marine sediments [6–10]. Chang et al. [7] reported isolation of SD magnetite of biogenic origin from modern marine carbonate oozes and calcareous laminated sediments. They also reported isolation of Fe_3O_4 particles, with morphologies analogous to magnetosomes in current magnetotactic bacteria, in Cambrian limestones dated to 500 million years. Petersen et al. [8] have also isolated chains of SD sized particles of Fe_3O_4 with similar morphologies from deep sea sediment cores dated to 50 million years.

Aquaspirillum magnetotacticum is a freshwater magnetotactic bacterium. This organism is currently the only magnetotactic microorganism available in pure culture [11]. *A. magnetotacticum* contains a single chain of magnetosomes that longitudinally traverses the cell, as shown in fig. 1. The Fe_3O_4 particles in this organism have linear dimensions of 40 to 50 nm and are separated from adjacent particles in the chain by approximately 4 to 10 nm [3]. The particles are well crystallized with truncated octahedral morphology and are oriented so that [111] faces are perpendicular to the magnetosome chain axis [4]. The number of magnetosomes per cell is variable within a population, but the average number is typically 10 to 20 magnetosomes per cell [3]. The average number of magnetosomes also varies with culture conditions, especially chelated iron concentration and dissolved oxygen tension [12]. Intact chains of magnetosomes can be separated from cell debris following cell rupture [13].

Rosenblatt et al. used static light scattering [14] and magnetically induced birefringence [15] to measure the average magnetic dipole moment per cell in suspensions of whole cells of *A. magnetotacticum* in water. Their results were consistent with estimates based on the amount of cellular Fe_3O_4 obtained from electron micrographs.

Initial bulk magnetic measurements on freeze-dried cells and isolated magnetosome chains of *A. magnetotacticum* were reported by Denham et al. [16]. The saturation magnetization (J_s) of the freeze-dried cells were consistent with an Fe_3O_4 content of about 1% dry weight of the cells. A saturation remanent magnetization (J_r) approximately equal to one-half the saturation magnetization confirmed the SD nature of the magnetosome chains. However, the coercive force (H_c) of 21.9 mT was inconsistent with the Stoner–Wohlfarth (SW) model [17] for magnetization reversal by coherent rotation. Instead, Denham et al. [16] suggested that the chain of spheres or fanning model, as proposed by Jacobs and Bean [18], was a better representation of magnetization reversal along a chain of magnetosomes. In addition, the saturation magnetization on a unit weight basis was higher for the isolated magnetosomes chains whereas J_r/J_s and H_c were lower than for the whole cells, suggesting stronger chain–chain magnetic interactions after removal of the cellular surroundings.

In this paper, we present a detailed magnetic study of magnetosomes in *A. magnetotacticum* grown in pure culture. A variety of magnetic properties have been measured on freeze-dried whole cells and magnetosomes chains separated from cells. An important result was that the acquisition and demagnetization of various type of remanent magnetizations were markedly different for the two samples and suggested that remanence was substantially affected by magnetostatic interactions. The magnetic properties of biogenic and comparably sized synthetic magnetites are also compared and discussed. In addition, hysteresis data for whole cells are shown to be consistent with predictions based on the chain of spheres model for magnetization reversal. Implications for paleomagnetism will be discussed.

2. Experimental procedures

2.1. Sample preparation

A. magnetotacticum was grown in batch culture in chemically defined medium as described previously [11]. Cells were harvested by filtration and washed in phosphate buffer. A portion of the washed cells was fixed in 1% glutaraldehyde and

subsequently freeze-dried after removal of the fixative, or kept in suspension [12]. Cells were disrupted with a French pressure cell and the magnetic cell fraction separated in a strong magnetic field gradient. This fraction was washed and resuspended 10 times in fresh buffer, treated with 1 M NaCl and again washed several times to remove adventitious protein. Electron microscopy showed that magnetosomes in this fraction were primarily in chains. The magnetosome chains were subsequently fixed in 1% glutaraldehyde and freeze-dried or kept in suspension.

Two samples of freeze-dried materials were studied: (1) M-1, which consisted of the intact whole cells and (2) M-2, which consisted of magnetosomes chains separated from cells. Measurements of saturation magnetization were consistent with a magnetite content of about 1% dry weight of the cells for M-1 and about 14% for M-2. The freeze-dried powders were mixed in a non-magnetic matrix of epoxy for remanence measurements. It should be emphasized that because of the higher concentration of magnetite in M-2, particle agglomeration was more likely to occur and therefore local concentrations in M-2 may be much higher than the average of 14%.

2.2. Magnetic measurements

Hysteresis loops were measured with an ac gradient force magnetometer [19]. Samples of whole cells or extracted magnetosomes were dried onto mylar film substrates and measurements made in the plane of the film. Using the ac gradient force magnetometer, the anisotropy field distribution was determined by saturating the sample magnetically, reducing the external field to zero, rotating the sample by approximately 6° for a randomly dispersed sample, or by 90° for an aligned sample, and measuring the component of magnetization normal to the field H. The field is cycled between zero and a maximum field whose value increases on consecutive cycles [19]. The average anisotropy field H_A was determined from the initial susceptibility (χ_0) of a spinning sample using a novel Hall method [20]. Rotational hysteresis W_R as a function of field was measured as a sample was spun clockwise and then counter clockwise at a frequency greater than 1000 rpm (see ref. [20] for more details). Magnetization measurements of whole cells in a water suspension before and after freezing in an applied field were made with a SQUID magnetometer.

Remanent magnetization (RM) was measured with a Schonstedt spinner magnetometer. Single- and multi-axis alternating field (af) demagnetization was conducted in a low-field environment using an af solenoid demagnetizer. For single-axis demagnetization, the axis of demagnetization was the axis along which RM was induced. Isothermal remanent magnetization (IRM) was produced using either a short-duration pulse discharge coil, with a peak field of 100 mT, or an iron-cored electromagnet, with a peak field of 800 mT. IRM acquisition curves were measured by applying incrementally increasing fields to initially demagnetized samples and noting the IRM produced. Static field demagnetization curves were measured by applying increasingly higher reverse-polarity dc fields to a saturation IRM (SIRM). Anhysteretic remanent magnetization (ARM) was imparted to the sample, initially af demagnetized at 120 mT, by applying an af of 100 mT simultaneously with a small dc field. The af was reduced slowly to zero and the remanent magnetization recorded. All ARM's were produced by dc fields that were always parallel to the axis of the alternating field. Zero-field decay of a viscous remanent magnetization (VRM) was measured after the sample was initially af demagnetized at 120 mT and then exposed to a constant field of 0.5 mT for approximately 16 h. Low-field initial susceptibility was measured using an ac susceptibility bridge.

3. Remanence curves and coercive forces

To facilitate comparisons among different remanent magnetization (RM) curves and their respective average coercivities, the following notation is used. All RM curves are normalized with respect to saturation remanence. IRM acquisition and dc demagnetization curves are denoted by $J_{ir}(H)$ and $J_d(H)$, respectively. The remanent coercive force, H_r, is the reverse dc field necessary to reduce an initial SIRM to zero. The comple-

ment to this is H_r', which is the dc field at which $J_{ir}(H)$ is 0.5. AF demagnetization curves of SIRM or ARM are denoted by $J_{ir}(\tilde{H})$ or $J_{arm}(\tilde{H})$, where $\tilde{H}$ is the peak alternating field. The median destructive field, $H_{1/2}$, is the af necessary to reduce an initial remanence by half. In addition, to estimate the spectral widths of the coercivity distributions exhibited by the various RM curves, let H_1 and H_2 be the fields at which the normalized intensity is, respectively, 15% and 85% of saturation (e.g., ref. [21]).

For an ensemble of non-interacting single-domain grains, Wohlfarth [22] has shown that the following relationships hold among the different RM curves:

$$J_d(H) = 1 - 2J_{ir}(H), \tag{1a}$$

$$J_{ir}(\tilde{H}) = \tfrac{1}{2}(1 + J_d(H)) = d(h), \tag{1b}$$

$$J_{ir}(\tilde{H}) = 1 - J_{ir}(H) = r(h). \tag{1c}$$

These relations also predict that $H_{1/2} = H_r' = H_r$ and on a plot of $J_{ir}(\tilde{H})$ and $J_{ir}(H)$, the crossover point occurs at a value $R = 0.5$ [21–26].

Particle interactions, however, will tend to offset the coercivity spectra of the different RM curves, and, as a result, relations (1a–c) will not be satisfied (e.g., refs. [21–26]). Instead, Kneller [26] proposed that the effects of particle interactions will produce two types of magnetic behavior with respect to relations (1a–c). Type I materials are characterized by $J_{ir}(\tilde{H}) < d(H) < r(H)$, $R < 0.5$ and $H_{1/2} < H_r' < H_r$. In contrast, type II materials are characterized by $J_{ir}(\tilde{H}) > d(H) \geq r(H)$, $R > 0.5$ and $H_{1/2} > H_r' \geq H_r$. Dispersed powders of SD particles, in which agglomeration of particles occur, are type I materials, whereas, SD precipitates in a non-magnetic matrix, in which minimal agglomeration occurs, are type II materials [26]. Multi-domain materials are always type I [26]. According to Kneller [26], the difference between type I and II interactions is effectively long-range interactions expressed via a mean field and short-range, or nearest-neighbor interactions, respectively. As will be shown subsequently, the magnetic properties of M-1 and M-2 correspond to type II and type I materials, respectively.

4. Results

4.1. Hysteresis measurements

Fig. 2 shows the hysteresis curve of a random dispersion of M-1. For this sample, $J_s = 0.6$ Am^2/Kg, $H_c = 26.8$ mT and $J_r/J_s = 0.53$. The value of J_s was equivalent to an Fe_3O_4 content of about 1% dry weight of the cells. The remanence ratio was consistent with the theoretical value of 0.5 for a randomly oriented ensemble of uniaxial SD particles, and agrees with an earlier study by Denham et al. [16].

The anisotropy field in M-1 was determined by three different methods. First, the distribution of anisotropy fields in a randomly oriented sample of M-1 was determined as outlined above. The resulting distribution in H_A is plotted in fig. 3 (curve A) and peaks at approximately 43.8 mT. Second, this value was checked by measuring the initial susceptibility of a spinning sample with the Hall probe technique [20]. The result from this measurement was $H_A = 47.8$ mT, in good agreement with the first method. Third, the anisotropy distribution for a water suspension of whole cells (M-1) dried onto a mylar film substrate in an external field of 13 T was determined. The anisotropy field distribution determined from this experiment (curve B, fig. 3) was nearly identical with the results obtained from the randomly dispersed sample used in the first two methods.

Hysteresis loops were also measured parallel to the direction of an orientating field. Here, a water suspension of whole cells (M-1) was dried onto

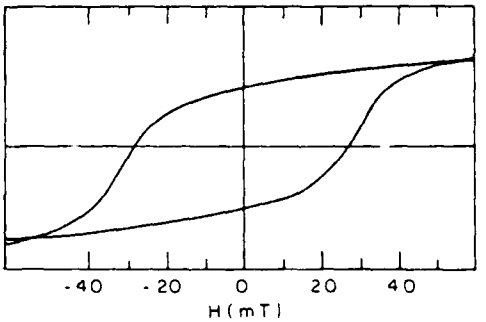

Fig. 2. Hysteresis loop for a random dispersion of freeze-dried whole cells of magnetic bacteria (M-1).

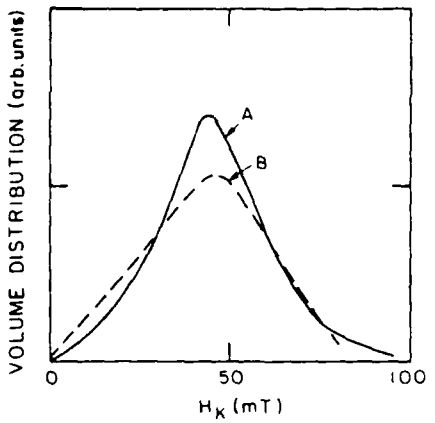

Fig. 3. Comparison of anisotropy field distribution for an aligned (curve A) and random (curve B) dispersion of freeze-dried whole cells. The aligned sample was produced by drying a water suspension of whole cells on a mylar film in an external field of 13 T.

mylar film substrates in either an external field of 0.6 T (aligned sample) or in the earth's field (random sample) and the results of this experiment are given in table 1. Theoretically, for the state of perfect alignment, the coercive force and remanence ratio in a parallel direction are $H_{c\parallel} = H_A$ and $J_{r\parallel}/J_s = 1.0$ [17]. However, $H_{c\parallel} \approx 0.6H_A$ and was approximately equal to the coercive force in the random dispersion. The latter result was consistent with the chain of spheres model [18].

Hysteresis loops and the distribution of anisotropy fields were also determined for a water suspension of extracted magnetosome chains (M-2) as a function of drying time in the earth's field. The effect of drying produces an increase in volume concentration. The results showed a dramatic decrease in the coercive force from 13.8 mT for a wet sample to 3.7 mT for a completely dried sample. The distributions of H_A also shifted to lower values as the sample dried, as shown in fig. 4. Moreover, the coercive force for a completely dried sample of magnetosome chains was approximately 90% lower than the value obtained for a sample of whole cells (M-1). In contrast, J_r/J_s decreased only slightly from 0.53 (wet) to 0.41 (dried).

Table 1
Coercive forces and remanence ratios for aligned and random dispersions of whole cells

Sample	H_c (mT)	J_r/J_s
aligned	28	0.85
random	28	0.53

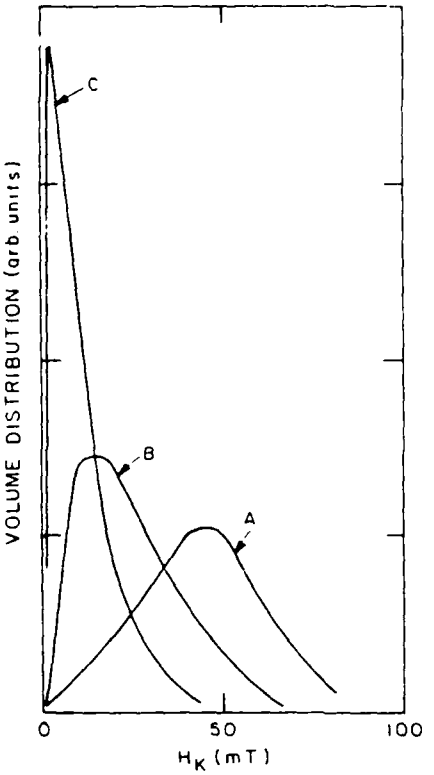

Fig. 4. Comparison of anisotropy field distributions for a random dispersion of freeze-dried whole cells (curve A) and for magnetosome chains separated from cells for samples partially dried after 30 min (curve B) and completely dried after 3 days (curve C).

Rotational hysteresis loss $W_R(H)$ as a function of field for M-1 is shown in fig. 5. The dimensionless parameter, $R_1 = \int [W_R(H)/J_s]\, dH^{-1}$, depends on the mode of magnetization reversal and provides a means to distinguish between coherent and incoherent modes [26]. From the data in fig. 5, R_1 is equal to 0.92 and is 2.5 times the value predicted by the SW model but is close to the value of 1.02 that is predicted for a random assembly of particles reversing their magnetization by fanning [26].

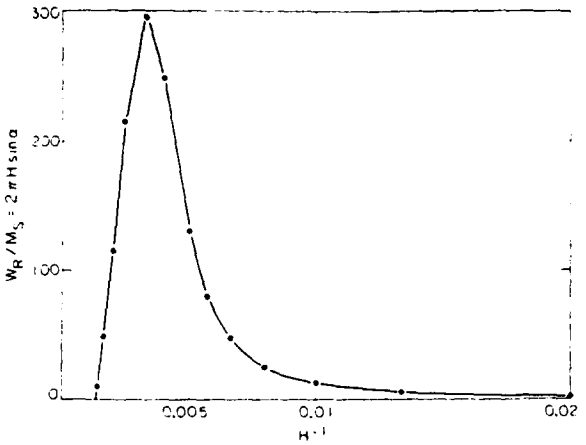

Fig. 5. Rotational hysteresis loss W_R versus H^{-1} (in mT) for random dispersion of freeze-dried whole cells. W_R is related to the experimental rotational lag angle α.

Measurements of the magnetic orientation of whole cells in a water suspension at 300 K were made with a SQUID magnetometer. The magnetization approached saturation for fields above 1.0 mT, as expected for an array of permanent magnetic dipoles with moments of the order of 3×10^{-16} Am^2.

Hysteresis loops were also determined for the suspension of cells after freezing in an applied field in the SQUID magnetometer. By measuring the magnetic moment during the cooling process, it was determined that the suspension froze below 265 K. The freezing process was found to disrupt

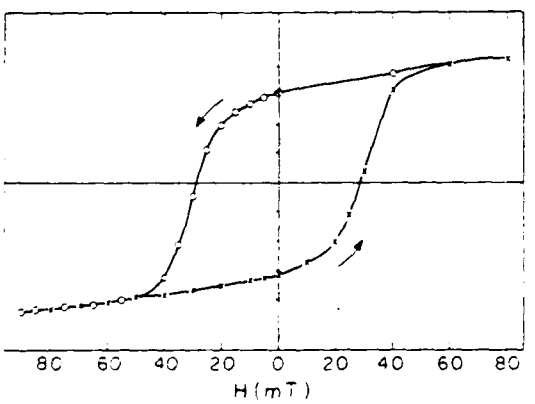

Fig. 6. Hysteresis loop for a suspension of fixed cells in water frozen in 0.9 T and measured in SQUID magnetometer.

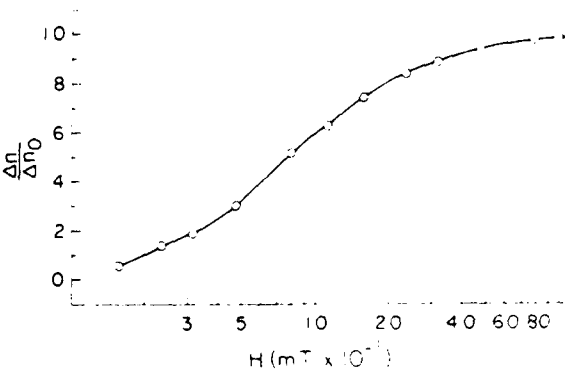

Fig. 7. Relative sample birefringence of suspension of whole cells in water as a function of applied magnetic field. The solid curve is the best fit to the data assuming an average magnetic moment per cell of 2.4×10^{-16} Am^2.

the alignment of the cells to an extent that depended on the applied field. At 115 mT, the moment decreased to 95% of the saturation value, but at 10 mT, the moment decreased to about 60% of the saturation value. The reason for this is unclear. The complete hysteresis loop for this sample is shown in fig. 6. From this curve, $H_c = 28$ mT and $J_r/J_s = 0.91$ and agree with the results in table 1.

4.2. Magnetically induced birefringence

Determination of the average magnetic dipole moment per cell was made by measuring the magnetically induced birefringence of the freeze-dried cells after resuspension in water [15]. The data in fig. 7 were fitted with an average magnetic moment per cell of 2.4×10^{-16} Am^2. This value agrees with results from other studies [14,15]. Using an estimated volume of Fe_3O_4 per cell from electron micrographs, the average magnetic moment corresponded to about 10 magnetosomes per cell.

4.3. Acquisition and demagnetization of IRM

Normalized RM curves of $J_{ir}(\tilde{H})$ and $J_{ir}(H)$ for M-1 and M-2 are shown in fig. 8 and coercivities and spectral parameters are listed in table 2. Both samples saturated by 60 mT, but M-1 had a slightly narrower coercivity spectrum for IRM acquisition (table 2) and approached saturation at

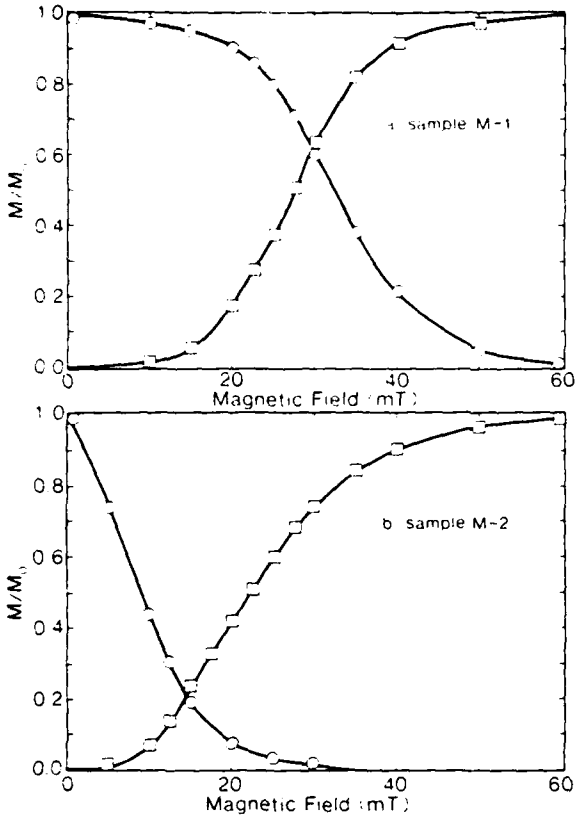

Fig. 8. Normalized curves of acquisition and af demagnetization of SIRM for (a) freeze-dried whole cells (M-1) and (b) freeze-dried magnetosome chains separated from cells (M-2).

Table 2
Coercivities and coercivity distribution parameters for whole and separated magnetosomes

Coercivity (mT)	M-1	M-2
H_c	26.7	3.7
H_r	27.6	16.6
H_r	27.5	22.4
$H_{1\ irm}$	32.2	9.0
$H_{1\ arm}$	33.7	12.3
$(H_1/H_2)_{irm}$ [a]	0.53	0.36
$(H_1/H_2)_{irm}$ [b]	0.50	0.19
$(H_1/H_2)_{irm}$ [c]	0.54	0.17
$(H_1/H_2)_{arm}$ [d]	0.55	0.30

[a] Distribution parameters for IRM acquisition.
[b] Distribution parameters for dc demagnetization of SIRM.
[c] Distribution parameters for af demagnetization of SIRM.
[d] Distribution parameters for af demagnetization of 0.1 mT ARM.

a slightly faster rate than M-2. In contrast, there were marked differences between samples during the demagnetization of SIRM, as illustrated in fig. 8. M-2 exhibited a wider spectral width ($\tilde{H}_1/\tilde{H}_2 = 0.17$), SIRM decayed more rapidly with $\tilde{H}$. R was equal to 0.21, complete demagnetization occurred at approximately 30 mT, and the af demagnetization spectrum was offset towards lower fields with respect to its dc magnetization spectrum. For M-1, however, the spectral width was narrower ($\tilde{H}_1/\tilde{H}_2 = 0.54$), R was equal to 0.62, complete demagnetization occurred at approximately 60 mT, and the af demagnetization

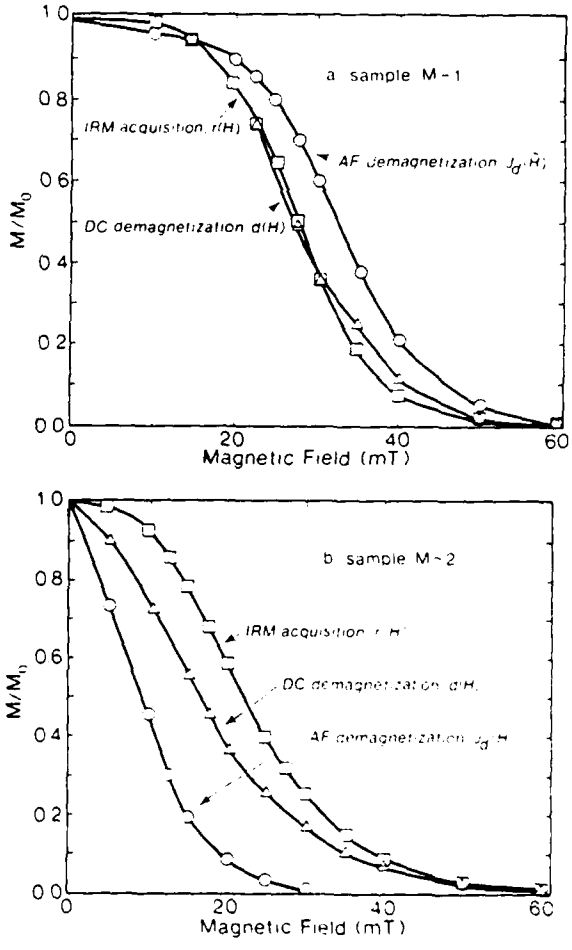

Fig. 9. Normalized remanence curves as a function of the applied field for (a) M-1 and (b) M-2. For comparison, all curves are plotted in terms of the af demagnetization curve according to the Wohlfarth relationships [eq. (1) of text].

spectrum was offset towards higher fields with respect to its dc magnetization spectrum. The various estimates of coercivities were also significantly different between the two samples (see table 2). Ratios of $H_{1/2}/H_r$ and H_r'/H_r were 1.17 and 1.00 for M-1 and 0.54 and 1.35 for M-2.

The difference in demagnetization characteristics between M-1 and M-2 was demonstrated further when remanence data were plotted in terms of $J_{ir}(\tilde{H})$, according to relations (1a–c). The results are shown in fig. 9 and confirmed that M-1 exhibited type II behavior, whereas M-2 exhibited type I behavior using the classification scheme of Kneller [26]. The results also illustrated that the most efficient method for erasing an SIRM was af demagnetization in M-2 and dc demagnetization in M-1. It should be noted, however, that when multi-axis af demagnetization was employed, it was found to be more efficient than either single-axis af or dc demagnetization methods. Furthermore, the R parameter determined from multi-axis af demagnetization of SIRM was lower than its value obtained from single-axis demagnetization [23].

4.4. Anhysteretic remanent magnetization

Fig. 10 compare ARM induction curves for M-1 and M-2. The approach to saturation was much more rapid in M-1 and M-2. For example, the ARM of M-1 was approximately 70% of saturation in a field of only 0.6 mT, whereas M-2

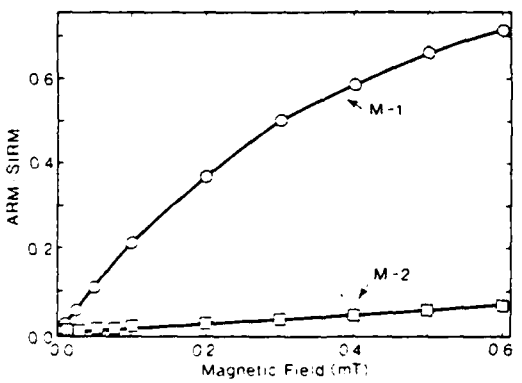

Fig. 10. Normalized acquisition of anhysteretic remanent magnetization as a function of applied dc field for M-1 and M-2.

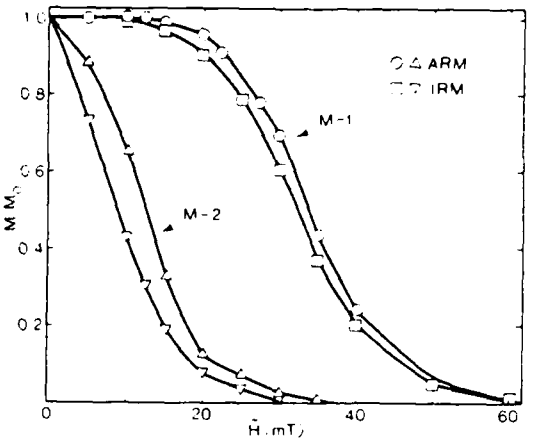

Fig. 11. Normalized af demagnetization curves of ARM and SIRM. ARM was acquired in dc field of 0.1 mT.

was barely at 10% of saturation in the same field. As a comparison, for comparable sized dispersed single-domain powders, ARM was less than 30% of saturation by 0.6 mT [27,28]. Initial anhysteretic susceptibilities (actually χ_{arm}/SIRM) were 2.68 $(kA/m)^{-1}$ and 0.13 $(kA/m)^{-1}$ for M-1 and M-2, respectively.

4.5. Lowrie–Fuller test

A commonly used procedure in rock magnetism is the Lowrie–Fuller test [29,30], in which the af demagnetization spectra of a strong-field remanence, such as SIRM, is compared to a weak-field remanence, such as ARM. This test has been shown to discriminate between SD-like and MD-like particles. For example, weak-field ARM in SD and small MD particles exhibit more resistance to af demagnetization than strong-field IRM, whereas large MD particles exhibit the opposite behavior (see ref. [30] for a complete discussion).

The results of the Lowrie–Fuller test for M-1 and M-2 are shown in fig. 11 and predicted that the domain state was SD, as one would have suspected based on particle size alone. The ARM and SIRM demagnetization curves were also similar in form for each sample but quite different between samples. The initial plateaus in the ARM and SIRM curves in M-1, which were missing in M-2, indicated that a threshold field must be

reached before demagnetization started. In contrast, the rapid demagnetization of ARM and SIRM in M-2, reminiscent of demagnetization curves for multi-domain materials, suggested that moments with very low coercivities were present. Variable and strong interaction fields in M-2 may be responsible for its low stability to af demagnetization. The results of fig. 11 also demonstrated that interactions in SD materials apparently do not effect the outcome of the Lowrie–Fuller test and agree with results obtained by Cisowski [23].

The ARM and SIRM data can be compared directly to results given in ref. [8], which were obtained from deep-sea sediments that possibly contained biogenic magnetite. Petersen et al. [8] used the parameters $\Delta LF = H_{1,2arm} - H_{1,2irm}$, ARM/SIRM, and $H_{1,2irm}$ to distinguish between biogenic SD and inorganic MD magnetite. The magnetic properties of some of their samples, which were later found to contain magnetite particles with morphologies that suggested a biogenic origin, fell within a narrow range of values (their A component) with $\Delta LF \approx 4.5$–7.0 mT, ARM/SIRM ≈ 0.07–0.10 and $H_{1/2irm} \approx 12$–15 mT. By contrast, our magnetic results on biogenic magnetite were significantly different from those attributed to their A component; specifically, $\Delta LF = 1.5$ mT, ARM/SIRM = 0.11 and $H_{1/2irm} = 32.2$ mT for M-1 and $\Delta LF = 3.3$, ARM/SIRM = 0.005 and $H_{1/2irm} = 9.0$ mT for M-2.

4.6. Viscous remanent magnetization

There were also significant differences in VRM behavior between M-1 and M-2. The viscous moments normalized to SIRM, acquired in a steady field of 0.5 mT after $t_a = 16$ h, were approximately 0.08% for M-1 and 0.76% for M-2. The zero field decay of VRM is shown in fig. 12 The experimental decay curves were fitted to polynomial functions in ln t by step-wise regression. For decay times t_d less than t_a,M-1 exhibited a linear logarithmic decay (VRM $\propto$ ln t). In contrast, the best fit polynomial for M-2 consisted of a constant term plus a term proportional to $(\ln t)^3$. After 16 h ($t_d > t_a$), the decay curves started to tail off but with a significant fraction (40–50%) of the original VRM remaining after a decay time equal to the original exposure time, this effect being more pronounced in M-2. In other words, acquisition of VRM proceeded more rapidly than its subsequent decay.

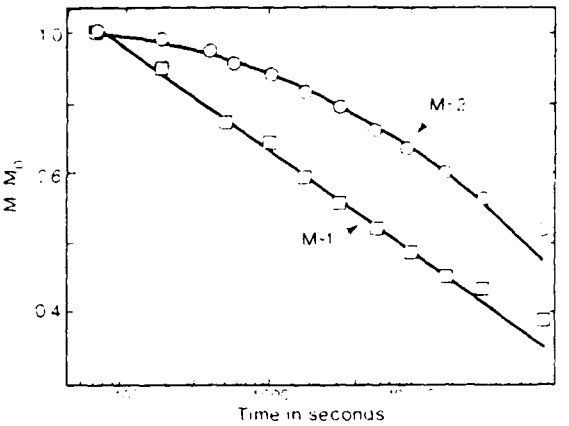

Fig. 12. Normalized zero-field decay of VRM. Solid lines are best fit polynomials in ln t to the data.

5. Discussion

5.1. Magnetostatic interactions

Magnetostatic interactions are most likely responsible for the marked contrast between the magnetization and demagnetization characteristics of M-1 and M-2. Stronger particle interactions are assumed to correspond to greater degree of particle agglomerations. Particle agglomeration is much more likely to occur in M-2 because the extracted magnetosome chains are no longer separated by the cell membranes and cytoplasm of the bacteria and, hence, are closer together on average. In this case, the interaction fields make it more difficult to magnetize than to demagnetize a sample (type I behavior). The offsets between the coercivity spectra, as observed in M-2, also have been observed in rocks, dispersed magnetic powders and magnetic recording media [21,23,25]. In contrast, the individual chains are still intact within the bacteria in M-1 and are therefore separated from one another by the cell membranes and cytoplasm. Thus, agglomeration of the chains should be reduced considerably. In this case, the

af spectra are shifted towards higher fields and the dc spectra are shifted towards lower fields. The apparent reduction in agglomeration is apparently sufficient to produce type II behavior, but interactions must still be important in M-1; otherwise, the RM curves should be described exactly by the Wohlfarth relations. This type of behavior has not been reported in samples consisting of dispersed powders, although it has been observed in certain precipitation alloys [26].

It is well known that magnetic interactions are responsible for ARM properties [26]. An estimate of the magnitude of the interaction fields in M-1 and M-2 can be obtained from the ARM results following Jaep [31,32]. Strictly speaking, Jaep's theory is valid only for interactions that are long-range and can be modeled by a mean field approximation [33]; however, adjusting the theory to take into account short-range interactions results in a similar equation of ARM [33]. For the region where the intensity of ARM is linearly dependent on the external field h_{dc}, the ARM in an ensemble of interacting single-domain grains is approximately,

$$\mathrm{ARM/SIRM} = Bh_{dc}/(kT/J_s + \lambda), \qquad (2)$$

where h_{dc} is the applied field, λ is the interaction field, $B \approx J_{sb}/J_s\ (T/T_b)^{1/2}$, and the subscript "b" refers to the value of the parameter at the blocking temperature [31,32]. However, the experimental blocking temperature and, subsequently B and λ, for the bacterial magnetites were not determined directly because of the possible adverse chemical changes which could be induced by heating the sample close to its Curie temperature. Nevertheless, estimates of λ can still be obtained from estimates of B by using reasonable limits for T_b as follows.

The parameter B was calculated for different values of T_b at 5° intervals between 500 and 575°C with J_s taken from Pauthenet [34]. λ was then determined using eq. (2) and the initial slope of the ARM induction curve (fig. 10). Using the limits for T_b, λ was found to very between 0.012 and 0.065 mT for M-1, and between 0.98 and 2.4 mT for M-2 and indicated that the interaction fields were approximately 50 times greater in M-2. In addition, an average distance between chains of particles (assuming an average chain length of 10 particles) that would be necessary to produce a field equal to λ was also determined. This calculation predicted that the particle chains were 1–3 μm apart in M-1, but only 0.3–0.4 μm apart in M-2. The former estimate was consistent with the average size of an individual bacterium.

The time dependence of magnetization can also be related qualitatively to the degree of particle interactions. For example, most theories of magnetic viscosity for non-interacting SD particles predict a linear ln t dependence of magnetization [35]. However, the time dependence commonly observed is non-linear in ln t for many rocks, dilute fine-particle dispersions and spin glasses (e.g., refs. [36–40]). Using a mean random field approach, Walton and Dunlop [39] predicted that the aquisition and decay of VRM should follow a polynomial ln t dependence. As our ARM results suggested, interactions fields were much lower in M-1, which exhibited a linear ln t dependence, than in M-2, which did not. The distinct curvature exhibited by the time dependence of magnetization of M-2 has also been observed in synthetic SD and small MD magnetites [36].

However, to explain the observation that acquisition of VRM is faster than the corresponding decay, a different distribution of activation times must be involved during acquisition and decay. It is possible that a distribution of interactions fields could produce the asymmetry between acquisition in an external field and decay in zero field. This asymmetry has also been observed in many other SD and MD materials (e.g., refs. [36,37]); however, there is not yet a satisfactory theoretical explanation for this observation.

5.2. *Bacterial versus synthetic magnetite*

The results of our experiments also offer an excellent opportunity to compare and contrast the magnetic properties of bacterial magnetite to comparably size synthetic magnetite, particularly concerning the role of magnetostatic interactions. The importance of interactions is dispersed magnetic powders has been suggested often (e.g. refs. [21,23,26]). Invariably, for samples consisting of

dilute dispersions of magnetite in a non-magnetic matrix, particle interactions are prevalent due to particle agglomerations. Moreover, most synthetic magnetites are compared of a distribution of particle sizes. The combined effects of magnetostatic interactions and a distribution of particle sizes play an important role in determining the magnetic properties of an ensemble of SD particles. The separation of these two effects is particularly important for various methods of magnetic granulometry, which are being used in many studies of the environmental applications of magnetism (e.g., ref. [41]). The narrow particle size distribution of the bacterial magnetite effectively removes particle size as a variable; hence, differences in magnetic properties between the freeze-dried samples should be due to interactions alone.

Magnetic properties of synthetic magnetites have been taken from the rock magnetic literature [21,42–45] and included: (1) chemically precipitated equidimensional particles, with grain sizes ranging from 25 to 220 nm; and (2) acicular particles with axial ratios of 8 : 1 and 7 : 1 and absolute dimensions of 30×200 nm^2 and 40×3500 m^2, respectively. The acicular particles have similar grain dimensions to the magnetosome chains in M-1. These samples were chosen for comparison because their ARM, SIRM, χ_0, S_d and coercivity data were available in the literature. Additionally, to eliminate errors arising from uncertainties in the concentration of magnetite in our samples, ratios of magnetic parameters that are independent of concentration were used for comparisons. Parameter ratios are summarized in table 3 and coercivity data are summarized in table 4.

Table 3
Magnetic parameters of bacterial and synthetic magnetite

Parameter	M-1	M-2	Cubic [a]	Acicular [b]
χ_{arm}/χ_0	148.7	1.46	5.19–9.76	5.98–38.2
χ_{arm}/SIRM ($1/kAm^{-1}$)	2.675	0.125	0.150–0.188	0.113
χ_0/J_s ($\times 10^{-3}$ ($1/kAm^{-1}$))	9.86	34.88	8.75	6.87
SIRM/χ_0 (kAm^{-1})	55.58	11.73	32.08–51.68	53.12
S_d/J_s ($\times 10^{-4}$)	0.26	0.92	0.60	–
J_r/J_s	0.53	0.41	0.28	0.36–0.45
H_r/H_c	1.02	4.49	1–2	1–2

[a] Values were interpolated for a grain size of 42 nm. Results were taken from refs. [42–45].
[b] Acicular magnetites were 30×200 nm^2 [45] and 40×350 nm^2 (King, unpublished).

Table 4
Coercivities of bacterial and synthetic magnetites

Coercivity (mT)	M-1	M-2	Cubic [a]	Acicular [b]
H_c	26.7	3.7	21.3	30.5–43.8
H_r	27.6	16.6	38.4	50.5–60.0
H_r'	27.5	22.4	50.6	67.7
$H_{1/2irm}$	32.2	9.0	28.3	43.4
$H_{1/2arm}$	33.7	12.3	–	57.1

[a] Values were interpolated for a grain size of 42 nm. Results were taken from ref. [21].
[b] Acicular magnetites were 30×200 nm^2 [21] and 40×350 nm^2 [44].

5.2.1. Parameter ratios

Particle interactions should have a pronounced effect on the ratios χ_{arm}/χ_0 and χ_{arm}/SIRM with χ_{arm} decreasing and χ_0 increasing with the strength of the interaction field [26]. The ratios χ_{arm}/χ_0 and χ_{arm}/SIRM for M-2 were similar to, but slightly lower than, those for the equant magnetites. On the other hand, the same ratios for M-1 were at least 10 times higher than the equant magnetites and 4–10 times higher than the acicular magnetites. The similar ARM results between M-2 and the synthetic magnetites suggest that similar interactions, presumably due to agglomeration effects are responsible for ARM in both types of materials. This conclusion is supported further by the observation that all synthetic dispersed magnetites exhibit type I behavior [21,23], just like M-2. Significantly, it is interesting to note that the volume percent of magnetite in M-2 is higher than the dispersed synthetic powders and suggests that dilution alone does not reduce agglomeration. The higher values of χ_{arm}/χ_0 and χ_{arm}/SIRM for M-1, undoubtedly related to the reduced effects of agglomerations, indicate that acicular magnetite is not a good analog for ARM

in M-1, even though the particle dimensions are approximately the same.

The χ_0/J_s and SIRM/χ_0 parameters for M-1 were at the high end of the range of values reported for synthetic magnetites (table 3). By contrast, for M-2, χ_0/J_s was higher and SIRM/χ_0 lower than the values in M-1 and the synthetic magnetites. The effects of particle agglomerations on χ_0 are probably responsible for these differences because the effects of agglomerations on the intensity of SIRM appear to be minor, as evidenced by the smaller decrease in J_r/J_s between M-1 and M-2 (table 3). Particle agglomerations can produce an increase in χ_0 by effectively producing a general decrease in shape anisotropy in a dispersion of particles. The shift in the anisotropy field distribution toward lower fields with drying time (or equivalently with increasing agglomeration, see fig. 4) is consistent with a decrease in shape anisotropy.

The ratio S_d/J_s for the bacterial and synthetic magnetites, reduced to $h = 0.1$ mT, is shown in table 3. The trend in this ratio, M-2 > equant magnetite > M-1, corresponds to the increase in the volume concentration of magnetite in each sample and suggests that increased particle interactions also increases the viscosity coefficient.

5.2.2. Coercivity

Values of coercivities for bacterial and synthetic magnetites are summarized in table 4. For M-1, H_c and $H_{1/2}$ were higher and H_r and H_r' lower than they were for equant magnetites and reflected the difference between the interaction fields in type I (synthetic equant magnetite) and type II (M-1) materials. Dankers [24] observed that in weakly magnetic SD hematite, where interactions should be negligible, $H_r' \approx H_r$, in agreement with the results for M-1. In contrast, M-2 had $H_r' > H_r$, as well as much lower coercivities than observed in the synthetic magnetites, presumably due to the increased in particle interactions in M-2. However, Dunlop [45] observed only minor changes in coercivity in nearly SD sized magnetites with concentrations up to 30% by volume.

Whereas the absolute values of coercivities between M-2 and the synthetic magnetites are different, the ratios $H_{1/2}/H_r$ and H_r'/H_4 are not. For example, Dunlop [21] found that H_r'/H_r = 1.25–1.38 and $H_{1/2}/H_r = 0.62$–0.86 for dispersed SD magnetites. In comparison, in M-2, H_r'/H_r = 1.35 and $H_{1/2}/H_r = 0.54$. However, the similar value of these ratios for the two sets of samples is only an expression of the more general relationship, $H_r' + H_{1/2} \approx 2H_r$, which was found to hold for dispersed samples of magnetite ranging in size from 0.1 to 250 μm [21,24]. According to Kneller [26], $H_r' + H_{1/2} = 2H_r$ is predicted for interacting type I SD materials, in which interactions can be modeled by a mean field approximation. However, M-1, a type II material, also approximately obeys this relationship, so its significance is unclear.

It is also interesting to compare the ratio H_r/H_c between sample M-1 and M-2 (table 3). Theoretically, in a randomly oriented ensemble of coherently reversing SD particles, $1 < H_r/H_c < 2$ [26]. The data for M-1 and the synthetic magnetites agree with the predicted SD values. However, H_r/H_c for M-2 is significantly higher than predicted. The high value of H_r/H_c is due to the much greater decrease of H_c when the magnetosomes are extracted from the cells. H_c decreases nearly 90% but H_r decreases only 40% upon extraction. High values of H_r/H_c often indicate the presence of SP particles or a mixture of soft and hard coercivity components [26], although in our case SP particles seem unlikely. On the other hand, interactions may either produce low coercivity components or produce an increase in susceptibility such that J_r is balanced only by the induced magnetization $-\chi_0 H_c$ [21]. The af demagnetization of SIRM and ARM for M-2, however, is consistent with low coercivity moments.

5.3. Chain-of-spheres model

The SW model for coherent rotation of magnetization due to shape anisotropy predicts that the coercive force in M-1 should be approximately 140 mT for an axial ratio of 10 : 1 (i.e., a chain length of 10 particles). The much lower observed coercive force of 23.8 mT in M-1 suggests a noncoherent reversal mechanism. A likely mechanism for moment reversal along a chain of magneto-

somes is the fanning or chain of spheres model [18], as first suggested by Denham et al. [16].

The chain-of-spheres model was originally developed to explain the coercive force in elongated single domain grains [18]. This model should be ideal to describe the reversal mode in M-1 because of the unique linear arrangement of equidimensional particles in bacterium. Experimental values for the rotational hysteresis integral and the ratio of coercive forces for random and aligned sample for M-1 are compared with predictions based on the SW and chain-of-spheres models in table 5. The experimental data are in excellent agreement with the chain-of-spheres model.

In the original chain-of-spheres calculations [18], however, the spheres were assumed to be touching. It is clear from electron micrographs that this is not the case for magnetosomes in magnetotactic bacteria. To account for a finite separation distance, the model coercive forces must be reduced by $(1+\beta)^{-3}$, where $\beta = x/a$, a is the particle diameter and x is the separation distance. This correction assumes that β is a constant along the chain length in an individual bacterium. Coercive force for randomly oriented chains as a function of β are plotted in fig. 13 for three different reversal models [18]: (1) symmetric fanning (model A), where the magnitude of the angle of fanning is constant along the length of the chain; (2) non-symmetric fanning (model A′), where the angle of fanning is not constant; and (3) parallel rotation (model B). The results of these calculations are as follows.

First, H_c increases continuously with chain length for both models A and B, whereas, in model A′, H_c is nearly independent of chain length for n greater than 6 [18]. Second, the values for β estimated from the observed coercive force for

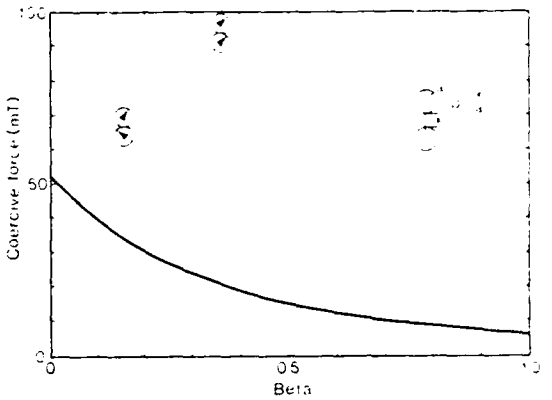

Fig. 13. Coercive forces for a randomly oriented chain of spheres as a function of sphere separation (β). Model calculations are based on the the chain of spheres model [18]. The dark stipple curve is for parallel rotation (model B), the light stipple curve is for symmetric fanning (model A), and the solid curve is for non-symmetric fanning (model A′). The width of each curve takes into account different chain lengths from 6 to an infinite number of spheres. See text for further details.

M-1 ($H_c = 26.7$ mT) using fig. 13 are (1) 0.25 for model A′, (2) 0.37–0.46 for model A and (3) 0.8–0.9 for model B. Models A and A′ predict values of β that are consistent with observation ($x \approx 3$–18 nm, $\beta \approx 0.07$–0.43 [3]). In contrast, model B predicts values of β that are too high and therefore it seems unlikely that coherent rotation is important. Third, to account for the observed coercivity spectrum (i.e., $H_1/H_2 \neq 1$, see table 1), or the distribution of anisotropy fields (fig. 3) in M-1, either a distribution in chain length (model A only), or a distribution of β (model A or A′), or both, must be assumed. Finally, it is interesting to note that the acicular magnetites had significantly higher values of coercivity than M-1 (see table 4), even though the particle dimensions were comparable. This disagreement may partly reflect the finite separation of magnetosomes along the chain length. This result may also indicate a completely different reversal mechanisms for acicular particles as suggested by Knowles [46].

Table 5
Calculated and observed values for selected magnetic parameters. Model values are based on an ensemble of random uniaxial particles

Parameter	SW model	Fanning model	M-1
R_1	0.380	1.02	0.92
H_c(random)/H_c(aligned)	0.479	1.08–1.13	0.93

5.4. Implications for paleomagnetism

Despite the successes of paleomagnetism, the mechanisms by which the remanent magnetization of marine sediments is acquired, and subsequently

retained over geologic time remains poorly understood. Rock magnetic studies indicate that the remanence in many marine sediments reside in SD-like particles of magnetite (e.g., ref. [47]). Yet, the exact identification of these particles, in many cases, has not been made. Since the discovery of magnetotactic bacteria, it has been suggested that fossil biogenic SD magnetite may be the primary carrier of remanent magnetization in marine sediment [6–10].

Petersen et al. [8] proposed some simple magnetic measurements to demonstrate the existence of biogenic magnetite in deep-sea sediments. However, our results, using the same measurements, are not consistent with those in ref. [8]. There are several possible explanations for this discrepancy. First, the parameters used in ref. [8] are likely to distinguish between any type of SD from MD particle, and not just biogenic magnetite. Second, we do not know if different species, or ancient species, of magnetotactic bacteria would exhibit slightly different magnetic properties. Third, the fossil biogenic magnetite could conceivably act as individual particles, whereas in our samples they are still in chains. For all these reasons, it is not too surprising that our results differ significantly from those in ref. [8].

The SD nature of magnetosomes is clearly demonstrated. The problem is how the magnetosomes are incorporated into the sediments. Do the chains remain intact, or do the individual particles separate and then agglomerate? Preliminary results [7–10] suggests that the chains remain intact after deposition. If so, the marked contrast between acquisition and demagnetization of SIRM (fig. 8) for M-1 and M-2 would suggest a simple magnetic test for the presence of magnetosome chains. The unique type II behavior exhibited by M-1 would be diagnostic for intact magnetosomes. However, several factors could serve to mask the type II behavior. As far as we know, all non-biogenic magnetic phases in rocks exhibit type I behavior. Therefore, the presence of any non-biogenic magnetite or any other magnetic phases, in sufficient quantity, could dominate the SIRM behavior. Finally, our results suggest that until a type II response is observed in marine sediments, electron microscope observation of magnetite morphologies is the only unambiguous technique for distinguishing between lithogenic and biogenic magnetite.

6. Conclusions

(1) Freeze-dried powders of *A. magnetotacticum* containing either intact whole cells (M-1) or magnetosome chains separated from cells (M-2) exhibited single-domain behavior.

(2) An average magnetic dipole moment per cell of 2.4×10^{-11} Am^2 was determined by magnetically induced birefringence. The average magnetic moment corresponded to about 10 magnetosomes per cell.

(3) The acquisition and demagnetization of IRM and ARM and the time dependence of VRM were significantly different between M-1 and M-2. This contrast in magnetic behavior was attributed to different degrees of particle agglomerations or, equivalently, to differences in the strength of the interaction fields in each sample. Particle agglomeration was greater and interaction fields larger in M-2 because the extracted magnetosomes chains were no longer separated from one another by the cell membranes and cytoplasm of the bacteria.

(4) AF demagnetization spectrum of SIRM was shifted towards higher fields with respect to the dc spectra for M-1, whereas the opposite behavior was observed for M-2. According to the classification scheme of Kneller [26]; M-1 and M-2 exhibited type II and type I behavior, respectively. The reason for this difference, although qualitatively related to magnetostatic interactions, was unclear.

(5) M-1 exhibited magnetic properties that were markedly different from those in synthetic dispersed powders of comparable grain size.

(6) The chain-of-spheres model predicted values for the coercive force, the rotational hysteresis parameter, and the ratio H_c(random)/H_c(aligned) that agreed with experimental values for M-1. This model was consistent with unique linear arrangement of equidimensional single-domain particles in *A. magnetotacticum*.

(7) The unique type II behavior of M-1 would suggest a simple magnetic method for determining the presence of intact magnetosome chains in sediments, although several factors could mask this effect in natural samples.

Acknowledgements

This research was partially supported by DARPA through Biomagnetech Corporation. We thank Y. Gorby and N. Blakemore for sample preparation. C.R. Rosenblatt for birefringence measurements and Naoma Doherty for remanence measurements. RBF was partially supported by the Office of Naval Research.

References

[1] R.P. Blakemore, Ann. Rev. Microbiol. 36 (1982) 217.
[2] R.B. Frankel, Ann. Rev. Biophys. Bioeng. 13 (1984) 85.
[3] D.L. Balkwill, D. Maratea and R.P. Blakemore, J. Bacteriol. 141 (1980) 1399.
[4] S. Mann, R.B. Frankel and R.P. Blakemore, Nature 310 (1984) 405.
[5] R.B. Frankel and R.P. Blakemore, J. Magn. Magn. Mat. 15–18 (1980) 1562.
[6] J.L. Kirschvink and H. Lowenstam, Earth Planet. Sci. Lett. 44 (1979) 193.
[7] S.B.R. Chang, J.L. Kirschvink and J.F. Stoltz, Phys. Earth. Planet. Inter. 46 (1987) 289.
[8] N. Petersen, T. von Dobeneck and H. Vali, Nature 320 (1986) 611.
[9] J.L. Kirschvink and S.R. Chang, Geology 12 (1984) 559.
[10] J.F. Stolz, S.R. Chang and J.L. Kirschvink, Nature 321 (1986) 849.
[11] R.P. Blakemore, D. Maratea and R.S. Wolfe, J. Bacteriol. 140 (1979) 720.
[12] Y. Gorby, T.J. Beveridge and R.P. Blakemore, J. Bacteriol. 170 (1988) in press.
[13] R.P. Blakemore, K.A. Short, D.A. Bazylinski, C. Rosenblatt and R.B. Frankel, Geomicrobiol. J. 4 (1985) 53.
[14] C. Rosenblatt, F.F.T. de Araujo and R.B. Frankel, J. Appl. Phys. 53 (1982) 2727.
[15] C. Rosenblatt, F.F.T. de Araujo and R.B. Frankel, Biophys. J. 40 (1982) 83.
[16] C.R. Denham, R.P. Blackemore and R.B. Frankel, IEEE Trans. Magn. MAG-16 (1980) 1006.
[17] E.C. Stoner and W.F. Wohlfarth, Trans. Roy. Soc. (London) A240 (1948) 599.
[18] I.S. Jacobs and C.P. Bean, Phys. Rev. 100 (1955) 1060.
[19] P.J. Flanders, J. Appl. Phys. (1988) in press.
[20] P.J. Flanders, IEEE Trans. Magn. MAG-21 (1985) 1584.
[21] D. Dunlop, Earth Planet. Sci. Lett. 78 (1986) 288.
[22] E.P. Wohlfarth, J. Appl. Phys. 29 (1958) 595.
[23] S. Cisowski, Phys. Earth Planet. Inter. 26 (1981) 56.
[24] P. Dankers, Geophys. J. Roy. Astron. Soc. 64 (1981) 447.
[25] G.W.D. Spratt, P.R. Bissell and R.W. Chantrell, IEEE Trans. Magn. MAG-22 (1986) 659.
[26] E. Kneller, in: Magnetism and Metallurgy, eds. A.E. Berkowitz and E. Kneller (Academic Press, New York, 1969) p. 366.
[27] D.J. Dunlop and G.F. West, Rev. Geophys. Space Phys. 7 (1969) 709.
[28] E. Schmidbauer and N. Schembera, Phys. Earth Planet. Inter. 46 (1987) 77.
[29] W. Lowrie and M. Fuller, J. Geophys. Res. 76 (1971) 6339.
[30] M.E. Bailey and D.J. Dunlop, Earth Planet. Sci. Lett. 63 (1983) 335.
[31] W.F. Jaep, J. Appl. Phys. 42 (1971) 2790.
[32] S.K. Banerjee and J.P. Mellema, Earth Planet. Sci. Lett. 23 (1974) 177.
[33] R.W. Chantrell and E.P. Wohlfarth, J. Magn. Magn. Mat. 40 (1983) 1.
[34] R. Pauthenet, C.R. Acad. Sci. (1950) 1842.
[35] L. Néel, Ann. Geophys. 5 (1949) 99.
[36] D.J. Dunlop, Geophys. J. Roy. Astron. Soc. 74 (1983) 667.
[37] B.M. Moskowitz, Geophys. J. Roy. Astron. Soc. 82 (1985) 143.
[38] R.V. Chamberlin, J. Appl. Phys. 57 (1985) 3377.
[39] D. Walton and D.J. Dunlop, Solid State Commun. 53 (1985) 359.
[40] R.H. Chantrell, M. Fearon and E.P. Wohlfarth, Phys. Stat. Sol. (a) 97 (1986) 213.
[41] R. Thompson and F. Oldfield, Environmental Magnetism (Allen and Unwin, London, 1986) p. 227.
[42] D.J. Dunlop, J. Geophys. Res. 78 (1973) 7602.
[43] D.J. Dunlop, M.E. Bailey and M.F. Westcott-Lewis, Geochim. Cosmochim. Acta 39 (Suppl. 6) (1975) 3063.
[44] J.W. King, S.K. Banerjee and J. Marvin, J. Geophys. Res. 88 (1983) 5911.
[45] D.J. Dunlop, J. Geophys. Res. 91 (1986) 9569.
[46] J.E. Knowles, IEEE Trans. Mag. MAG-20 (1984) 84.
[47] R. Freeman, Geophys. J. Roy. Astr. Soc. 85 (1986) 433.

CHAPTER 6

Biomineralization by magnetogenic bacteria

RICHARD P.BLAKEMORE[1] and RICHARD B.FRANKEL[2]

[1]*Department of Microbiology, University of New Hampshire, Durham, NH 03824, USA and* [2]*Department of Physics, California Polytechnic State University, San Luis Obispo, CA 93407, USA*

Introduction

As indicated by the contributions to this symposium, microbes and metals interact in a multitude of ways, in which the latter may have roles ranging from being vital structural and functional cell components to being toxic agents. The magnetotactic bacteria (Blakemore, 1975, 1982; Frankel, 1982) transform extracellular iron into the mixed-valence iron oxide mineral magnetite (Fe_3O_4) comprising an intracellular magnetic navigational apparatus (*Figure 1*); they provide a fascinating example of the seemingly unlimited capacity of life to adapt to the physical and chemical world. Readers interested in the role of biogenic magnetite in magnetotaxis and cell navigation in the magnetotactic bacteria and other organisms are referred to several reviews (Frankel, 1982, 1984; Blakemore, 1982; Blakemore *et al.*, 1988).

A purpose of this chapter is to give further emphasis to the poorly characterized physiological group of bacteria, the 'dissimilatory iron-reducers' (a term first suggested in a footnote on page 190 of Ehrlich, 1981; see also Short and Blakemore, 1986; Lovley, 1987) by reviewing aspects of those members that produce magnetite as a biomineralization product. The term 'magnetogenic' bacteria is proposed for these dissimilatory iron reducers. As is apparent from study of their physiology, occurrence and distribution, the magnetotactic bacteria appear to be (facultative) dissimilatory iron-reducers. Recently, dissimilatory iron-reducing bacteria which produce extracellular magnetite have been reported (Lovley *et al.*, 1987; Bell *et al.*, 1987). Each of these types of magnetogens carries out a different manner of biomineralization, producing different forms of the same mineral. Bacterial magnetite, especially as being a biomineralization product of these bacteria and a mineral of biogeochemical interest, is examined in more detail in the pages which follow. Recent reviews by Lovley (1987) and Jones (1986) provide a more comprehensive treatment of the broader subject of dissimilatory iron reduction by microorganisms.

Prokaryotes and respiratory diversity

Diversity is a hallmark of prokaryotes. As with eukaryotes, this is evident from their great variation in structure and morphology. But it is in respect to their physiological diversity that bacteria simply outclass the rest of life. The bacterium *Escherichia coli*